

Optimization Problems for Design and Maintenance of Forces and Shape of Tension Structures

Jingyao ZHANG

Dept. of Architecture and Architectural Engineering
Kyoto University, Japan

A thesis submitted for the degree of
Master of Engineering

14th, Feb., 2005

Acknowledgements

First, I would like to thank my family. The debts that I have accumulated during my six and a half years apart from them, four at Zhejiang and two and a half years here in Japan, are numerous. Without their encourages, I never would have made it to my Master's degree. I feel very lucky to have such a wonderfully supportive family, and very sorry for my having not spent much time with them.

My deepest thanks go to my supervisor at Kyoto, Professor Makoto OHSAKI, for his patient guidance and support throughout my master's degree. He always encourages my research interests and goals, although some may sound unusual. Over the past two years, I have learned a tremendous amount from him about both research and life, and I am grateful to have had the opportunity to work with him. And I feel very lucky to have the opportunities to take part in many conferences and seminars, with the support from prof. OHSAKI.

I would like to thank Professor Naoki KATO, Yoshikazu ARAKI and Dr. Y. KANNO. Prof. KATO has given me many advices on my study and research, and shown me the fantastic aspects of optimization problems, in which I have been interested but not done much work. I have had some discussions with Prof. ARAKI on my thesis and got many advices and guides from him, especially in the field of identification problem. The initial idea of the new direct approach for form-finding method for tensegrity structures in Chapter 2 came from Dr. KANNO's research, the method could not have been worked out without the discussion with him.

I would also like to thank the other current or former members of the former Architectural Information System Lab. (AIS) for their useful discussion and supports.

I am also indebted a lot to Professor Motoyuki SUZUKI, my former advisor at Tohoku University, and sorry very much for not being able to enjoy with him for a longer duration due to my research interest's shifting into another area. I can never forget two scenes: he marked circles on Hangzhou, where the university I graduated from locates, and Guangzhou, where I come from, on a map and encouraged me to work hard on research at the first meeting with him in his office; and, at the last meeting, he wrote on the calendar to remind himself the date of my leaving for Kyoto. I did at Kyoto as what I have promised him and will keep on hard working for my doctoral degree.

Contents

1	Introduction	1
1.1	Introduction of Tension Structures	1
1.1.1	Classification of Tension Structure	2
1.1.2	Tensegrity Structures	3
1.1.3	Tensile Structures	5
1.2	Background & Research Goals	6
1.3	Thesis Outline	8
I	Form-finding Problem of Tensegrity Structures	10
2	Direct Approach for Form-finding Problem of Tensegrity Structures	11
2.1	Background	11
2.1.1	Current Studies	12
2.1.2	Motivation & Outline	13
2.2	Equilibrium Analysis	14
2.3	Geometrical Constraints	18
2.3.1	Member Directions	19
2.3.2	Directions of Fixed Members	20
2.3.3	Symmetry Properties	21
2.4	Form-finding Process	23
2.4.1	Design of Forces	23
2.4.2	Design of Nodal Coordinates	25
2.4.3	Stress States	26

2.4.4	Summary of Design Procedures	27
2.5	Numerical Examples	27
2.5.1	Two-dimensional Prestressed Tensegrity System	28
2.5.2	A three-dimensional prestressed tensegrity structure	29
2.5.3	Diamond-shaped Tensegrity	31
2.5.4	Prism-shaped Tensegrity	35
2.5.5	Evaluation of Design Errors	35
2.6	Discussions and Conclusions	36
3	Adaptive Force Density Method	40
3.1	Introduction & Outline	40
3.2	Force Density Method	41
3.3	Force Density Method	42
3.3.1	Formulation of Equilibrium Matrix with respect to Nodal Coordinates	42
3.3.2	Force Density Method for Tensegrity Structures	45
3.4	Adaptive Force Density Method	47
3.4.1	Formulation of Force Density Vector	47
3.4.2	Singular Value Decomposition	49
3.4.3	Form-finding Process	50
3.4.3.1	Feasible Force Densities	50
3.4.3.2	Determination of Nodal Coordinates	51
3.5	Numerical Examples	52
3.5.1	Two-stage Tensegrity Structures	52
3.5.2	Three-stage Tensegrity Structure	55
3.6	Discussions and Conclusions	56
 II Optimal Measurement Positions of Tension Structures for the Identification of Prestress Distribution		 58
4	Optimal Measurement Positions I	59
4.1	Introduction	59
4.1.1	Maintenance Problem of Membrane Structures	60

4.1.2	Maintenance & Health Monitoring of Tensegrity Structures	61
4.1.3	Motivation & Outline	61
4.2	Equilibrium Analysis	62
4.3	Mean Identification Error (MIE)	64
4.3.1	Formulation of MIE	65
4.3.2	Characteristics of MIE	66
4.4	Formulation of Optimization Problem	67
4.5	Stingy Method	68
4.6	Greedy Method	69
4.6.1	Simulated annealing (SA)	69
4.6.1.1	Feasible Solutions	70
4.6.1.2	Transition of Solutions	71
4.6.1.3	Cooling Schedule & Termination Conditions	71
4.7	SLS & GLS	73
4.8	Numerical examples	73
4.8.1	Cable Net Model of Membrane Structure	74
4.8.1.1	21-member Cable Net Model	75
4.8.1.2	40-member Cable Net Model	76
4.8.1.3	Optimal Measurement Positions by Stingy Method	77
4.8.2	Two-dimensional Cable Dome	78
4.8.3	Two-dimensional Self-stressing Pin-jointed Arch	80
4.8.4	Three-dimensional Tensegric Truss Dome	81
4.9	Conclusions & Discussions	82
5	Optimal Measurement Positions II	85
5.1	Introduction	85
5.1.1	Motivation	86
5.1.2	Outline	86
5.2	Equilibrium Analysis	86
5.3	Sensitivity Analysis of Equilibrium Matrix	88
5.3.1	Sensitivity Analysis of Length Matrix	88
5.3.2	Sensitivity Analysis of Coordinate Difference Matrices	89
5.4	Formulation of Identification Error (IE)	90

5.4.1	Formulation of Force Errors	90
5.4.2	Mean and Variance-covariance	91
5.4.3	Definition of Identification Error (IE)	92
5.5	Formulation and Solution of Optimal Positions	93
5.5.1	Formulation	93
5.5.2	Solution	94
5.5.2.1	Improved Simulated Annealing (ISA)	95
5.6	Numerical Example 1: 21-member Cable Net Model	95
5.6.1	Enumeration method	96
5.6.2	Efficiency and Accuracy of Improved SA (ISA)	98
5.7	Other Numerical Examples	99
5.7.1	Example 2: Two-dimensional Self-stressing Arch	99
5.7.2	Example 3: A Three-dimensional Cable Dome	101
5.8	Conclusion	102
6	Conclusions	103
6.1	Form-finding Problem of Tensegrity Structures	103
6.1.1	Direct Approach	103
6.1.2	Adaptive Force Density Method	104
6.2	Optimal Measurement Positions	105
6.2.1	Consider Measurement Errors of Forces only	105
6.2.2	Consider Errors of Forces and Configuration	106
6.3	Future Study	107
A	Reduced Row-Echelon Form	108
B	Least Square Solution	110

List of Figures

1.1	Simple examples of tensegrity structures.	3
1.2	Needle Tower, by Kenneth Snelson in 1968.	5
1.3	Millennium Dome built in Greenwich, UK	6
1.4	German Pavilion at the 1967 MONTREAL EXPOSITION (1967-68)	7
2.1	Definition of axial force vector \mathbf{v}_k	15
2.2	A two-dimensional tensegrity system.	16
2.3	The two-dimensional tensegrity system with fixed members.	17
2.4	Coordinate difference vector \mathbf{d}_k of member k	20
2.5	Rotational symmetry properties of a two-dimensional structure.	22
2.6	Two-dimensional tensegrity system.	28
2.7	Perspective view of a three-dimensional prestressed tensegrity system.	29
2.8	Example 1 of a three-dimensional prestressed tensegrity system.	30
2.9	Example 1 of a three-dimensional prestressed tensegrity system.	31
2.10	Example 1 of diamond-shaped tensegrity	32
2.11	Example 2 of diamond-shaped tensegrity.	33
2.12	Example 3 of diamond-shaped tensegrity.	34
2.13	Examples 1'-3' of diamond-shaped tensegrity.	35
2.14	Example 1 of rotationally symmetric prism-shaped tensegrity	36
2.15	Example 2 of rotationally symmetric prism-shaped tensegrity with $v_9^y = 2$	37
2.16	Example 3 of rotationally symmetric prism-shaped tensegrity with $v_9^y = 0.5$	37
2.17	Prism-shaped tensegrities with reversed stress states	38

LIST OF FIGURES

3.1	A two-dimensional cable net.	43
3.2	A two dimensional tensegrity structure.	46
3.3	A two-stage tensegrity structure.	52
3.4	Example 1: a two-stage tensegrity structure.	53
3.5	Convergence of the algorithm for feasible force densities.	54
3.6	Example 2: a two-stage tensegrity structure.	54
3.7	Example 3: a two-stage tensegrity structure.	55
3.8	Example 4: a "two" stage tensegrity structure.	55
3.9	Example 5: a three-stage self-stressed structure.	56
4.1	Stress relaxation of membrane.	60
4.2	Top view of the 176-member cable net model.	74
4.3	Side view of the 176-member cable net model.	74
4.4	Optimal measurement members - $m = 40, h = 13, \bar{E}/e = 1.5$. . .	75
4.5	Numerical experiments of the proposed methods ($m = 40, h = 13$). .	76
4.6	Optimal measurement members - $m = 176, h = 29, \bar{E}/e = 2.0$. . .	77
4.7	A two-dimensional tensegrity structure.	78
4.8	MIE of a 2D tensegrity structure by Stingy Method.	79
4.9	Optimal measurement members by Stingy method ($\bar{E}/e = 1.5$). . .	79
4.10	A two-dimensional prestressed pin-jointed arch.	80
4.11	System truss unit.	81
4.12	Multi-objective Dome of Kirara Sports Park.	82
4.13	A three-dimensional tensegric dome.	83
4.14	A three-dimensional tensegric dome.	84
5.1	A membrane structure modeled by a cable net with 176 members. .	96
5.2	A membrane structure modeled by a cable net with 21 members. .	96
5.3	21-member cable net.	97
5.4	Ex. 2-1 of optimal measurement members ($\bar{p} = 13$).	100
5.5	Ex. 2-2 of optimal measurement members ($\bar{p} = 13$).	100
5.6	A three-dimensional cable dome.	101
5.7	12 optimal measurement members of a three-dimensional cable dome.	102

Chapter 1

Introduction

Less is more.

– by Mies van der Rohe

This saying marks the architecture in 1920's. After the war, young architects, engineers, and entrepreneurs had been looking for new peaceful architectural forms, which should not counteract nature, but could be a integrated part of it instead. It was of prime importance, with the minimal material and energy, to rebuild the destroyed cities in a more effective and beautiful way at that time ([Ishii, 1999](#)).

The thought, "less can also be more", makes sense even today. For now it is recognized for the first time that conservation and care of nature and a livable, sustainable environment should be taken into account in the process of selection and design of architectural forms. It is not only about the development of new structural technologies, construction methods, and materials to fulfill actual needs, but also about the realization and creation of new aesthetic environments. It is essential to conserve and protect the fundamental home of our mankind.

1.1 Introduction of Tension Structures

Tension structure is a kind of structure considered to be born from these thought and recognition. Besides pursuing higher and higher buildings in crowd cities nowadays, human beings have been also making their consecutive efforts to find

novel structural materials and forms, which can provide the same level of safety as the traditional structural ones, to facilitate the framing of large spaces and create bright, variegated interior spaces.

Tension structures can greatly extend architects' imagination because of their lightweight characteristics by making use of tensile materials, cables and/or membranes. This kind of structure can achieve the desired geometrical configuration and capacity of resisting external loads by the introduction of prestress. The last few decades have seen a rapid expansion in the growth of number and range of applications of them.

1.1.1 Classification of Tension Structure

There have been many definitions for tension structures. Some scholars consider that tensile membrane structures should be included in the category of tension structure, however, some others disagree and consider it as just a kind of roof material. Base on the fact that stability of tension structure is provided by the prestresses in it, we regard tensile membrane structure as a kind of tension structure. And we classify tension structures into two major classes as follows in this study, according to the stress states, in compression and/or in tension, of their structural elements:

1. *Tensegrity Structure* – consisting of both compressive and tensile elements.
2. *Tensile Structure* – consisting of only tensile elements.

There exist both tensile and compressive elements in a tensegrity structure. It is a prestressed cable-strut system, of which structural elements are usually assumed to be connected by pin joints.

Tensile structure is made of tensile materials, cables and/or membranes, in which there is no bending, compression nor torsion but only tension forces/stresses exist. It is usually used as a large-span structure because of the light-weight characteristics of the structural materials and absence of elements that may have buckling.

As described in the coming chapters, all of the structures being dealt with in this study accept the common used assumption in structural engineering that

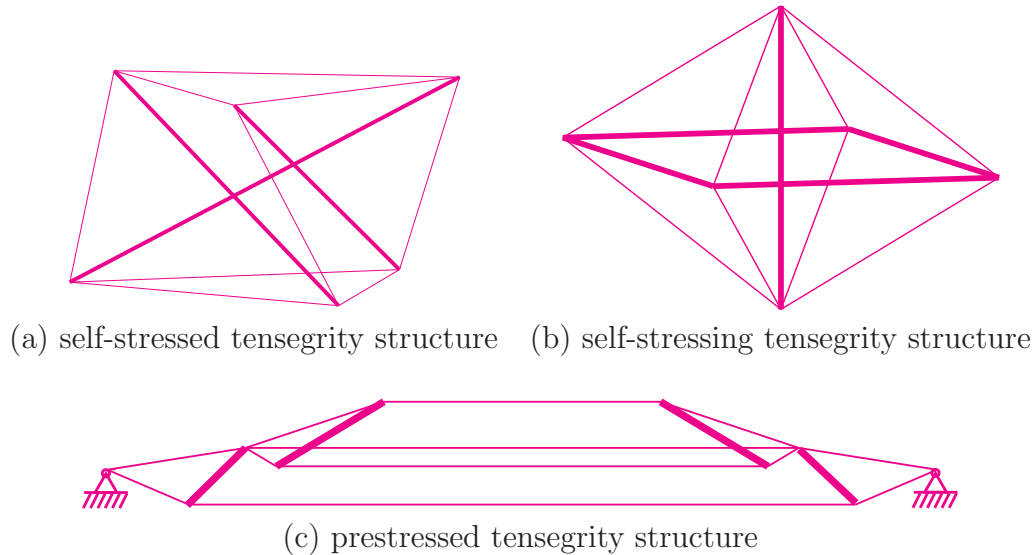


Figure 1.1: Simple examples of tensegrity structures.

all elements of them are or are transformed to be connected by pin-joints with prestresses in them.

1.1.2 Tensegrity Structures

Inspired by Kenneth Snelson sculptures created in 1948, Buckminster Fuller patented a class of cable-strut structures, which he called *TENSEGRITY* structures (Fuller, 1975) - an acronym, a contraction of *TENSional inteGRITY*. Structural elements of a tensegrity structure are usually assumed to be connected by pin joints, and the external loads are applied at the nodes. So structural elements of the structure transmit only axial forces, either tension or compression, and the geometrical configuration of the structure can be described in terms of nodal coordinates.

A strict definition of tensegrity structure is that the structure is composed of a set of continuous tensile elements (usually cables), and a set of *physically discontinuous* compressive elements (usually struts). In the following of this thesis, the cables and struts mean the tensile and compressive elements of the structure, respectively. Many structures developed nowadays from the basic idea of tensegrity

1.1 Introduction of Tension Structures

structure do not fit the definition exactly. According to their mechanical characteristics and physical connections of different structural elements, tensegrity structures can be classified into three classes as follows (Motro, 1996):

1. *Self-stressed Tensegrity Structure*, which consists of physically discontinuous struts without support.
2. *Self-stressing Tensegrity Structure*, which consists of physically continuous struts without support.
3. *Prestressed Tensegrity Structure*, which is attached to supports.

Self-stressed and self-stressing tensegrity structures belong to the kind of free-standing cable-strut system. This kind of structures maintains (self-)equilibrium by the prestress introduced. Among these, the self-stressed structure fits the initial strict definition of tensegrity structure exactly: no strut (compressive element) is physically connected with each others by ends. And self-stressing tensegrity structure is a degenerated one of the self-stressed structure, of which some struts (compressive elements) are physically touching each other by ends. The prestressed tensegrity structure, such as tensegric dome or cable dome which are often used as large-span structures, belongs to the third class. Supports, which are called fixed nodes in the following of the thesis since they cannot have any displacement while subjected to external loads, are necessary for the structure to maintain its equilibrium state against external loads.

Concepts of these three types of tensegrity structures are shown in Fig. 1.1(a), (b) and (c), respectively. A multi-layer tensegrity structure in practice, named *Needle Tower*, is shown in Fig. 1.2. It is designed for and installed in the Hirshhorn Museum and Sculpture Garden, Smithsonian Institution, Washington DC., by Kenneth Snelson in 1968.

Because the nodes of a tensegrity structure have a predictable, linear response over a wide range of different shapes, it attracts research interests of many researchers and engineers. Some new developments are currently taking place in the field, driven by a growing interest in smart structures, of which shape can be actively adjusted and controlled, since the control systems (sensors and actuators)

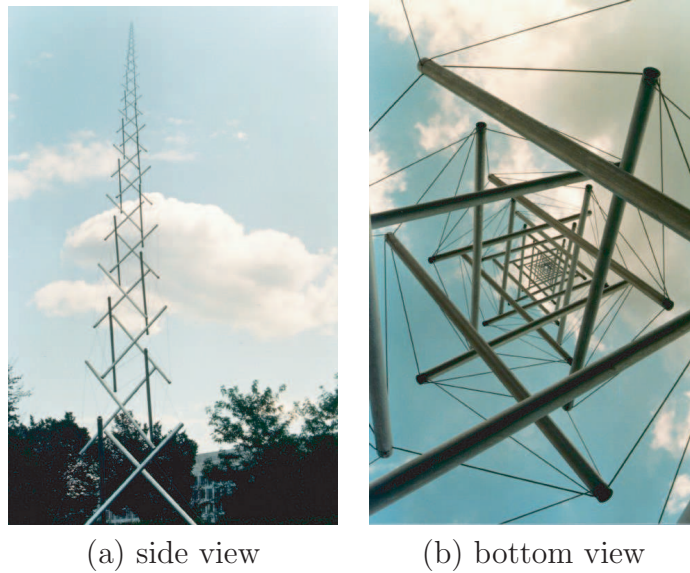


Figure 1.2: Needle Tower, by Kenneth Snelson in 1968.

can be easily embedded in this kind of structures, e.g. a concept of adjustable tensegrity structure proposed by [Fest et al. \(2003\)](#).

Tensegrity structures have also aroused the interest of the bio-medical community. [Ingber \(1993\)](#) has extended the tensegrity structure as a model for the cellular structure from its earlier version for viruses by [Caspar and Klug \(1962\)](#). These models have been utilized to explain how various types of cells (such as nerve cells, smooth muscles) resist shape distortion in different external environment. Some reports have confirmed that the results of static numerical analysis of a tensegrity structure model are in good agreement with biological experimental measurements of a cell's static properties.

1.1.3 Tensile Structures

Tensile structure is made of only tensile materials, membranes and/or cables. Only tensile forces (stresses) exist in this kind of structure. It can be used to cover a very large area by the introduction of prestress because there is no need to consider the buckling of compressive elements.

Tensile structure is indeed a very old structural form, that can be traced back



Figure 1.3: Millennium Dome built in Greenwich, UK

to tents made of animals' skins and widely used by the nomadic tribes in the ancient time. Nevertheless, it is a very new constructive system used today. It opens the eyes of people who have been seeking technically advanced, ecologically sustainable, and thereby aesthetically pleasing non-column architectures.

Building with coated fabrics and/or nets, which are held in position with cables, frames, masts or air pressure, tensile structure has come to be the symbol of the modern age. Halls, stadiums, roof, which can be unfurled in few minutes, and pneumatic skins over cities and industrial parks, show the fascination with the near ethereal.

There is now a well established base of projects, both temporary and permanent, ranging from simple free-standing shade elements through to complex wall and roofing elements that form an integrated part of or even a whole building. E.g. the Millennium Dome, a famous membrane structure built in Greenwich, UK as shown in Fig. 1.3, and the German Pavilion at the 1967 Montreal Exposition, a cable net as shown in Fig. 1.4, are two famous examples of this kind of structural form.

1.2 Background & Research Goals

Geometrical configuration of a tension structure and the prestress in it are the two highly interdependent parameters. They provide the structure the capability of maintaining its desired shape against external loads. So tension structure is



Figure 1.4: German Pavilion at the 1967 MONTREAL EXPOSITION (1967-68)

said to be the perfect combination of architectural form and mechanics. However, these attracting characteristics lead to difficulties in design and maintenance processes, which may also be regarded as great challenges to structural engineers and one of the most important technical barriers for its popularization.

A key step in the design of tensegrity structures is the determination of their geometrical configuration, well known as *form-finding* or *shape-finding*. Methods that can help architects control the shape of the structure and structural engineers control its mechanical properties, or have the ability of searching novel stable and prestressable configuration, turn to be necessary. These requirements motivate us to propose more powerful new methods based on the current studies, which is discussed in detail in the first part - *Form-finding Problem of Tensegrity Structures* of this study. Although no optimization problem is discussed in this part in this stage, some basic formulations in the study can be used for optimization problems to simplify the problem in future study.

It has been well known that the stiffness of tension structure, which provides resistance ability against external loads, is highly sensitive to the geometrical configuration and the prestress in it. The change of prestress due to construction error, material properties, e.g. stress relaxation phenomena in membrane materials, or affect of external environment, may change the geometrical configu-

ration of the structure significantly. This could cause problems of wrinkle, stress concentration or even damage of membrane structure under just design loads, or lose the normal function of tensegrity structures, e.g. the structure used in space cannot receive and send signals correctly due to the change of shape or orientation. So engineers/researchers would like to adjust the prestress in the structure to maintain it the desired configuration and function.

Before the maintenance or health monitoring of tension structure, prestress distribution is necessary to be known. In order to identify the prestress distribution, measurements of stresses or forces are usually needed. In this case, how to find an optimal set of measurement positions to achieve high enough identification accuracy with the minimal costs on construction and measurement devices, is also the research goal of this study. The details are demonstrated in the second part - *Optimization Methods for the Maintenance Problem of Tension Structures*.

1.3 Thesis Outline

The coming contents of this thesis are organized as follows:

- Chapter 2 describes a direct approach for the form-finding problem of tensegrity structures. The proposed method can satisfy architects' requirements on control of configuration and structural engineers' on mechanical properties by introducing linear equations of specified geometrical and mechanical properties. The method is highly efficient in computation cost because only linear equations need to be solved, and is able to search for new configurations by modifying the values of the parameters. The difficulties and drawbacks of the approach are also discussed.
- Chapter 3 presents an numerical method based on the idea of force density method, which is originally developed for the form-finding problem of cable nets. Equilibrium matrix is formulated in terms of nodal coordinates and topology matrix, and singular value decomposition of it is used to find a feasible set of force densities to make the equilibrium matrix have the required rank deficiency. A few numerical examples demonstrate the high capability

of searching new configurations, although designers may lose exact controls over geometrical and mechanical properties of the structure.

- Chapter 4 formulates an equation of mean identification error (MIE) to evaluate the accuracy of the prestress identification of a tension structure, based on the sensitivity analysis of equilibrium equations, while assuming that the nodal coordinates of it are given or measured without any error. Four heuristic methods are then proposed for finding the minimal number of measurement positions subjected to the upper-bound constraint on mean identification error. Efficiencies and accuracies of the presented methods are investigated by several numerical examples.
- Chapter 5 reformulates the identification error (IE) of stress distribution of a tension structure, taking into account of the measurement errors of not only member forces but also its nodal coordinates to reflect the problem in practice. An improved simulated annealing (ISA), which starts from an initial solution found by Stingy method proposed in Chapter 4 rather than a random one, is used to find a specific number of measurement positions to minimize the identification error.
- Chapter 6 concludes the study and give some discussions of future study on the design and maintenance problems of tension structures.

Part I

Form-finding Problem of Tensegrity Structures

Chapter 2

Direct Approach for Form-finding Problem of Tensegrity Structures

In the process of designing a tensegrity system, some constraints are usually introduced for geometry and/or forces to ensure uniqueness of the solution, because the tensegrity systems are underdetermined in most cases (Haber and Abel, 1982). In this chapter, a new approach is presented to enable designers to specify independent sets of axial forces and nodal coordinates consecutively, under the equilibrium conditions and the given geometrical constraints. Therefore, the method can satisfy the distinctly different requirements of architects and structural engineers. The proposed method can be used very efficiently for practical applications because only linear algebraic equations are to be solved, and no equation of kinematics or material property is needed. Some numerical examples are given to show not only efficiency of the proposed method but also its ability of searching new configurations.

2.1 Background

The basic parameters involved in the shape design of tensegrity systems can be concluded as follows:

- topology
- internal forces

- external loads
- configuration
- geometrical constraints

Among these, topology defines the connectivity of members and nodes. In the design of tensegrity systems, members are assumed to be pin-jointed and external loads are applied at nodes if exist. So the members transmit only axial forces, either in tension or compression. The geometrical configuration is described in terms of nodal coordinates.

Determination of geometrical configuration at the equilibrium state is known as *form-finding* or *shape-finding* that is considered a key step in the design of tensegrity systems. Geometrical constraints, such as locations and directions of members and symmetry properties, are often needed to ensure a unique solution of the form-finding problem because most of the tensegrity systems are under-determined; i.e. the member forces and nodal locations cannot be determined uniquely only from the equilibrium conditions.

2.1.1 Current Studies

There have been extensive researches on analysis and design of tensegrity structures, such as [Hanaor \(1988\)](#); [Pellegriano \(1990\)](#); [Pelegriano and Calladine \(1986\)](#); [Sultan et al. \(2001\)](#); [Jager and Skelton \(2004\)](#); [Motro et al. \(1986\)](#).

A key step in the design of tensegrity structures is the determination of their geometrical configuration, well known as *form-finding* or *shape-finding*. Many methods have also been proposed for the shape analysis of them. Some of them, such as dynamic relaxation by [Barnes \(1999\)](#) and [Motro \(1984\)](#) and force density method by [Schek \(1974\)](#) and [Vassart and Motro \(1999\)](#), have been originally used for the form-finding problem of membrane structure and cable net and then extended to tensegrity system.

[Tibert and Pellegriano \(2003\)](#) classified the existing methods for the form-finding of tensegrity structures into the following two categories:

- kinematical methods,

- statical methods.

The kinematical methods determine the geometrical configuration of a given tensegrity structures by maximizing the lengths of the struts while keeping the lengths of the cables constant, or by minimizing the total length of cables while the lengths of cables are kept constant. There are three methods consist in this category: (a) analytical approach(Connelly, 1995), (b) non-linear optimization method, and (c) pseudo-dynamic iterative methods.

The statical methods search for equilibrium configurations that allow existence of a state of prestress in the structure with given topology and forces, where the force density method can be effectively used. There are four methods belong to this category: methods (i) and (ii) establish linear nodal equations of equilibrium in terms of so-called force densities and solve these equations for the nodal coordinates, either analytically in method (i) or by setting up a force density matrix in method (ii). Method (iii) is based on an energy minimization approach, which is shown to produce a matrix identical to the force-density matrix, and introduces the concept of super-stable tensegrities. Method (iv) searches for equilibrium configurations of a set of rigid bodies, i.e. the struts of the tensegrity structure, connected by cables whose lengths are to be determined. A reduced set of equilibrium equations for the struts are determined by virtual work, making use of symmetry condition, and are then solved in symbolic form.

2.1.2 Motivation & Outline

For the design of a tensegrity structure in architectural application, it is desirable for architects that the characteristics of configuration, such as directions and locations of members or locations of supports, can be specified, while structural engineers are concerned with its mechanical properties defined by the member forces. However, there has been no method developed so far that can satisfy both of these requirements simultaneously, which motivates us to present a new approach.

Ohsaki and Kanno (2003) have pointed out that the set of member axial forces cannot be specified arbitrarily because the equilibrium conditions and geometrical constraints may be violated. For a tensegrity with fixed configuration, the number

of independent member force vectors at self-equilibrium can be easily found by investigating the rank of the equilibrium matrix. However, no method exists for directly finding the number of independent member directions (force vectors), and nodal locations of tensegrity system with unknown geometry with given topology.

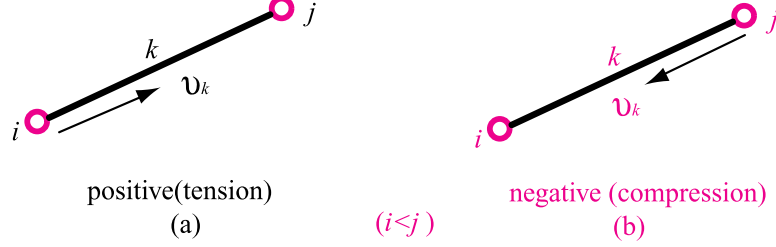
In this chapter, a new approach is presented for specifying independent set of axial forces and then nodal coordinates consecutively, under equilibrium conditions and geometrical constraints. The incidence matrix of a directed graph (Harary, 1969; Kaveh, 1992), is used in the formulation of the equilibrium conditions. The components of the member force vector are taken as the variables (Williamson and Skelton, 2003) at the first stage, and then the nodal coordinates at the second stage of the approach.

The rest of this chapter is organized as follows: Section 2 describes the equilibrium conditions of the structures by using the graph theory. In Section 3, the geometrical constraints are formulated to represent designer's preferences, including (a) member directions, (b) member locations, and (c) symmetry properties, in terms of axial force vector. Section 4 describes the form-finding approach proposed in detail. And some numerical examples will be presented in Section 5 to illustrate the validity of the proposed method for generating various shapes, and finally conclusions are given in Section 6.

2.2 Equilibrium Analysis

The following commonly accepted assumptions in the form-finding problem of tensegrity structures are adopted for simplicity:

- a. The topology of the structure, which is defined by the designer, is known.
- b. Members are connected by pin joints.
- c. No external load is applied and the self-weight of the structure is neglected during the design procedure.
- d. The possibility of buckling of the struts is disregarded.


 Figure 2.1: Definition of axial force vector \mathbf{v}_k

Since the incidence matrix of a directed graph is used for formulating the equilibrium equations in terms of the member force vectors, we start with a brief description of the graph theory as described by [Harary \(1969\)](#).

The words *edge* and *node* in graph theory are called *member* with direction and *node*, respectively. Let m denote the number of members including cables and struts. And the number of nodes including the supports of a structure is denoted by n .

Suppose member k is connected to nodes i and j , and directed from node i to j ($i < j$). The incidence matrix $\bar{\mathbf{B}} = (\bar{\mathbf{B}}_{(k,p)}) \in \mathfrak{R}^{m \times n}$ of the structure regarded as a directed graph can be defined as

$$\bar{\mathbf{B}}_{(k,p)} = \begin{cases} 1 & p = i \\ -1 & p = j \\ 0 & \text{in other cases} \end{cases} \quad (2.1)$$

By using $\bar{\mathbf{B}}$, the equilibrium matrix \mathbf{B} is defined as

$$\mathbf{B} = \bar{\mathbf{B}} \otimes \mathbf{I}$$

where \otimes and $\mathbf{I} \in \mathfrak{R}^{s \times s}$ denote tensor product and identity matrix, respectively, and s is the number of dimension of the space; i.e. $s = 2$ or 3 .

Let $\mathbf{v}_k \in \mathfrak{R}^s$ denote the axial force vector of member k that is connected to nodes i and j ($i < j$). We define the positive direction, i.e., tensile state, of \mathbf{v}_k as shown in Fig. 2.1(a), starting from i and directing to j . Fig. 2.1(b) shows the negative direction of \mathbf{v}_k , which means that member k is in compression.

For member k of a two-dimensional structure, its force components of \mathbf{v}_k are written as $\mathbf{v}_k = (v_k^x, v_k^y)^\top$. In three-dimensional space, $\mathbf{v}_k = (v_k^x, v_k^y, v_k^z)^\top$. The

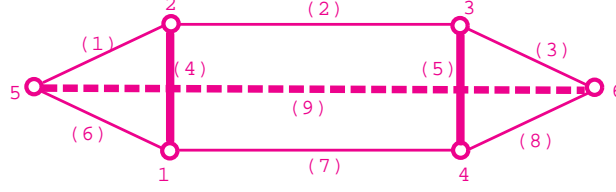


Figure 2.3: The two-dimensional tensegrity system with fixed members.

Since all the free nodes are in self-equilibrium state, the equilibrium equations of a free node, e.g. node 4, are written as

$$\begin{aligned} -v_5^x - v_7^x + v_8^x &= 0 \\ -v_5^y - v_7^y + v_8^y &= 0 \end{aligned} \quad (2.2)$$

Eq. (2.2) can be rewritten by using the equilibrium matrix as

$$\begin{aligned} (\mathbf{B}^\top)_7 \mathbf{v} &= 0 \\ (\mathbf{B}^\top)_8 \mathbf{v} &= 0 \end{aligned}$$

where $(\mathbf{B}^\top)_i$ denotes the i th row of \mathbf{B}^\top . $(\mathbf{B}^\top)_7$ and $(\mathbf{B}^\top)_8$ correspond to the x - and y -directions, respectively, of node 4. So the global equilibrium condition of all the free nodes in terms of unknown generalized axial force vector \mathbf{v} can be written as

$$\mathbf{B}^a \mathbf{v} = \mathbf{0} \quad (2.3)$$

In designing tensegrity systems with supports, the locations of the supports should be specified. In Section 3, a direct approach is presented for specifying force vectors and member directions. In the proposed approach, some components of force vectors are first specified. However, if we specify a set of axial force vectors arbitrarily satisfying Eq. (2.3), the form finding process may end up with an undesirable configuration as shown in the dotted lines in Fig. 2.2; i.e. nodes 5 and 6 are located unfavorably, because the locations of the fixed nodes (supports in this example) have not been incorporated in Eq. (2.3).

To present a unified approach to shape design of structures with and without supports, we introduce auxiliary members called *fixed members* to connect the

2.3 Geometrical Constraints

supports. For the structure shown in Fig. 2.2, we connect nodes 5 and 6 with the auxiliary member 9 as shown in Fig. 2.3. The locations of the auxiliary members are to be fixed in Section 4 to transform the supported tensegrity into a selfstressing or selfstressed system.

Let m_f and n_f denote the numbers of fixed members and nodes, respectively, where $m_f = 1$ and $n_f = 2$ for the structure in Fig. 2.3. Note that the members and nodes are numbered such that the nodes $\{1, \dots, n - n_f\}$ and members $\{1, \dots, m - m_f\}$ correspond to free nodes and members, respectively. So $\mathbf{B}^f \in \mathfrak{R}^{sm_f \times sn_f}$ corresponding to fixed members and nodes is placed in the lower-right of \mathbf{B} as

$$\mathbf{B} = \left(\begin{array}{c|c} \mathbf{B}^a & \mathbf{B}^b \\ \mathbf{O} & \mathbf{B}^f \end{array} \right) = \begin{array}{c} m_1^x \\ m_1^y \\ m_2^x \\ m_2^y \\ m_3^x \\ m_3^y \\ m_4^x \\ m_4^y \\ m_5^x \\ m_5^y \\ m_6^x \\ m_6^y \\ m_7^x \\ m_7^y \\ m_8^x \\ m_8^y \\ m_9^x \\ m_9^y \end{array} \left| \begin{array}{cccc|cccc|cccc} n_1^x & n_1^y & n_2^x & n_2^y & n_3^x & n_3^y & n_4^x & n_4^y & n_5^x & n_5^y & n_6^x & n_6^y \\ \hline 0 & 0 & 1 & 0 & 0 & 0 & 0 & 0 & -1 & 0 & 0 & 0 \\ 0 & 0 & 0 & 1 & 0 & 0 & 0 & 0 & 0 & -1 & 0 & 0 \\ 0 & 0 & 1 & 0 & -1 & 0 & 0 & 0 & 0 & 0 & 0 & 0 \\ 0 & 0 & 0 & 1 & 0 & -1 & 0 & 0 & 0 & 0 & 0 & 0 \\ 0 & 0 & 0 & 0 & 1 & 0 & 0 & 0 & 0 & 0 & -1 & 0 \\ 0 & 0 & 0 & 0 & 0 & 1 & 0 & 0 & 0 & 0 & 0 & -1 \\ 1 & 0 & -1 & 0 & 0 & 0 & 0 & 0 & 0 & 0 & 0 & 0 \\ 0 & 1 & 0 & -1 & 0 & 0 & 0 & 0 & 0 & 0 & 0 & 0 \\ 0 & 0 & 0 & 0 & 1 & 0 & -1 & 0 & 0 & 0 & 0 & 0 \\ 0 & 0 & 0 & 0 & 0 & 1 & 0 & -1 & 0 & 0 & 0 & 0 \\ 1 & 0 & 0 & 0 & 0 & 0 & 0 & 0 & -1 & 0 & 0 & 0 \\ 0 & 1 & 0 & 0 & 0 & 0 & 0 & 0 & 0 & -1 & 0 & 0 \\ 1 & 0 & 0 & 0 & 0 & 0 & -1 & 0 & 0 & 0 & 0 & 0 \\ 0 & 1 & 0 & 0 & 0 & 0 & 0 & -1 & 0 & 0 & 0 & 0 \\ 0 & 0 & 0 & 0 & 0 & 0 & 1 & 0 & 0 & 0 & -1 & 0 \\ 0 & 0 & 0 & 0 & 0 & 0 & 0 & 1 & 0 & 0 & 0 & -1 \\ \hline 0 & 0 & 0 & 0 & 0 & 0 & 0 & 0 & 1 & 0 & -1 & 0 \\ 0 & 0 & 0 & 0 & 0 & 0 & 0 & 0 & 0 & 1 & 0 & -1 \end{array} \right.$$

This way, all the fixed nodes are converted to free nodes, and the equilibrium equation of the structure can be written as

$$\mathbf{B}^\top \mathbf{v} = \mathbf{0} \tag{2.4}$$

2.3 Geometrical Constraints

To design a tensegrity system with desired geometrical properties, such as directions of members and symmetric properties, geometrical constraints are usu-

ally assigned at the first step of the form-finding of it. Geometrical constraints can also reduce the number of unknown parameters in the form-finding process, which helps to simplify the problem as in the case of the proposed method in this chapter. This section formulate all these geometrical constraints on a tensegrity system in terms of nodal coordinates.

2.3.1 Member Directions

In the design process of tensegrity systems, it is desirable that the directions of some members can be directly specified. The direction of a member, however, should coincide with that of its force vector, because members of a tensegrity system can transmit only axial forces.

Consider a tensegrity system in three-dimensional space, and let $\mathbf{e}_k = (e_k^x, e_k^y, e_k^z)^\top$ denote a vector in the direction of member k . The vector \mathbf{e}_k of some members are defined by designer's preference. The direction vector \mathbf{e}_k and the force vector \mathbf{v}_k of member k should satisfy the relation $\mathbf{e}_k \times \mathbf{v}_k = \mathbf{0}$ which is explicitly written as

$$\begin{aligned} e_k^x v_k^y &= e_k^y v_k^x \\ e_k^y v_k^z &= e_k^z v_k^y \\ e_k^z v_k^x &= e_k^x v_k^z \end{aligned} \tag{2.5}$$

Let $\bar{\mathbf{T}}$ be defined as

$$\bar{\mathbf{T}} = \begin{pmatrix} 0 & 1 & 0 \\ 0 & 0 & 1 \\ 1 & 0 & 0 \end{pmatrix}$$

Eq. (2.5) can be written as

$$\text{diag}(\mathbf{e}_k) \bar{\mathbf{T}} \mathbf{v}_k - \text{diag}(\bar{\mathbf{T}} \mathbf{e}_k) \mathbf{v}_k = \mathbf{0} \tag{2.6}$$

where $\text{diag}(\mathbf{x})$ is the diagonal matrix of which the i th diagonal component is equal to the i th component x_i of \mathbf{x} . By letting

$$\mathbf{D}_k = \text{diag}(\mathbf{e}_k) \bar{\mathbf{T}} - \text{diag}(\bar{\mathbf{T}} \mathbf{e}_k)$$

Eq. (2.6) can be rewritten as

$$\mathbf{D}_k \mathbf{v}_k = \mathbf{0} \tag{2.7}$$

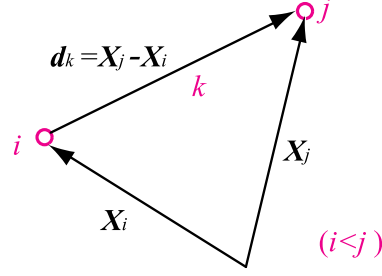


Figure 2.4: Coordinate difference vector \mathbf{d}_k of member k

By assembling Eq. (2.7) through all members for which the direction is specified, the following linear relation is derived for \mathbf{v} :

$$\mathbf{D}\mathbf{v} = \mathbf{0} \quad (2.8)$$

2.3.2 Directions of Fixed Members

In order to consider the fixed nodes (supports) in a similar manner as free nodes (internal nodes) in the self-equilibrium equation, we have introduced the concept of auxiliary fixed members, of which the directions are to be specified.

For a three-dimensional structure, let $\mathbf{X}_i = (x_i, y_i, z_i)^\top$ denote the coordinate vector of node i . The coordinate difference vector $\mathbf{d}_k = (d_k^x, d_k^y, d_k^z)^\top$ of member k that connects nodes i and j is defined as

$$\mathbf{d}_k = \mathbf{X}_j - \mathbf{X}_i \quad (2.9)$$

which is illustrated in Fig. 2.4.

Using the relation between the direction of a member and its force vector, $\mathbf{d}_k \times \mathbf{v}_k = \mathbf{0}$ should be satisfied; i.e.

$$\begin{aligned} d_k^x v_k^y &= d_k^y v_k^x \\ d_k^y v_k^z &= d_k^z v_k^y \\ d_k^z v_k^x &= d_k^x v_k^z \end{aligned} \quad (2.10)$$

Since Eq. (2.10) has a same form as Eq. (2.5), the relation similar to Eq. (2.6) can be easily obtained as

$$\text{diag}(\mathbf{d}_k) \bar{\mathbf{T}} \mathbf{v}_k - \text{diag}(\bar{\mathbf{T}} \mathbf{d}_k) \mathbf{v}_k = \mathbf{0} \quad (2.11)$$

\mathbf{d}_k can be expressed as follows using Eq. (2.9):

$$\mathbf{d}_k = -\mathbf{B}_k \mathbf{X} \quad (2.12)$$

where the rows of $\mathbf{B}_k \in \mathfrak{R}^{3 \times 3n}$ consist of the $(3k - 2)$ th, $(3k - 1)$ th, and $(3k)$ th rows of \mathbf{B} .

Let $\mathbf{d}^f \in \mathfrak{R}^{3m_f}$ denote the vector consisting of the coordinate difference vectors of the fixed members. The relation between \mathbf{d}^f and \mathbf{X}^f is written as

$$\mathbf{d}^f = -\mathbf{B}^f \mathbf{X}^f \quad (2.13)$$

The vector consisting of force vectors of the fixed members is denoted by $\mathbf{v}^f \in \mathfrak{R}^{3m_f}$. Let $\mathbf{I}^f \in \mathfrak{R}^{m_f \times m_f}$ denote the identity matrix. By using $\mathbf{T}^f = \mathbf{I}^f \otimes \bar{\mathbf{T}}$, Eq. (2.11) is assembled as

$$\text{diag}(\mathbf{d}^f) \mathbf{T}^f \mathbf{v}^f - \text{diag}(\mathbf{T}^f \mathbf{d}^f) \mathbf{v}^f = \mathbf{0} \quad (2.14)$$

In Eq. (2.14), \mathbf{d}^f is known after the coordinates \mathbf{X}^f of the fixed nodes are specified, and \mathbf{T}^f is a constant matrix. Since \mathbf{v}^f is the selected components of \mathbf{v} , it is easy to see that Eq. (2.14) can be rewritten by using a known matrix \mathbf{C} as

$$\mathbf{C} \mathbf{v} = \mathbf{0} \quad (2.15)$$

2.3.3 Symmetry Properties

The configuration of a tensegrity system usually has symmetry properties; i.e. invariance conditions to reflection with respect to some planes and/or rotation around some axes. Therefore, the member direction vectors should be specified to satisfy such symmetry conditions. The same axial forces should be assigned to the symmetrically located members.

For example, consider a part of a two-dimensional structure shown in Fig. 2.5(a), whose members are rotationally arranged by $\alpha (= \pi/3)$. Select two adjacent members k and k' as shown in Fig. 2.5(b) to illustrate the process of formulating their rotational symmetry properties. Members k and k' connect pairs of nodes (i, j) and (i', j') , respectively. The rotation matrix is defined as

$$\mathbf{M}_l = \begin{pmatrix} \cos \alpha & \sin \alpha & 0 \\ -\sin \alpha & \cos \alpha & 0 \\ 0 & 0 & 1 \end{pmatrix}$$

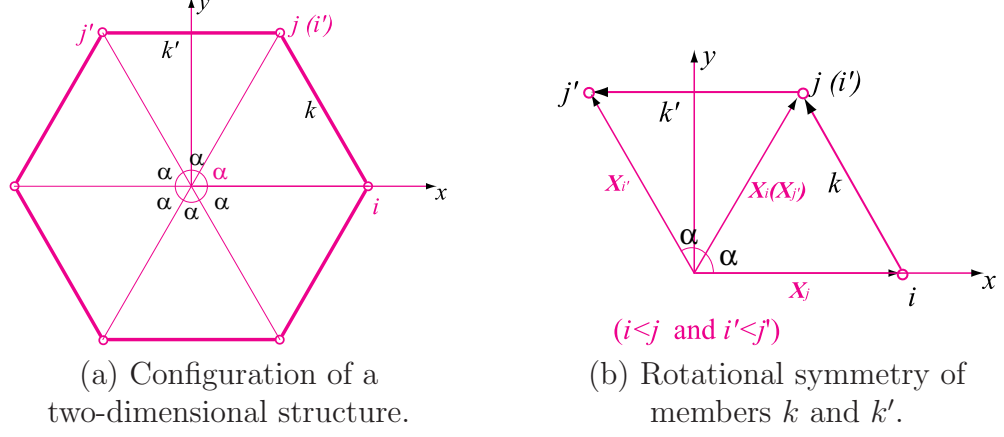


Figure 2.5: Rotational symmetry properties of a two-dimensional structure.

Then the relation between the coordinate difference vectors of members k and k' is written as

$$\mathbf{d}_{k'} = \mathbf{M}_l \mathbf{d}_k$$

From Figs. 2.1 and 2.4, we know that the direction of \mathbf{d}_k is the same with the positive direction of \mathbf{v}_k . So the symmetry properties of axial forces of members k and k' can be written as

$$\mathbf{v}_{k'} = \mathbf{M}_l \mathbf{v}_k \quad (2.16)$$

. By letting $\mathbf{S}_l = (\mathbf{0} \cdots \mathbf{M}_l \cdots -\mathbf{I} \cdots \mathbf{0})$, Eq. (2.16) can be rewritten as

$$\mathbf{S}_l \mathbf{v} = \mathbf{0} \quad (2.17)$$

The rotational symmetry of all other members of the structure can be formulated in a similar way. Reflectional symmetry can be also written in a form of Eq. (2.17). By combining Eq. (2.17) through all the symmetry conditions, the following linear equations are obtained:

$$\mathbf{S} \mathbf{v} = \mathbf{0} \quad (2.18)$$

2.4 Form-finding Process

In this section, we introduce an algorithm for directly specifying the member axial forces and nodal coordinates consecutively at two separated processes, in which all the specified components are independent so that the final unique configuration of the structure holds are of exactly the axial forces and nodal coordinates specified. Since only linear equations need to be solved in the form-finding process, the proposed algorithm can be used very efficiently.

2.4.1 Design of Forces

From the equilibrium condition (2.4) and the geometrical constraints (2.8), (2.15) and (2.18), we obtain a linear equation formulated based on the equilibrium equations and geometrical constraints in terms of the generalized force vector as

$$\begin{pmatrix} \mathbf{B}^\top \\ \mathbf{D} \\ \mathbf{C} \\ \mathbf{S} \end{pmatrix} \mathbf{v} = \mathbf{0} \quad (2.19)$$

By letting $\mathbf{H}^\top = (\mathbf{B}, \mathbf{D}^\top, \mathbf{C}^\top, \mathbf{S}^\top)$, Eq. (2.19) can be rewritten as

$$\mathbf{H}\mathbf{v} = \mathbf{0} \quad (2.20)$$

At this stage, our task is to find a non-trivial solution $\mathbf{v} \neq \mathbf{0}$ to Eq. (2.20). Let $h = 3m - \text{rank}(\mathbf{H})$ for a three dimensional structure. If $h = 0$, then there exists only trivial solution $\mathbf{v} = \mathbf{0}$. If $h < 0$, then Eq. (2.20) is overdetermined, and some geometrical constraints and/or symmetry properties should be relaxed. If $h > 0$, then the static relation (2.20) is underdetermined. Tensegrity systems will often fall into this category. So we will focus only on the underdetermined cases in this study.

The solution of Eq. (2.20) can be written by using a matrix $\mathbf{G} \in \mathfrak{R}^{3m \times h}$ as

$$\mathbf{v} = \mathbf{G}\boldsymbol{\alpha} \quad (2.21)$$

where the columns of \mathbf{G} are self-equilibrium modes and the i th element α_i of $\boldsymbol{\alpha} \in \mathfrak{R}^h$ is the coefficient of the i th self-equilibrium mode. Since $\boldsymbol{\alpha}$ has no explicit

mechanical meaning, we will obtain $\boldsymbol{\alpha}$ by specifying $\bar{\mathbf{v}}$ that consists of a set of independent components of generalized force vector.

Let $\mathcal{J} \subseteq \{1, \dots, 3m\}$ denote the set of indices of components of \mathbf{v} to be specified. $\bar{\mathbf{v}}$ is defined as the vector consisting of the component v_j ($\forall j \in \mathcal{J}$) of \mathbf{v} . By assembling the corresponding rows of \mathbf{G} to generate a submatrix $\bar{\mathbf{G}}$, the relation between $\bar{\mathbf{v}}$ and $\boldsymbol{\alpha}$ is written as

$$\bar{\mathbf{v}} = \bar{\mathbf{G}}\boldsymbol{\alpha} \quad (2.22)$$

If $\bar{\mathbf{G}} \in \mathfrak{R}^{h \times h}$ and is full-rank, Eq. (2.22) can be solved as

$$\boldsymbol{\alpha} = \bar{\mathbf{G}}^{-1}\bar{\mathbf{v}} \quad (2.23)$$

By substituting $\boldsymbol{\alpha}$ back to Eq. (2.21), the force vector \mathbf{v} of all members is obtained as

$$\mathbf{v} = \mathbf{G}\bar{\mathbf{G}}^{-1}\bar{\mathbf{v}} \quad (2.24)$$

Let $(\mathbf{G})_k$ denote the k th row vector of \mathbf{G} . $\Pi = \{\pi(l) | l = 1, 2, \dots, 3m\}$ denotes a permutation of $3m$ indices $1, 2, \dots, 3m$, where $\pi(l)$ stands for the location of index l in Π . The following algorithm generates \mathcal{J} and $\bar{\mathbf{G}}$, where the Reduced Row-Echelon Form (RREF) (Borse, 1997) summarized in Appendix is effectively used:

Algorithm 1:

Step 0 Let $\mathcal{J} = \emptyset$, feasible set $\mathcal{A} = \{1, 2, \dots, 3m\}$, $\Pi^0 = \{\pi^0(l) | l = 1, 2, \dots, 3m\}$, and $\pi^0(l) = l$ ($l = 1, \dots, 3m$). Set $i := 0$.

Step 1 If $i = h$, then $\bar{\mathbf{G}} := \hat{\mathbf{G}}$, and STOP. Otherwise, set $i \leftarrow i + 1$.

Step 2 Choose $j \in \mathcal{A}$. Update $\mathcal{J} := \mathcal{J} \cup j$. Define $\Pi^i = \{\pi^i(l) | l = 1, 2, \dots, 3m\}$ by

$$\pi^i(l) = \begin{cases} \pi^{i-1}(l) & (l < j), \\ 3m & (l = j), \\ \pi^{i-1}(l) - 1 & (l > j). \end{cases}$$

Step 3 Generate \mathbf{Q} by eliminating $(\mathbf{G})_k$ ($\forall k \in \mathcal{J}$) from \mathbf{G} . Let $\hat{\mathbf{G}}$ be the matrix consisting of $(\mathbf{G})_k$ ($\forall k \in \mathcal{J}$).

Step 4 Compute the RREF of the matrix $(\hat{\mathbf{G}}^\top, \mathbf{Q}^\top)$ in a form of

$$\mathbf{W} = \begin{pmatrix} \mathbf{I} & \mathbf{W}^U \\ \mathbf{O} & \mathbf{W}^L \end{pmatrix},$$

where $\mathbf{W}^U \in \mathfrak{R}^{i \times (3m-i)}$ and $\mathbf{W}^L \in \mathfrak{R}^{(h-i) \times (3m-i)}$.

Step 5 Update \mathcal{A} as

$$\mathcal{A} = \left\{ l \mid |(\mathbf{W}^L)_{\pi^i(l)}^\top \neq \mathbf{0} \quad (\pi^i(l) = 1, \dots, 3m-i) \right\}.$$

and go to Step 1.

2.4.2 Design of Nodal Coordinates

Knowing only the generalized force vector \mathbf{v} , we are still unable to determine configuration uniquely. Since \mathbf{v}_k for all members are known by using the procedure presented in Section 4.1, Eq. (2.11) is rewritten as

$$\text{diag}(\bar{\mathbf{T}}\mathbf{v}_k)\mathbf{d}_k - \text{diag}(\mathbf{v}_k)\bar{\mathbf{T}}\mathbf{d}_k = \mathbf{0} \quad (2.25)$$

Let $\mathbf{I} \in \mathfrak{R}^{m \times m}$ denote the identity matrix. By using $\mathbf{T} = \mathbf{I} \otimes \bar{\mathbf{T}}$, Eq. (2.25) is assembled through all members as

$$\text{diag}(\mathbf{T}\mathbf{v})\mathbf{d} - \text{diag}(\mathbf{v})\mathbf{T}\mathbf{d} = \mathbf{0} \quad (2.26)$$

where $\mathbf{d} = (\mathbf{d}_1, \dots, \mathbf{d}_m)^\top$.

Incorporating Eq. (2.12) into Eq. (2.26), the constraints on \mathbf{X} can be written in the following form:

$$\mathbf{F}\mathbf{X} = \mathbf{0} \quad (2.27)$$

where

$$\mathbf{F} = \text{diag}(\mathbf{T}\mathbf{v})\mathbf{B} - \text{diag}(\mathbf{v})\mathbf{T}\mathbf{B}$$

is a known matrix. Since the same axial forces should be assigned to the symmetrically located members, the symmetry conditions are included in Eq. (2.27).

Let $\gamma = 3n - \text{rank}(\mathbf{F})$ and suppose an underdetermined case $\gamma > 0$. The solution of Eq. (2.27) can be written as

$$\mathbf{X} = \mathbf{P}\boldsymbol{\beta} \quad (2.28)$$

where $\boldsymbol{\beta} \in \mathfrak{R}^\gamma$ is the coefficient vector and $\mathbf{P} \in \mathfrak{R}^{3n \times \gamma}$. The nodal coordinates are divided into unknown components $\mathbf{X}^c \in \mathfrak{R}^{3n_c}$ of the free nodes and specified components $\mathbf{X}^f \in \mathfrak{R}^{3n_f}$ of the fixed nodes (supports). The matrix \mathbf{P} is divided into \mathbf{P}^c and \mathbf{P}^f , accordingly. Hence Eq. (3.23) is rewritten as

$$\begin{pmatrix} \mathbf{X}^c \\ \mathbf{X}^f \end{pmatrix} = \begin{pmatrix} \mathbf{P}^c \\ \mathbf{P}^f \end{pmatrix} \boldsymbol{\beta} \quad (2.29)$$

Let $r_f = \text{rank}(\mathbf{P}^f)$. Select r_f independent rows from \mathbf{P}^f to obtain matrix $\bar{\mathbf{P}}$ utilizing RREF forms. The vector $\bar{\mathbf{X}}$ of independent nodal coordinates are selected from \mathbf{X}^f accordingly. If $r_f = \gamma$, we can calculate the coordinate vector \mathbf{X} directly by

$$\mathbf{X} = \mathbf{P}\bar{\mathbf{P}}^{-1}\bar{\mathbf{X}} \quad (2.30)$$

Otherwise, we are able to specify $(\gamma - r_f)$ nodal coordinates to obtain $\bar{\mathbf{X}}$ by using the same procedure described in Section 4.1 .

2.4.3 Stress States

For a tensegrity system, it is important to know whether each member is in tension or in compression. From Figs. 2.1 and 2.4, we can see that the direction of \mathbf{d}_k is same as that of the member force vector in tension. So the inner product g_k of \mathbf{d}_k and \mathbf{v}_k have the following properties

$$g_k = \mathbf{v}_k^\top \mathbf{d}_k \quad \begin{cases} > 0 & \text{tension} \\ < 0 & \text{compression} \\ = 0 & \text{member } k \text{ is removable} \end{cases} \quad (2.31)$$

For the case of $g_k = 0$, member k can be removed because

- a. If $\mathbf{v}_k = \mathbf{0}$, then there exists no force in member k , and its existence is unnecessary.
- b. If $\mathbf{d}_k = \mathbf{0}$, then nodes i and j coincide. So member k and node i or j can be removed.

2.4.4 Summary of Design Procedures

In Sections 4.1 and 4.2, we have presented the procedure and algorithm for designing a tensegrity system. In order to show how to design a tensegrity system systematically, we conclude the design procedure as follows:

Design procedure:

Step 1: Generate the self-equilibrium system by replacing the supports with the auxiliary fixed members.

Step 2: Give the topology, represented by the incidence matrix \mathbf{B} .

Step 3: Give the symmetry property by the matrix \mathbf{S} . Define the directions of some members, and coordinates of supports so as to define in \mathbf{D} and \mathbf{C} , respectively.

Step 4: Specify $\bar{\mathbf{v}}$ and obtain $\bar{\mathbf{G}}$ by using Algorithm 1. Compute \mathbf{v} from Eq. (2.24).

Step 5: Specify $\bar{\mathbf{X}}$ and obtain $\bar{\mathbf{P}}$ by using the algorithm described in Section 4.2. Compute \mathbf{X} from Eq. (3.24).

Step 6: Remove member k satisfying $\mathbf{v}_k^\top \mathbf{d}_k = 0$. Convert the auxiliary fixed members back to supports.

2.5 Numerical Examples

In this section, a simple two-dimensional prestressed tensegrity system is presented firstly to show how the auxiliary fixed members are used effectively. Diamond-shaped and prism-shaped tensegrity systems are then investigated to demonstrate the capability of the proposed method for generating various shapes.

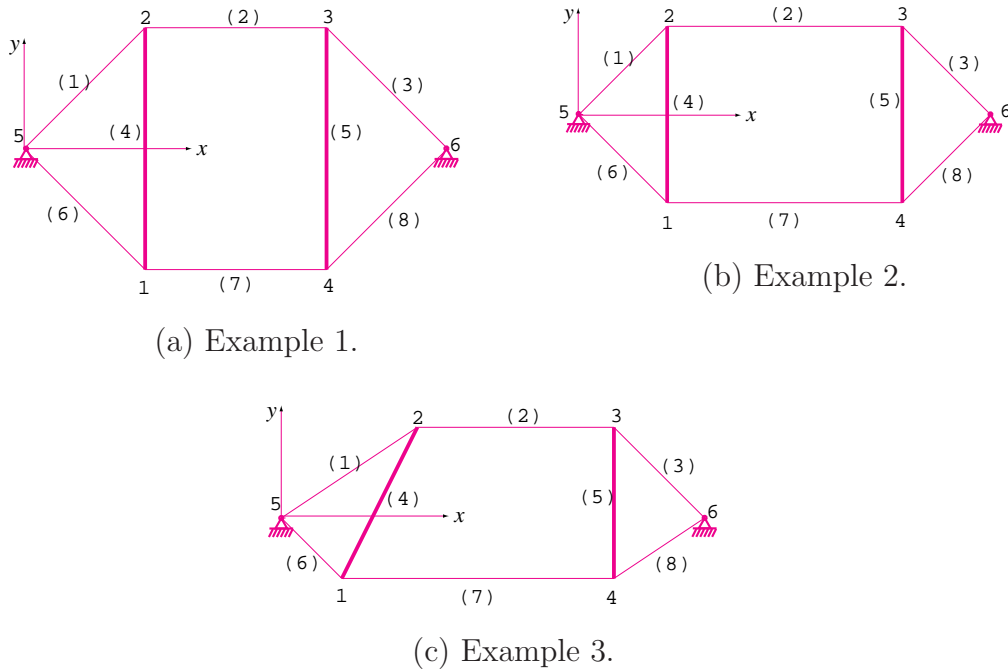


Figure 2.6: Two-dimensional tensegrity system.

2.5.1 Two-dimensional Prestressed Tensegrity System

The initial topology of a two-dimensional structure in this example is shown in Fig. 2.2. It may be reduced from a three-dimensional structure by using some of its geometrical characteristics; e.g. symmetry properties (Ohsaki and Kanno, 2003).

We have discussed in Section 2 that the supports can be converted into free nodes by using the concept of auxiliary fixed member, in order to obtain the desirable configuration. After implementation of form-finding using the method proposed in Section 4, the auxiliary fixed member may be removed to convert the two nodes connected by it back to be supports.

To illustrate the procedure of specifying the member directions, member 5 is assigned to be vertical. The nodal coordinates of the two supports are specified as (0,0) and (7,0). By connecting the two supports with auxiliary fixed member 9, the new topology of the structure is shown in Fig. 2.3. After defining the

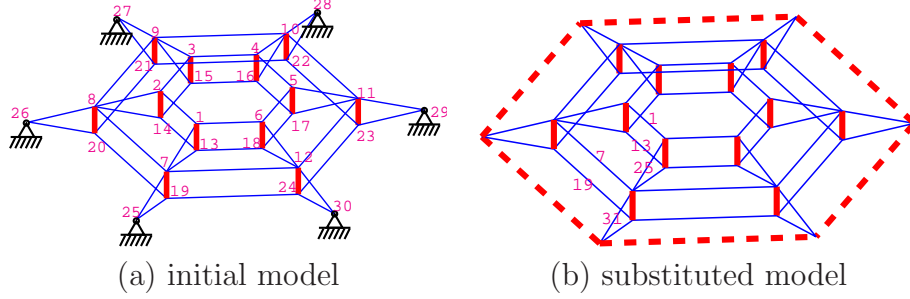


Figure 2.7: Perspective view of a three-dimensional prestressed tensegrity system.

directions of members 5 and 9, the rank of matrix \mathbf{H} has been computed to obtain $h = 6$; i.e. we are able to specify 6 axial force components.

As Example 1, if we specify $\bar{\mathbf{v}} = (\mathbf{v}_2, \mathbf{v}_4, v_5^y, v_6^x)^\top = ((1, 0), (0, -1), 1, -1)^\top$ consecutively based on Algorithm 1, the axial force components of all the members are obtained as $\mathbf{v} = ((-1, -1), (1, 0), (1, -1), (0, -1), (0, 1), (-1, 1), (1, 0), (1, 1), (-2, 0))^\top$.

The rank of matrix \mathbf{F} is computed to obtain $\gamma - r_f = 4 - 3 = 1$. So we can specify one nodal coordinate except those of the defined fixed nodes 5 and 6. If $X_1^x = 2$, the structure as shown in Fig. 2.6(a) is obtained, where the thick lines represent members in compression, the thin lines are in tension, and the auxiliary fixed member 9 has been removed. If $X_2^y = 1.5$ as Example 2, we will achieve the configuration in Fig. 2.6(b).

The direction of member 4 is not necessarily vertical. If we specify $\mathbf{v}_4 = (0.5, 1)^\top$ as Example 3, and specify other variables the same as in Example 2, the configuration as shown in Fig. 2.6(c) is obtained. This way, the directions of the struts can be easily controlled based on the designer's preference.

2.5.2 A three-dimensional prestressed tensegrity structure

The three-dimensional prestressed tensegrity structure shown in Fig. 4.13(a) consists of 24 free nodes, 8 fixed nodes and 60 members. The fixed nodes are located on a circle with radius of 15. In order to make use of the proposed approach, auxiliary fixed members, which are shown as dashed lines in Fig. 4.13(b), are

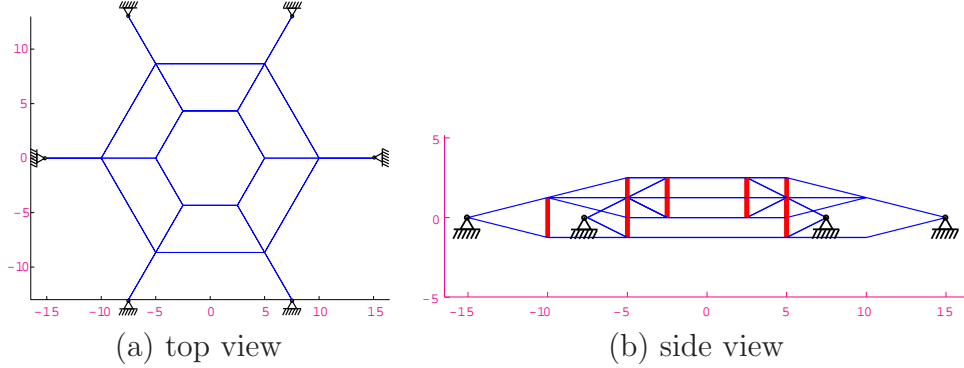


Figure 2.8: Example 1 of a three-dimensional prestressed tensegrity system.

utilized to transform the structure into a selfstressing structure. Therefore, there are 66 members for the substituted model.

Without introducing any geometrical and mechanical constraints to the structure, there are totally $(h=)99$ independent components of axial forces that can be specified arbitrarily, which may be thought as a burden rather than benefit for specifying such a large number of axial forces. According to locations and rotational distribution of the cables, we can separate them into 8 groups, six cables a group, and specify rotationally symmetric around z -axis by $\pi/3$ for the cables of each group. This way, there are only $(h=)14$ independent components of axial forces need to be specified.

As in Example 1, we specify the 14 independent axial forces as $\bar{\mathbf{v}}^\top = (\mathbf{v}_1, \mathbf{v}_7, v_{13}^x, v_{13}^y, v_{19}^x, \mathbf{v}_{25}, \mathbf{v}_{31}) = ((-1, 1.7321, 0), (-1, 1.7321, 0), -1, 1.7321, -3, (-1, -1.7321, -0.5), (-3, -5.1963, -1.5))$, where the numbers of the specified members are shown in Fig. 4.13(b), and then obtain the number of nodal coordinates that can be specified arbitrarily as $\gamma - r_f = 2$. If we specify the independent x -coordinates of nodes 2 and 8 as -5 and -10 , respectively, we can obtain the configuration of the structure as shown in Fig. 4.13(a) and Fig. 2.8, where the auxiliary fixed members have been removed.

If we change the values of v_{31}^x and v_{31}^y in Example 1 to -2 and 3.4642 , respectively, for Example 2 without changing the values of other parameters, we can achieve the configuration as shown in Fig. 2.9.

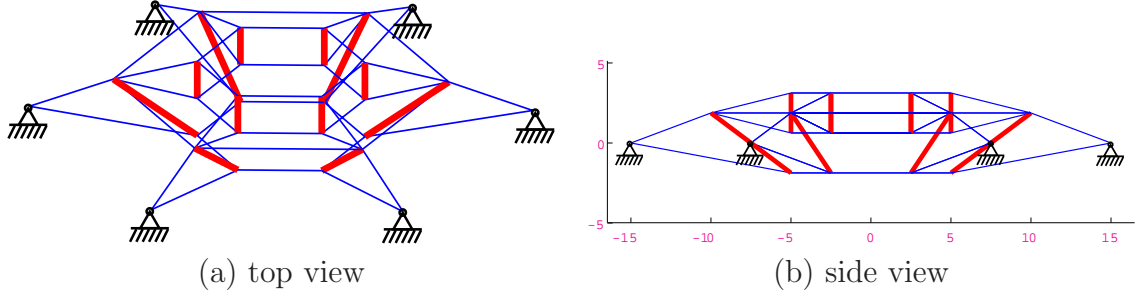


Figure 2.9: Example 1 of a three-dimensional prestressed tensegrity system.

2.5.3 Diamond-shaped Tensegrity

Consider a tensegrity system that consists of 6 nodes and 13 members as shown in Fig. 2.10. The configurations are found for the following six cases:

Consider firstly Example 1 without any explicit geometrical constraint. The rank of matrix \mathbf{H} has been computed to find $h = 22$; i.e. there are 22 axial force components needed to be specified. By using the algorithm presented in section 4.1, we specify the forces in members 5, 6, 7 and 8 as shown in *variables* in Table 2.1. The feasible set obtained by using the RREF form is $(\mathbf{v}_1, \mathbf{v}_2, \mathbf{v}_3, \mathbf{v}_4, \mathbf{v}_9, \mathbf{v}_{10}, \mathbf{v}_{11}, \mathbf{v}_{12}, v_{13}^z)$. The axial forces $(\mathbf{v}_1, \mathbf{v}_2, \mathbf{v}_9, v_{10}^z)$ have been selected from the feasible set consecutively by using Algorithm 1 as shown in *variables* in Table 2.1. Then the results computed by Eq. (2.24) are as shown in *results*.

The rank of matrix \mathbf{F} has been computed to find $\gamma = 4$; i.e. there exist 4 nodal coordinates needed to be specified. The specified 4 nodal coordinates and the results using the similar method for specifying force components are shown in Table 2.2. The obtained configuration is as shown in Fig. 2.10. Note that the locations and force vectors of members 1–4 have been obtained to be rotationally symmetric around z -axis by $\pi/2$, although only the force vectors of members 1 and 2 have been specified.

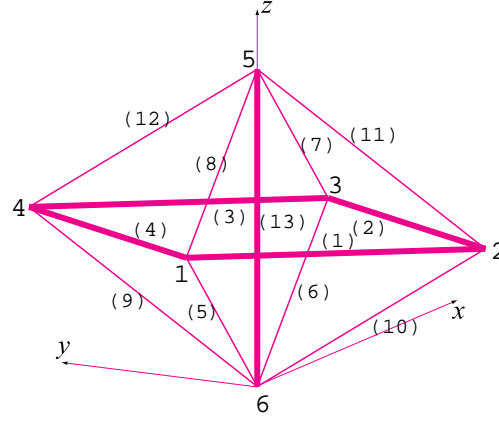


Figure 2.10: Example 1 of diamond-shaped tensegrity

Table 2.1: Axial forces of Example 1.

	Variables v_k								Results v_k					
k	1	2	5	6	7	8	9	10	3	4	10	11	12	13
x	1	1	-1	1	1	-1	0		-1	1	0	0	0	0
y	-1	1	0	0	0	0	1		1	1	-1	-1	1	0
z	0	0	1	1	-1	-1	1	1	0	0		-1	-1	-4

If we specify $v_{10}^z = 3$, which is different from $v_{10}^z = 1$ in the previous example, then all nodes will be degenerated into one node with only three nodal coordinates that can be specified; i.e. $\gamma = 3$. It means that we cannot obtain the desirable configuration although the generalized force vector \mathbf{v} satisfies the equilibrium conditions and all geometrical constraints.

In the following examples of the diamond-shaped tensegrity system, we will

Table 2.2: Nodal coordinate of Example 1.

	Variables X_i		Results X_i				
i	5	6	1	2	3	4	5
x		0	-2	0	2	0	0
y		0	0	-2	0	2	0
z	4	0	2	2	2	2	

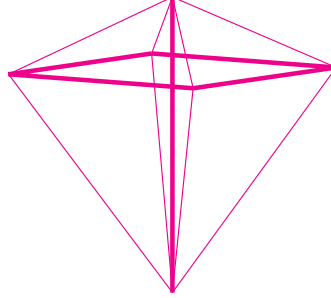


Figure 2.11: Example 2 of diamond-shaped tensegrity.

Table 2.3: Axial forces of Example 2.

	Variables v_k					Results v_k								
k	1	5	6	9	10	2	3	4	7	8	10	11	12	13
x	2	-1	1	0		2	-2	2	3	-3	0	0	0	0
y	-2	0	0	1		2	2	2	0	0	-1	-3	3	0
z	0	1	1	1	1	0	0	0	-1	-1		-1	-1	-4

show how to search new configuration practically by changing the values of some variables to be specified. To reduce the number of independent variables or to assign geometrical characteristics, we introduce some explicit geometrical constraints such that members 1–4 are symmetrically located around z -axis by $\pi/2$, and member 13 is chosen as a fixed member; i.e. the nodal coordinates of nodes 5 and 6 are given as $(0, 0, 4)$ and $(0, 0, 0)$, respectively. In this case, we have only 13 axial forces to specify; i.e. $h = 13$, and no nodal coordinate can be given because $r_f = \gamma = 4$.

Consider Example 2 with the symmetric geometrical constraints as described above. In this example, we specify $(\mathbf{v}_1)_{e2} = 2(\mathbf{v}_1)_{e1}$, where $(\mathbf{v}_1)_{ei}$ denote the axial force vector of member 1 in Example i . The axial forces of members 5, 6, 9 and 10 are same as those in Example 1. The specified variables and computed results of axial forces are as shown in Table 2.3. The results of nodal coordinates are listed in Table 2.4.

We can see from Fig. 2.11 that the compressive element consisting of symmetrically arranged members 1–4 is located at a higher place than in Example 1,

Table 2.4: Nodal coordinates of Example 2.

i	Variables X_i		Results X_i			
	5	6	1	2	3	4
x	0	0	-3	0	3	0
y	0	0	0	-3	0	3
z	4	0	3	3	3	3

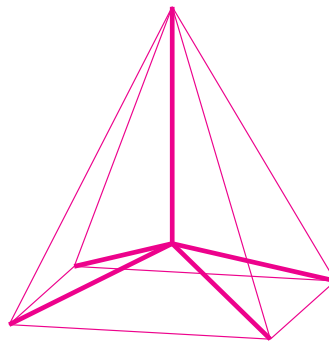


Figure 2.12: Example 3 of diamond-shaped tensegrity.

because larger values have been given for the axial force of member 1.

If we let $(\mathbf{v}_1)_{e3} = 0.2(\mathbf{v}_1)_{e2}$ and the other variables of axial forces remain the same as those in Example 2, then we obtain a new configuration as shown in Fig. 2.12 for Example 3. It may be interesting to see what happens if we reverse the sign of the specified variables of axial forces. Figs. 2.13(a)–(c) show the results for Examples 1'–3' that have axial forces reversed from Examples 1–3, respectively. We can see that the configurations of Examples 1, 2, 3 and 1', 2', 3', respectively, are exactly the same except the sign of the stress states of the members.

If we define the symmetry property such that the members 7, 8, 11 and 12 are symmetrically located with members 6, 5, 10 and 9, respectively, as shown in Fig. 2.10, instead of rotational symmetry, then there exist only 7 components of the generalized force vector to be specified.

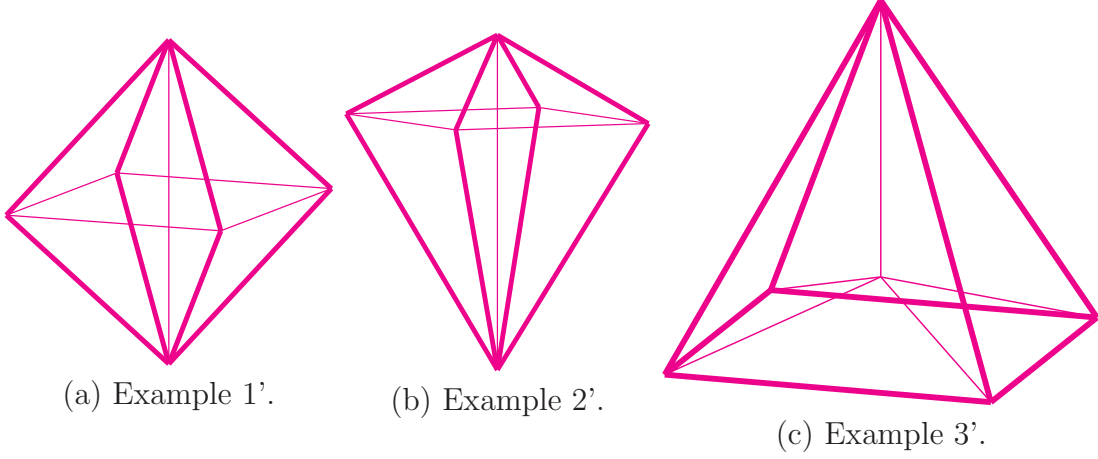


Figure 2.13: Examples 1'-3' of diamond-shaped tensegrity.

2.5.4 Prism-shaped Tensegrity

Consider a prism-shaped structure consisting of 6 nodes and 12 members as shown in Fig. 2.14. Member sets $\{1, 2, 3\}$, $\{7, 8, 9\}$ and $\{10, 11, 12\}$ are arranged, respectively, in rotationally symmetric locations. The rank of \mathbf{H} has been computed to find that there are 7 axial force components to be specified.

If we specify $(v_1^x, v_1^y, v_1^z, v_4^z, v_9^x, v_9^y, v_9^z)$ consecutively to be $(0.866, -0.5, 0, 1, 1, 0, 0)$ for $\bar{\mathbf{v}}^\top$ by using Algorithm 1 as Example 1, then we know that we can specify 4 nodal coordinates by computing the rank of \mathbf{F} . By specifying (x_1, y_1, z_1, x_2) to be $(0, 0, 0, 4)$ for $\bar{\mathbf{X}}^\top$, we obtain a configuration as shown in Fig. 2.14.

Let $v_9^y=2$ and $v_9^y=0.5$ for Examples 2 and 3, respectively, which are equal to twice and half of the value in Example 1. The configurations for Examples 2 and 3 are obtained as shown in Fig. 2.15 and Fig. 2.16, respectively, where the sizes of the top and bottom triangles are different.

In Examples 1'-3', we reverse the sign of $\bar{\mathbf{v}}$ in Example 1-3 to $-\bar{\mathbf{v}}$, respectively. Then we obtain the configurations in which the stress states of all members are reversed as shown in Fig. 2.17.

2.5.5 Evaluation of Design Errors

To investigate the accuracy of the calculation results of axial forces and nodal coordinates, equilibrium equations Eq. (2.20) and Eq. (2.27) in terms of general-

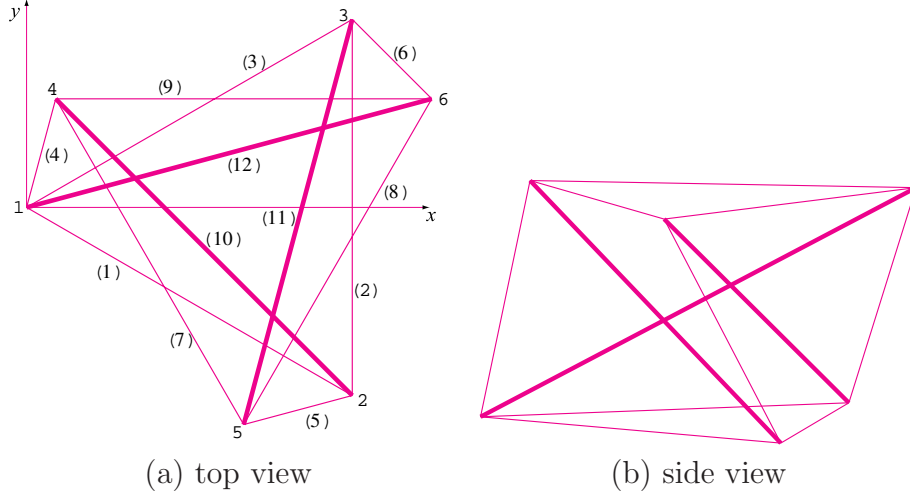


Figure 2.14: Example 1 of rotationally symmetric prism-shaped tensegrity

ized force vector and nodal coordinate vector are used to formulate the errors e_f and e_c , respectively, as

$$e_f = \sqrt{(\mathbf{H}\mathbf{v})^\top \mathbf{H}\mathbf{v}/(3m)} \quad (2.32)$$

$$e_c = \sqrt{(\mathbf{F}\mathbf{X})^\top \mathbf{F}\mathbf{X}/(3n)} \quad (2.33)$$

For each example given in Section 5, the design errors of forces and nodal coordinates by Eq. (2.32) and Eq. (2.33) are within 10^{-15} and 10^{-14} , respectively, by using Eq. (2.32) and Eq. (2.33), which illustrates the accuracy of the proposed method.

2.6 Discussions and Conclusions

A general method has been presented for direct design of member directions, force vectors and nodal locations of tensegrity systems with given topology, which is defined as a directed graph. The system of equilibrium equations is written in terms of the components of the member force vectors by using the incidence matrix.

The directions of members and symmetry properties are first assigned as the geometrical constraints, and the member force vectors are computed from the

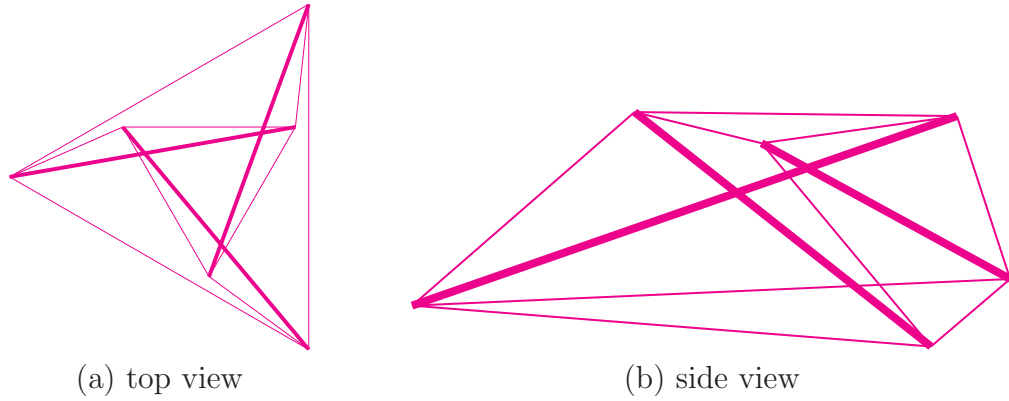


Figure 2.15: Example 2 of rotationally symmetric prism-shaped tensegrity with $v_9^y = 2$

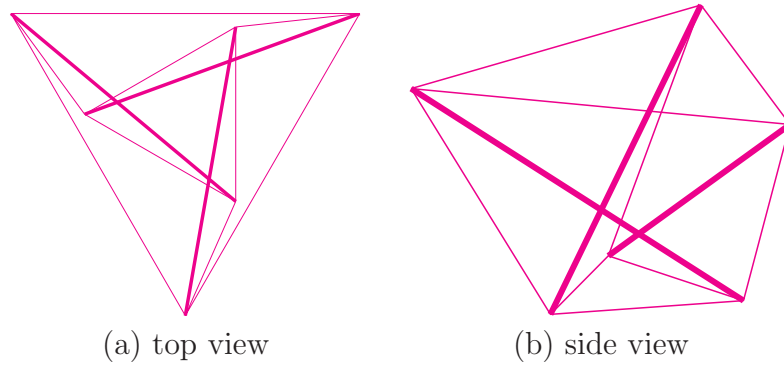


Figure 2.16: Example 3 of rotationally symmetric prism-shaped tensegrity with $v_9^y = 0.5$

constrained equilibrium equations. The locations of some nodes including the supports are then assigned to obtain the locations of all nodes. A concept of auxiliary (fixed) members is introduced to present a unified approach for tensegrity systems with or without supports.

The solution obtained by this method satisfies the equilibrium conditions and the geometrical constraints exactly. By using the proposed method, the designers can directly control the axial forces and the configuration simultaneously, which is considered a major advantage of the method. A new configuration can also be obtained by changing the forces and geometrical constraints.

The proposed method is very efficient because only linear equations need to be

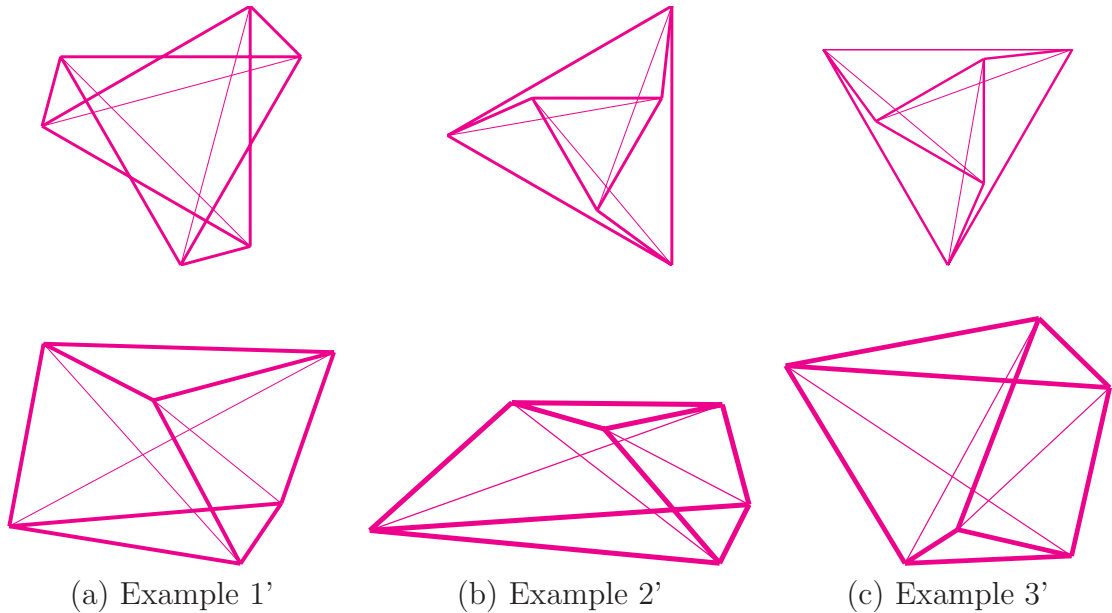


Figure 2.17: Prism-shaped tensegrities with reversed stress states

solved. A general algorithm has been presented to find the independent variables consecutively.

The effectiveness of the proposed method can be summarized as follows:

- a. The directions of some members can be specified directly based on the designer's preference.
- b. The numbers of components of the generalized force vector and the nodal coordinate vector that can be specified can be systematically obtained.
- c. The equilibrium conditions in large-deformation range can be formulated as a set of linear equations in terms of generalized force vector.
- d. The method presents a general procedure for checking the existence of solution to a form-finding problem.

Unfortunately, it is not an easy task to specify the members to be in tension or compression because the equilibrium shape is not known a priori.

In the case where the number of independent variables that should be specified is large, the geometrical constraints including the symmetry properties should be

2.6 Discussions and Conclusions

extensively used. In some cases, the obtained configuration may not be feasible, which means that some nodes may contact and some members may intersect with each other. For these cases, the variables to be specified should be gradually varied from a feasible solution. Introducing more geometrical constraints may be another way to prevent infeasible solutions.

Chapter 3

Adaptive Force Density Method

In this chapter, a new method, which is extended from force density method and based on singular value composition, is proposed for the form-finding problem of tensegrity structures. Since the initial given values of force densities can be adjusted to satisfy the requirement on rank deficiency of the equilibrium matrix, the method is called *adaptive force density method*. A few numerical examples are given to illustrate its powerful ability of searching new geometrical configurations of tensegrity structures with given topology, and the easiness for use.

3.1 Introduction & Outline

In Chapter 2, we have proposed a direct approach to let designers be able to specify some geometrical characteristics of configuration desired by architects, such as directions, locations of members and/or locations of supports, and some mechanical properties in terms of member forces, which are desired by structural engineers.

However, as have been pointed out, when the structure is relative complicated, e.g. a structure with a large number of members and highly underdetermined, the number of axial forces that can be (or have to be in another word) specified will come to be much more than designers' willing, which may turn out to be an additional burden than benefit. Introducing more geometrical constraints to the problem or solving it as an optimization problem by setting some expected initial values may be a promise way (details of this method can be found in the

graduation thesis of J. Kimura at Kyoto University). But it is still not a very easy task, especially when the designers have no much experience. On the other hand, the stress states of the members, either tensile or compressive, cannot be specified easily without advanced knowledge of the structure.

Force density method extended to the problem of tensegrity structures from tensile structure is a very promised one, in which only linear equations need to be solved and the stress states can be easily specified. A multi-parameter analyzing technique developed by [Vassart and Motro \(1999\)](#), based on force density method, is found to be particularly suitable to find new tensegrity structures that meet a set of given general requirements, although with some drawbacks which will be discussed in the follows.

The outline of this chapter following this introduction is summarized as follows. Section 2 introduces the initial idea and formulation of force density method originated for the form-finding problems in the field of tensile structures and then its extension to tensegrity structures. Section 3 gives out idea of the proposed adaptive force density method based on singular value decomposition of the equilibrium matrix in terms of nodal coordinates. And the design procedure using the proposed approach is summarized in Section 4. Section 5 discusses the prestressability and stability conditions for general tensegrity structures. Some numerical examples are given in Section 6 to illustrate the efficiency and ability of searching new configurations of the proposed method. Section 7 concludes this chapter and give some discussions based on the numerical experiments.

3.2 Force Density Method

The force density method, originated from the form-finding problem for cable structures by [Schek \(1974\)](#), uses a mathematical trick to transform the non-linear equilibrium equations of the free nodes into a set of linear equations, by prescribing a force density coefficient, a force-to length ration called *force density* in the paper, for each cable element. Based on this idea, [Maurin and Motro \(1998\)](#) developed it for membrane structures by cable net approximations, in which the continuum membrane material is substituted by virtual cables.

3.3 Force Density Method

The form-finding problem of tensegrity structures is very similar to that of cable nets, since they use almost the same assumptions described as follows except (d) and (e), which are adopted only for tensegrity structures:

- a. Members are connected by pin joints.
- b. Topology of the structure is known.
- c. No external load is applied and self-weight is neglected.
- d. Buckling of the struts is not considered.
- e. The structure is free-standing, without any support.

From these assumptions, we may know that (1) geometrical configuration of the structure can be described in terms of nodal coordinates; (2) members of the structure transmit only axial forces, either in compression or in tension; and (3) the structure is in a self-equilibrium state.

The force density method was originally developed for the form-finding problem of cable nets by [Schek \(1974\)](#). It uses a mathematical technique to transform the nonlinear equilibrium equations of free nodes into a set of linear equations by prescribing a force s_k to length l_k ratio $q_k = s_k/l_k$, called *force density*, for cable member k where $q_k > 0$. The formulation of equilibrium analysis of cable nets can be easily applied to the form-finding problem of tensegrity structures, since they use almost the same assumptions. However, some complications may arise because tensegrity structures are free-standing and there exists a strut with $q_k < 0$.

3.3.1 Formulation of Equilibrium Matrix with respect to Nodal Coordinates

We start with basic formulations of the force density method for cable nets. A typical cable net is attached to supports, called fixed nodes in the study since they cannot have any displacement. It maintains an equilibrium state and stiffness

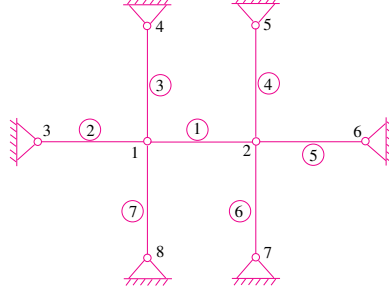


Figure 3.1: A two-dimensional cable net.

against external loads by the introduction of prestress. E.g., the two-dimensional cable net as shown in Fig. 3.1 has two free nodes 1 and 2, of which displacements are not constrained, and is attached to fixed nodes 3–8. The structural elements connected by nodes are called *members*.

For a structure with m members, n free nodes and n^f fixed nodes, its topology can be described by an incidence matrix $\mathbf{C}^s \in \mathfrak{R}^{m \times (n+n^f)}$ (Harary, 1969). If member k connects nodes i and j ($i < j$), then the i th and j th elements of the k th row of \mathbf{C}^s are set to 1 and -1 , respectively, as

$$\mathbf{C}_{(k,p)}^s = \begin{cases} 1 & p = i \\ -1 & p = j \\ 0 & \text{for other cases} \end{cases} \quad (3.1)$$

It is recommended that the fixed nodes are preceded by the free nodes in the numbering sequence for convenience, so that \mathbf{C}^s can be partitioned into two parts as

$$\mathbf{C}^s = (\mathbf{C}, \mathbf{C}^f) \quad (3.2)$$

where $\mathbf{C} \in \mathfrak{R}^{m \times n}$ and $\mathbf{C}^f \in \mathfrak{R}^{m \times n^f}$ describe the topologies of free and fixed nodes, respectively.

Let $\mathbf{x}, \mathbf{y}, \mathbf{z} (\in \mathfrak{R}^n)$ and $\mathbf{x}^f, \mathbf{y}^f, \mathbf{z}^f (\in \mathfrak{R}^{n^f})$ denote the nodal coordinate vectors of free and fixed nodes in x -, y - and z - directions, respectively. By denoting the force density vector $\mathbf{q} = (q_1, q_2, \dots, q_m)^\top \in \mathfrak{R}^m$, the equilibrium equations of

free nodes in each direction can be written as follows (Schek, 1974):

$$\begin{aligned}
 \mathbf{C}^\top \mathbf{Q} \mathbf{C} \mathbf{x} + \mathbf{C}^\top \mathbf{Q} \mathbf{C}^f \mathbf{x}^f &= \mathbf{p}^x \\
 \mathbf{C}^\top \mathbf{Q} \mathbf{C} \mathbf{y} + \mathbf{C}^\top \mathbf{Q} \mathbf{C}^f \mathbf{y}^f &= \mathbf{p}^y \\
 \mathbf{C}^\top \mathbf{Q} \mathbf{C} \mathbf{z} + \mathbf{C}^\top \mathbf{Q} \mathbf{C}^f \mathbf{z}^f &= \mathbf{p}^z
 \end{aligned} \tag{3.3}$$

where \mathbf{p}^x , \mathbf{p}^y and \mathbf{p}^z ($\in \mathfrak{R}^n$) denote the vectors of external loads applied at free nodes in x -, y - and z - directions, respectively, and force density matrix $\mathbf{Q} \in \mathfrak{R}^{m \times m}$ is calculated by

$$\mathbf{Q} = \text{diag}(\mathbf{q}) \tag{3.4}$$

For simplicity, let

$$\begin{aligned}
 \mathbf{E} &= \mathbf{C}^\top \mathbf{Q} \mathbf{C} \\
 \mathbf{E}^f &= \mathbf{C}^\top \mathbf{Q} \mathbf{C}^f
 \end{aligned} \tag{3.5}$$

It is obvious that $\mathbf{E} \in \mathfrak{R}^{n \times n}$ and $\mathbf{E}^f \in \mathfrak{R}^{n \times n^f}$ are constant when the force density matrix \mathbf{Q} is given. Therefore, the equilibrium equations without consideration of external loads can be rewritten as

$$\begin{aligned}
 \mathbf{E} \mathbf{x} &= -\mathbf{E}^f \mathbf{x}^f \\
 \mathbf{E} \mathbf{y} &= -\mathbf{E}^f \mathbf{y}^f \\
 \mathbf{E} \mathbf{z} &= -\mathbf{E}^f \mathbf{z}^f
 \end{aligned} \tag{3.6}$$

which are *linear* for determination of coordinates \mathbf{x} , \mathbf{y} and \mathbf{z} of free nodes while the coordinates of fixed nodes have given. Since \mathbf{E} represents the equilibrium of free nodes, it is called *equilibrium matrix* in this study. Instead of using \mathbf{C} and \mathbf{Q} as in Eq. (3.5), the equilibrium matrix \mathbf{E} can be written directly (Vassart and Motro, 1999). Let \mathcal{J} and p denote the set of members connected to free node i and the member connected to free nodes i and j , respectively. The (i, j) component $\mathbf{E}_{(i,j)}$ of \mathbf{E} is given as

$$\mathbf{E}_{(i,j)} = \begin{cases} \sum_{k \in \mathcal{J}} q_k & \text{if } i = j \\ -q_p & \text{if } i \neq j \\ 0 & \text{for other cases} \end{cases} \tag{3.7}$$

E.g., for a two-dimensional cable net as shown in Fig. 3.1, \mathbf{E} can be written directly by using Eq. (3.7) as

$$\mathbf{E} = \begin{pmatrix} q_1 + q_2 + q_3 + q_7 & -q_1 \\ -q_1 & q_1 + q_4 + q_5 + q_6 \end{pmatrix}$$

where $\mathbf{E} \in \mathfrak{R}^{n \times n}$ is always square and symmetric, and moreover, *positive definite* if all members are in tension, i.e. $q_k > 0$, without isolated free nodes. Therefore, \mathbf{E} is invertible, and the coordinates of free nodes can be uniquely determined by solving the linear equations in Eq. (3.6), which is the original idea of force density method for the form-finding problem of cable nets.

3.3.2 Force Density Method for Tensegrity Structures

A similar formulation to the force density method for cable nets can be easily applied to the form-finding problem of tensegrity structures, since they use almost the same assumptions. However, unlike the equilibrium matrix \mathbf{E} for a cable net attached to fixed nodes (supports), which is always positive definite as pointed out previously, \mathbf{E} has rank deficiency for a tensegrity structure because it is free-standing and has compressive members, i.e. $q_k < 0$. Therefore \mathbf{E} is not invertible.

For a tensegrity structure with no fixed node as well as no external load and self-weight, Eq. (3.6) becomes

$$\begin{aligned} \mathbf{E}\mathbf{x} &= \mathbf{0} \\ \mathbf{E}\mathbf{y} &= \mathbf{0} \\ \mathbf{E}\mathbf{z} &= \mathbf{0} \end{aligned} \tag{3.8}$$

For a two-dimensional tensegrity structure as shown in Fig. 3.2, where the thick solid lines denote struts and the thin ones denote cables, \mathbf{E} can be written as follows by using Eq. (3.7):

$$\mathbf{E} = \begin{pmatrix} q_1 + q_2 + q_3 + q_4 & -q_1 & -q_2 & -q_3 & -q_4 \\ -q_1 & q_1 + q_5 + q_7 & 0 & -q_5 & -q_7 \\ -q_2 & 0 & q_2 + q_6 + q_8 & -q_6 & -q_8 \\ -q_3 & -q_5 & -q_6 & q_3 + q_5 + q_6 & 0 \\ -q_4 & -q_7 & -q_8 & 0 & q_4 + q_7 + q_8 \end{pmatrix}$$

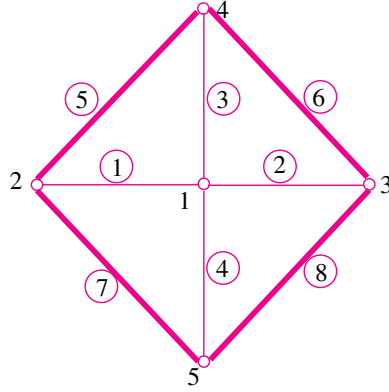


Figure 3.2: A two dimensional tensegrity structure.

It can be concluded that \mathbf{E} of a tensegrity structure is always square, symmetric and *singular*, with rank deficiency of at least 1 since sum of the rows or columns is always equal to zero. This is because the structure is free-standing, therefore, may have rigid body displacements. Moreover, with the existence of both positive and negative values of force densities for cables and struts, respectively, the rank deficiency of \mathbf{E} maybe larger if the force densities satisfy some specific conditions.

Since \mathbf{E} is singular, geometrical configuration of the structure, which is described in terms of nodal coordinates \mathbf{x} , \mathbf{y} and \mathbf{z} , cannot be uniquely determined. Define rank deficiency h of \mathbf{E} as

$$h = n - \text{rank}(\mathbf{E}) \quad (3.9)$$

Therefore, there are up to h independent components of \mathbf{x} , \mathbf{y} and \mathbf{z} , respectively, that can be specified arbitrarily.

It can be easily observed that a line can be determined by two points, a plane by three points and a three-dimensional object by four points. Therefore, in order to achieve a non-degenerate d -dimensional ($d=2$ or 3) tensegrity structure, which can be neither translated nor rotated, rank deficiency of \mathbf{E} has to satisfy $h = h^* = d + 1$. Hence, the problem of finding feasible shape for a tensegrity structure turns out to be that of finding a set of force densities corresponding to $h = h^*$.

Vassart and Motro (1999) presented three practical techniques for finding a feasible set of force densities to achieve the required rank deficiency: (1) intuitive, (2) iterative, and (3) analytical.

Among these three techniques, the first is suitable for structures with only a few members. The second technique is based on trial-and-error experiments, or more refined search for a set of force densities that yield the required deficiency step by step. The third technique is thought to be the most effective in these methods: the equilibrium matrix \mathbf{E} is analyzed based on Gaussian elimination in symbolic form to find the relationship of force densities, which has to be satisfied for achieving the required rank deficiency of \mathbf{E} .

3.4 Adaptive Force Density Method

The analytical approach mentioned above is not effective enough in view of simplicity since the force densities are analyzed in symbolic form. It will not be a easy task to apply this approach to relatively complicated structures, such as structures with many members. This motivates us to propose a new numerical method to achieve the required rank deficiency of \mathbf{E} with less human efforts, based on *singular value decomposition*. The proposed method is called *adaptive force density method* since it adjusts the values of force densities to adapt to the requirement on rank deficiency.

3.4.1 Formulation of Force Density Vector

Let \mathcal{J} and p denote the set of members connected to node i and the member connected to nodes i and j , respectively. From the direct definition of \mathbf{E} in Eq. (3.7), the i th column \mathbf{E}_i of \mathbf{E} can be written in terms of force density vector \mathbf{q} by a matrix $\mathbf{B}^i \in \mathfrak{R}^{n \times m}$ as

$$\mathbf{B}^i \mathbf{q} = \mathbf{E}_i \tag{3.10}$$

where (j, k) ($k \in \{1, 2, \dots, m\}$) component $\mathbf{B}_{(j,k)}^i$ of \mathbf{B}^i is defined as

$$\mathbf{B}_{(j,k)}^i = \begin{cases} 1 & \text{if } i = j \text{ and } k \in \mathcal{J} \\ -1 & \text{if } i \neq j \text{ and } k = p \\ 0 & \text{for other cases} \end{cases} \tag{3.11}$$

For the tensegrity structure shown in Fig. 3.2, e.g., the matrix \mathbf{B}^1 for the formulation of the first column \mathbf{E}_1 of \mathbf{E} can be written as

$$\mathbf{B}^1 = \begin{pmatrix} 1 & 1 & 1 & 1 & 0 & 0 & 0 & 0 \\ -1 & 0 & 0 & 0 & 0 & 0 & 0 & 0 \\ 0 & -1 & 0 & 0 & 0 & 0 & 0 & 0 \\ 0 & 0 & -1 & 0 & 0 & 0 & 0 & 0 \\ 0 & 0 & 0 & -1 & 0 & 0 & 0 & 0 \end{pmatrix}$$

By letting $\mathbf{B}^\top = (\mathbf{B}^{1\top}, \dots, \mathbf{B}^{i\top}, \dots, \mathbf{B}^{n\top})$ and $\mathbf{g}^\top = (\mathbf{E}_1^\top, \dots, \mathbf{E}_i^\top, \dots, \mathbf{E}_n^\top)$, \mathbf{q} can be expressed as

$$\mathbf{B}\mathbf{q} = \mathbf{g} \tag{3.12}$$

From the definition of \mathbf{B} , we can see that there must exist a row of which the k th ($\forall k \in \{1, 2, \dots, m\}$) element is -1 while the others are zero, so \mathbf{B} is a full-rank matrix.

Linear constraints on some specific force densities, e.g. relation between two values, and direct assignment of the force density, can be formulated as

$$\mathbf{B}^e \mathbf{q} = \mathbf{q}^e \tag{3.13}$$

where \mathbf{B}^e and \mathbf{q}^e denote the constraint matrix and the vector containing expected values, respectively. By letting $\bar{\mathbf{B}}^\top = (\mathbf{B}^\top, \mathbf{B}^{e\top})$ and $\bar{\mathbf{g}}^\top = (\mathbf{g}^\top, \mathbf{q}^{e\top})$, we obtain

$$\bar{\mathbf{B}}\mathbf{q} = \bar{\mathbf{g}} \tag{3.14}$$

where $\bar{\mathbf{B}}$ is constant and full-rank, and $\bar{\mathbf{g}}$ comes directly from \mathbf{E} and specified linear constraints on force densities. Since $\bar{\mathbf{B}}$ is full-rank, the least square solution of \mathbf{q} can be calculated by (Borse, 1997)

$$\mathbf{q} = \bar{\mathbf{B}}^- \bar{\mathbf{g}} \tag{3.15}$$

where $\bar{\mathbf{B}}^-$ denotes the generalized inverse matrix of $\bar{\mathbf{B}}$.

3.4.2 Singular Value Decomposition

Singular value decomposition (SVD) is a very powerful technique which can deal with a set of linear equations or matrices that are either singular or numerically very close to singular (Lay, 1996). By implementation of SVD, $\mathbf{E} \in \mathfrak{R}^{n \times n}$ can be written as the product of a column-orthogonal matrix $\mathbf{U} \in \mathfrak{R}^{n \times n}$, a diagonal matrix $\mathbf{\Lambda} \in \mathfrak{R}^{n \times n}$ with nonnegative elements, and the transpose of a column-orthogonal matrix $\mathbf{V} \in \mathfrak{R}^{n \times n}$:

$$\mathbf{E} = \mathbf{U}\mathbf{\Lambda}\mathbf{V}^\top \quad (3.16)$$

where

$$\begin{aligned} \mathbf{U}^\top \mathbf{U} &= \mathbf{I} \\ \mathbf{V}^\top \mathbf{V} &= \mathbf{I} \end{aligned} \quad (3.17)$$

and $\mathbf{I} \in \mathfrak{R}^{n \times n}$ denotes the identity matrix.

The diagonal elements of $\mathbf{\Lambda}$ are called *singular values*. If the rank of \mathbf{E} is r , then it has r positive and $n - r$ additional zero singular values. The positive singular values, $\lambda_1, \lambda_2, \dots, \lambda_r$, are numbered in non-increasing order as

$$\lambda_1 \geq \lambda_2 \geq \dots \geq \lambda_r > 0 \quad (3.18)$$

Since setting the smallest positive singular value of \mathbf{E} to zero may lead to minimal modification of it, we set the last smallest h^* singular values of \mathbf{E} to zero to make it have the required rank deficiency:

$$\lambda_{n-h^*+1} = \lambda_{n-h^*+2} = \dots = \lambda_n = 0 \quad (3.19)$$

Therefore, the updated version $\bar{\mathbf{\Lambda}}$, obtained by these new singular values, of $\mathbf{\Lambda}$ has rank deficiency h^* . The updated version $\bar{\mathbf{E}}$ of the equilibrium matrix can then be derived by

$$\bar{\mathbf{E}} = \mathbf{U}\bar{\mathbf{\Lambda}}\mathbf{V}^\top \quad (3.20)$$

3.4.3 Form-finding Process

By applying singular value decomposition to the equilibrium matrix \mathbf{E} and setting its smallest h^* singular values to zero so as to obtain $\bar{\mathbf{E}}$ from Eq. (3.20), *adaptive force density method* is presented first to obtain a feasible set of force densities. An independent set of nodal coordinates is then specified to determine a unique geometrical configuration of the structure.

3.4.3.1 Feasible Force Densities

By using Eqs. 3.19 and 3.20, we can easily obtain $\bar{\mathbf{E}}$, which has the required rank deficiency, from an initial \mathbf{E} calculated by the given force densities. A new set of force densities is then achieved by Eq. (3.15) with the updated $\mathbf{E}(=\bar{\mathbf{E}})$. But in general, the final feasible set of force densities has to be achieved by iterative computations since the least square solution is an approximate solution. Let $\hat{\mathbf{q}}$ denote the feasible force density vector, the algorithm can be summarized as follows

Algorithm 1:

- Step 0:** Specify an initial force density vector \mathbf{q}^0 to obtain \mathbf{E}^0 by Eq. (3.5). Formulate the linear constraints to obtain $\bar{\mathbf{B}}$ and $\bar{\mathbf{g}}^0$. Set $i := 0$.
- Step 1:** Apply singular value decomposition to \mathbf{E}^i and set its h^* smallest singular values to zero to obtain $\bar{\mathbf{E}}^i$ by Eq. (3.20).
- Step 2:** Set $\mathbf{E}^i := \bar{\mathbf{E}}^i$. Obtain $\bar{\mathbf{g}}^{i+1}$, calculate \mathbf{q}^{i+1} by Eq. (3.15) and update \mathbf{E}^{i+1} by Eq. (3.5).
- Step 3:** Check the rank of \mathbf{E}^{i+1} , i.e. if it satisfies $n - \text{rank}(\mathbf{E}^{i+1}) = h^*$, then let $\hat{\mathbf{q}} = \mathbf{q}^{i+1}$ and terminate the algorithm; otherwise, set $i \leftarrow i + 1$ and return to Step 1.

This way, we can achieve the feasible force density vector $\hat{\mathbf{q}}$ and then its corresponding equilibrium matrix $\hat{\mathbf{E}}$, which has the required rank deficiency h^* .

3.4.3.2 Determination of Nodal Coordinates

Let $\mathbf{H} \in \mathfrak{R}^{dn \times dn}$ denote the tensor product of the identity matrix $\mathbf{I} \in \mathfrak{R}^{d \times d}$ and $\hat{\mathbf{E}}$ as

$$\mathbf{H} = \mathbf{I} \otimes \hat{\mathbf{E}} \quad (3.21)$$

By letting $\mathbf{X}^\top = (\mathbf{x}^\top, \mathbf{y}^\top, \mathbf{z}^\top) \in \mathfrak{R}^{dn}$, the equilibrium equations (7) can be combined as follows:

$$\mathbf{H}\mathbf{X} = \mathbf{0} \quad (3.22)$$

The rank deficiency of \mathbf{H} , which is equal to dh^* , denotes the number of independent nodal coordinates that can be specified arbitrarily. It should be noticed that there are h^* components of nodal coordinates in each direction that can be specified since the rank deficiency of \mathbf{E} is equal to h^* . The solution of Eq. (3.22) can be written as

$$\mathbf{X} = \mathbf{P}\boldsymbol{\beta} \quad (3.23)$$

where the columns of $\mathbf{P} \in \mathfrak{R}^{dn \times dh^*}$ denote self-equilibrium modes, and $\boldsymbol{\beta} \in \mathfrak{R}^{dh^*}$ the coefficient vector. If we specify an independent set of nodal coordinates $\bar{\mathbf{X}} \in \mathfrak{R}^{dh^*}$, and then obtain its corresponding components $\bar{\mathbf{P}} \in \mathfrak{R}^{dh^* \times dh^*}$ in \mathbf{P} , where $\text{rank}(\bar{\mathbf{P}}) = dh^*$, configuration of the structure in terms of nodal coordinates \mathbf{X} can be uniquely determined as

$$\mathbf{X} = \mathbf{P}\bar{\mathbf{P}}^{-1}\bar{\mathbf{X}} \quad (3.24)$$

Since the nodes of a tensegrity structure are always in self-equilibrium, which can never be violated in the form-finding process, and system errors maybe introduced during the implementation of numerical computations, the design error vector $\boldsymbol{\epsilon} \in \mathfrak{R}^{dn}$ is defined as

$$\boldsymbol{\epsilon} = \mathbf{H}\mathbf{X} \quad (3.25)$$

To reflect the magnitude of this design error vector, the Euclidean norm of $\boldsymbol{\epsilon}$, or the Euclidean length of a vector in other words, is used to define design error e as

$$e = \|\boldsymbol{\epsilon}\| = \sqrt{\boldsymbol{\epsilon}^\top \boldsymbol{\epsilon}} \quad (3.26)$$

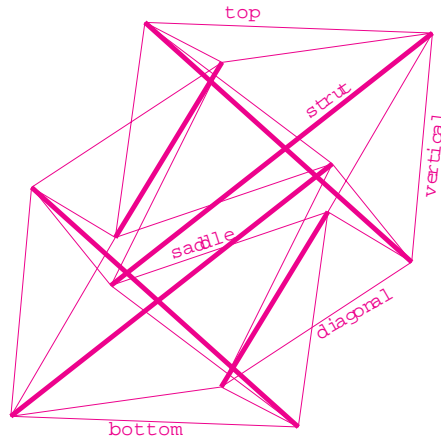


Figure 3.3: A two-stage tensegrity structure.

The design procedure of the proposed adaptive force density method can be summarized as follows:

Step 1: Specify linear constraints and an initial set of force densities.

Step 2: Obtain a feasible set of force densities by implementation of Algorithm 1.

Step 3: Specify an independent set of nodal coordinates to obtain a unique configuration of the structure.

3.5 Numerical Examples

In order to investigate the convergence property and ability of searching new configurations of the proposed adaptive force density method, numerical examples are presented for several simple and complicated tensegrity structures, by using MATLAB ver 6.5.1 (Borse, 1997).

3.5.1 Two-stage Tensegrity Structures

The proposed method is first applied to a two-stage tensegrity structure, composed of 12 nodes and 30 members, i.e. $n = 12$, $m = 30$. Its six struts are divided

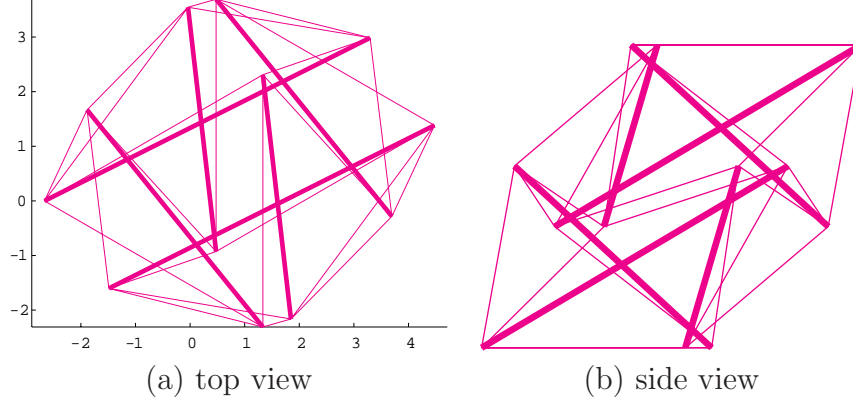


Figure 3.4: Example 1: a two-stage tensegrity structure.

into two groups: (1) struts of the upper stage, and (2) struts of the lower stage. The 24 cables are divided into: (3) the top and bottom bases, (4) saddle, (5) vertical, and (6) diagonal (Sultan et al., 2001), as shown in Fig. 3.3.

Example 1: By specifying an initial set of force densities as $\{-1.5, -1.5, 1, 2, 1, 1\}$, Algorithm 1 finds $\{-1.8376, -1.8376, 0.9281, 1.9918, 1.1737, 0.9958\}$ by 158 iterations. After specifying the coordinates of nodes a, b and c, which are defined in Fig. 3.4(a), as $\{(-2.6667, 0, 0), (1.3333, -2.3094, 0), (1.3334, 2.3094, 0)\}$ to make the bottom base locate on the xy -plane, and node d in the lower stage as $(-1.8867, 1.6666, 3.3333)$, configuration of the structure is achieved as shown in Fig. 3.4.

The relative error of force density vector at each iteration, defined as the Euclidean norm of the difference of \mathbf{q}^i to the final one $\hat{\mathbf{q}}$, $\|\mathbf{q}^i - \hat{\mathbf{q}}\|$, is plotted in Fig. 3.5. Termination condition of Algorithm 1 is that the equilibrium matrix $\hat{\mathbf{E}}$ has the required rank deficiency $h^*(=n - \text{rank}(\hat{\mathbf{E}}))$, where $\text{rank}(\hat{\mathbf{E}})$ is equal to the number of its singular values, which are larger than 10^{-5} . A very good and fast convergence of Algorithm 1 can be seen from the figure. The relative error comes very close to zero with only 20 iterations.

It can be observed from the formulations and design procedures presented in the previous section that the initial force densities and independent nodal coordinates can be arbitrarily given by the designers. Hence we can have some controls over the geometrical and mechanical properties of the structure. Furthermore,

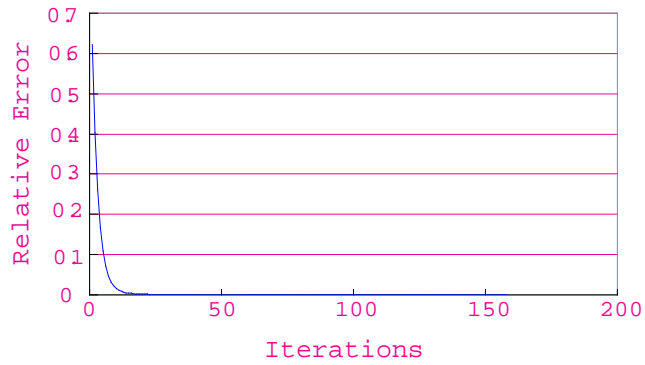


Figure 3.5: Convergence of the algorithm for feasible force densities.

new configurations can be easily found by changing the values of initial force densities and/or nodal coordinates.

Example 2: If x -coordinate of the fourth node is changed to -2.8867 from -1.8867 in Example 1 without modifying the others, a new configuration of the two-stage tensegrity structure is achieved as shown in Fig. 3.6. The design error of this example is 5.4866×10^{-14} .

Example 3: Besides changing nodal coordinates at the last step of the form-finding process, we can change the initial force densities at the first step as well to

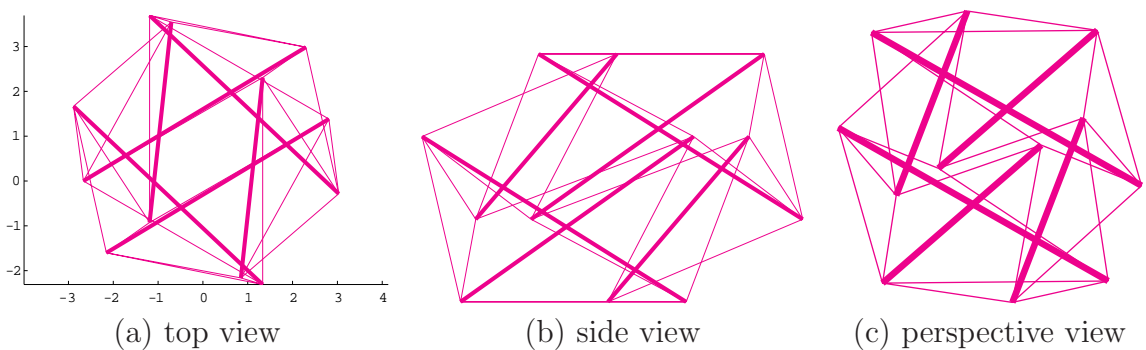


Figure 3.6: Example 2: a two-stage tensegrity structure.

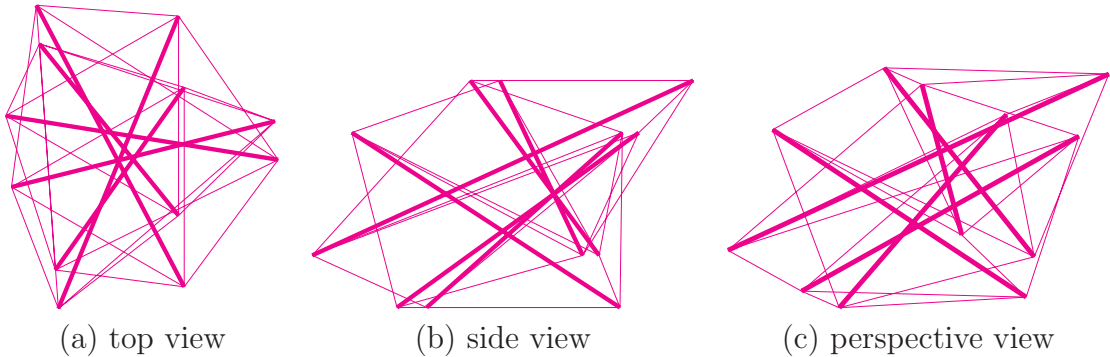


Figure 3.7: Example 3: a two-stage tensegrity structure.

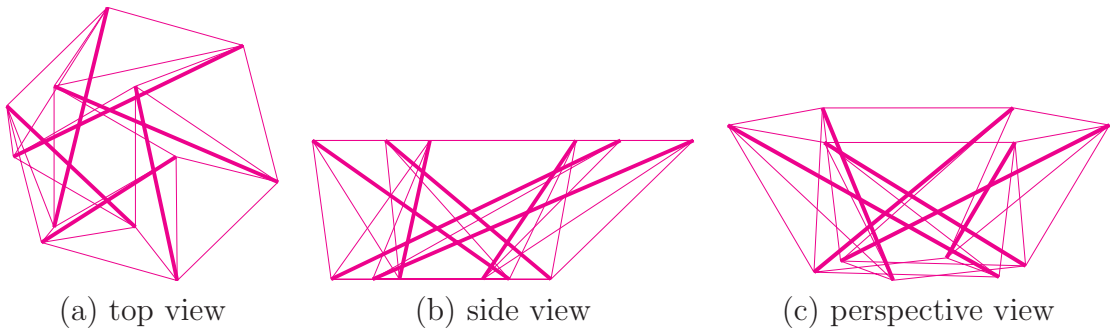


Figure 3.8: Example 4: a "two" stage tensegrity structure.

search for new configurations. If we change only the initial force density for the group of saddle to 0.5, and do not modify the nodal coordinates, the configuration is found as shown in Fig. 3.7, where the design error is 1.1573×10^{-13} . It is interesting to notice that there is no pair of parallel struts in this case.

Example 4: Another interesting example is shown in Fig. 3.8, where the initial force density of the vertical cable group is modified to 0.7. The "two"-stage tensegrity structure comes "down" to be only one stage but it has exactly the same topology as the other examples.

3.5.2 Three-stage Tensegrity Structure

Other than the relatively simple examples given previously, we applied the proposed form-finding method to a three-stage structure, which has upper, central

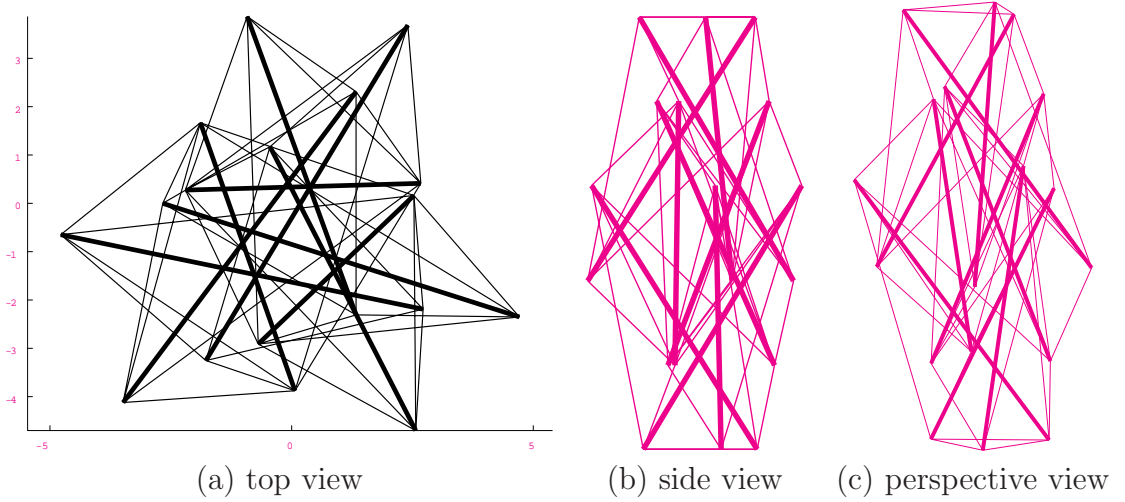


Figure 3.9: Example 5: a three-stage self-stressed structure.

and lower stages. The struts of this kind of structures are classified into two groups: (1) the six struts in the upper and lower stages, and (2) the three struts in the central stage. The cables are classified into the same groups as the two-stage tensegrity structure. So there are six groups in total.

Example 5: By specifying an initial set of force densities for these six groups as $\{-0.8, -1, 0.871, 0.3, 0.7244, 0.5\}$, and specifying the nodal coordinates of the bottom base and a lower node in the central stage as $\{(-2.6667, 0, 0), (1.3333, -2.3094, 0), (1.3334, 2.3094, 0)\}$ and $(-1.8867, 1.6666, 3.3333)$, respectively, we achieve the three-stage tensegrity structure as shown in Fig. 3.9.

It is of course not only the examples shown above can be achieved successfully. Other new configurations can be found by systematically changing the initial force densities and/or nodal coordinates.

3.6 Discussions and Conclusions

This paper has presented a method, called *adaptive force density method*, for the form-finding problem of tensegrity structures. The method is an extension of the basic idea of force density method for cable nets. The required rank deficiency of the equilibrium matrix for a non-degenerate structure has been discussed and the

singular value decomposition has been used to find a feasible set of force densities. After specifying an independent set of nodal coordinates, we can achieve a unique geometrical configuration of the structure.

In the proposed method, linear constraints on force densities can be included in the formulation, and the prestress state of each member can be specified as expected, i.e. tension for cables and compression for struts.

The algorithm finds the feasible set of force densities based on singular value decomposition of the equilibrium matrix and the least square solution of force density vector. A very good and fast convergence of the proposed algorithm has been demonstrated. To find a unique configuration, only topology, initial force densities given at the first step and an independent set of nodal coordinates specified at the last step are required. The proposed approach has also a very strong ability of searching new, feasible geometrical configurations by changing the initial set of force densities and/or nodal coordinates.

However, it cannot control the geometrical and mechanical properties of the structure exactly, since the parameters in the method are neither forces nor lengths but the force-to-length ratios. As discussed by [Tibert and Pellegrino \(2003\)](#), asymmetric configurations may be found for a given, symmetric force densities by the proposed method, because the member lengths cannot be described explicitly and linearly in the formulation.

Part II

Optimal Measurement Positions of Tension Structures for the Identification of Prestress Distribution

Chapter 4

Optimal Measurement Positions I

In this chapter, a formulation of mean identification error (MIE), which reflects the accuracy of the stress identification of a tension structure is introduced first. The formulation is based on the assumption of the configuration of the tension structure's being known and sensitivity analysis of equilibrium equations.

Four heuristic approaches are then proposed to find the optimal set of measurement members with the minimal number of measurements, subjected to an upper-bound constraint given on the mean identification error.

4.1 Introduction

Because of the light-weight characteristics and aesthetics, tension structures are built all over the world. Unlike any other conventional structural forms, which are made of steel, concrete, or wood, tension structure transmits neither moment nor torsion.

The geometric shape and prestress distribution of this kind of structure are tightly related. These two parameters are interdependent and can provide capability of maintaining the shape against external loads, so that it is said to be the perfect combination of structural form and mechanics. However, these characteristics lead to difficulties in design and maintenance processes, which are regarded as great challenges to structural engineers at the same time.

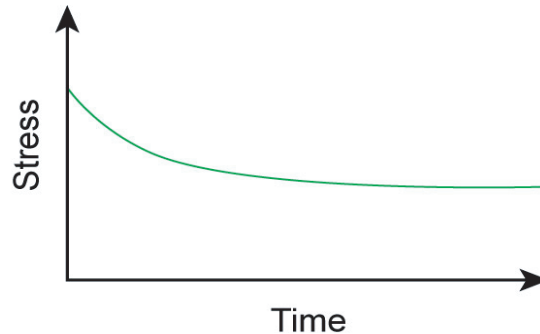


Figure 4.1: Stress relaxation of membrane.

4.1.1 Maintenance Problem of Membrane Structures

Due to the short and long term creep phenomena, prestress in membrane may be reduced as shown in Fig. 4.1 with the increment of construction time, which is well known as *stress relaxation* or *relaxation*. When relaxation takes place, wrinkle, stress concentration or even damage of membrane structure may occur under design loads.

Short-term creep can be prevented by pre-tensioning the membrane before installation. For protecting structures against long-term relaxation, there are two commonly used methods: (1) Introduce higher prestress than required; and (2) Re-tension the membrane to compensate the relaxation.

Higher prestress is not recommended because of: (a) Jack with much higher capacity is needed to handle much higher prestress; (b) Longer jacking distance to pull the membrane; (c) Higher friction between membrane and cable; (d) Longer installation period and longer exposure to unknown environment; (e) Larger and concentrated deformation in the membrane, especially at corners.

For the implementation of re-tension, the stress distribution of the structure should be known. Several numerical methods, based on approximate models of the mechanical property of membrane material, have been proposed to predict the stresses after relaxation. However, it is not easy to guarantee the reliability of the approximations, and structure may be exposed to unexpected external loads during its lifetime. So analytical methods are not reliable or accurate enough for

prediction of stress distribution, and stresses should be measured before carrying out re-tension.

4.1.2 Maintenance & Health Monitoring of Tensegrity Structures

The prestressed tensegrity structures, called cable domes also, used as the frame of a large span structure is a novel architectural form. A simplified two-dimensional prestressed tensegrity structure is shown in Fig. 4.7 in the example section in the follows. Roof materials, such as membranes etc., are used to cover them to prevent the internal space against external environment.

The introduction of prestress in cables is a great challenge to the engineers on site, since the configurations of these structures are highly sensitive to the prestress distribution in them. There have been some researches and examples in practice to the problem how to install the structures properly by introducing appropriate tension to achieve the desired shape with enough capacity of resisting design loads. E.g. the Kumatani Dome built in Aomori has used EM sensors to embed in all the cables to monitor the prestress real time during construction. However, this is obvious uneconomic, since each EM sensor costs several hundred thousands Japan Yens.

Also, to the tensegrity structures widely used in space because of their lightweight, easiness of control and deployability in some cases, the shape have to be controlled by actuators embedded in the members since the lose of their 'correct' shape may lose their formal function, e.g. a deployable tenant in space should maintain its configuration and maybe orientation to enable it receive and send signals between it and the earth. The structures used in a similar way, which monitor its prestress distribution by sensors and adjust the shape according to specific requirements, are called *Adaptive Structures*.

4.1.3 Motivation & Outline

From the discussion above, it is no doubt that the number of measurement members is preferred to be as small as possible, so the objective of this chapter is to

find a set of measurement positions with the minimal number, satisfying the need on accuracy evaluated by the mean identification error (MIE) in Section 3.

The measurement positions of axial forces of a prestressed pin-jointed structure can be represented in terms of members to be measured, called *measurement members*, and the ones to be estimated, called *estimation members*. To its identification problem, just as a design problem, the measurement members cannot be determined arbitrarily as described by Ohsaki and Kanno (2003), which is discussed further in Section 3 based on the equilibrium matrix.

In Section 4, an optimization problem of finding a set of measurement members with the minimal number is formulated, and four heuristic methods are proposed for the problem. Numerical examples are given in Section 5 to illustrate the efficiency and accuracy of the proposed methods. Section 6 gives a conclusion of this chapter.

4.2 Equilibrium Analysis

Force density method, described originally by Schek (1974), has been applied specifically to the form-finding of cable nets. Research in France has extended the concept to triangular surface elements, under the name of the *Surface Stress Density Method* (Maurin and Motro, 1998). The advantage of the method is that it provides a linearized solution to the equilibrium shape finding problem. The controlling element variable is that of force density or tension coefficient (e.g. s_k/l_k for a cable element of current tension s_k and length l_k). As noted in Maurin and Motro (1998), the main drawback of density methods is that the final distribution of stress is difficult to control. This can be overcome by iterating with updated force densities until the desired smooth stress distribution is achieved, but this would seem to negate the advantage of a linearized solution.

However, the shortcoming of the density methods is not a problem in our study since the geometrical configuration of the structure in terms of nodal coordinates is known by measurements.

Using the generally accepted assumption in structural engineering that external loads, if there is any, are or equivalently applied on the nodes. So that

members of a pin-jointed structure, connecting two adjacent nodes, transmit only axial forces, either in tension or compression.

Before formulating the equilibrium equations of the structure, we introduce the following assumptions:

1. Members of the structure are connected by pin joints.
2. Topology of the structure is known.
3. Configuration of the structure, in terms of nodal coordinates is known.
4. No external load is applied and the self-weight of the structure is neglected.

Let m , n and n^f denote number of members, free nodes and fixed nodes, respectively. Use the equilibrium equations of the structure formulated in the former chapter, which are

$$\begin{pmatrix} \mathbf{C}^\top \mathbf{U} \\ \mathbf{C}^\top \mathbf{V} \\ \mathbf{C}^\top \mathbf{W} \end{pmatrix} \mathbf{L}^{-1} \mathbf{s} = \begin{pmatrix} \mathbf{p}^x \\ \mathbf{p}^y \\ \mathbf{p}^z \end{pmatrix} \quad (4.1)$$

where the diagonal elements of the diagonal matrices \mathbf{U} , \mathbf{V} and \mathbf{W} denote the coordinate differences in x -, y - and z - directions, respectively. \mathbf{C} is a matrix defined the topology of the structure and \mathbf{p}^x , \mathbf{p}^y , \mathbf{p}^z are external loads.

By letting

$$\mathbf{D} = \begin{pmatrix} \mathbf{C}^\top \mathbf{U} \\ \mathbf{C}^\top \mathbf{V} \\ \mathbf{C}^\top \mathbf{W} \end{pmatrix} \mathbf{L}^{-1} \quad (4.2)$$

and

$$\mathbf{P} = \begin{pmatrix} \mathbf{p}^x \\ \mathbf{p}^y \\ \mathbf{p}^z \end{pmatrix}$$

Eq. (4.2) can be rewritten as

$$\mathbf{D} \mathbf{s} = \mathbf{P} \quad (4.3)$$

4.3 Mean Identification Error (MIE)

where $\mathbf{D} \in \mathfrak{R}^{3n \times m}$ is a matrix in terms of topology and nodal coordinates, and $\mathbf{s} \in \mathfrak{R}^m$ is the vector of axial forces of all members. From the assumptions 2 and 3, \mathbf{D} is a constant matrix.

Since there is no external load applied on the structure considered in this chapter and its self-weight is neglected, Eq. (4.4) becomes

$$\mathbf{D}\mathbf{s} = \mathbf{0} \tag{4.4}$$

Let

$$h = m - \text{rank}(\mathbf{D}) \tag{4.5}$$

Eq. (4.4) is overdetermined when $h < 0$, and underdetermined when $h > 0$. If $h = 0$, there exists only trivial solution $\mathbf{s} = \mathbf{0}$. Since tension structures often fall into the underdetermined category (Haber and Abel, 1982), we will focus on only this case in this study. This also means that there are at least h members to be measured to identify the others.

The solution of Eq. (4.4) can be written by using a matrix $\mathbf{G} \in \mathfrak{R}^{m \times h}$ as

$$\mathbf{s} = \mathbf{G}\alpha \tag{4.6}$$

where the columns of \mathbf{G} are self-equilibrium modes, and α_i , the i th element of $\alpha \in \mathfrak{R}^h$, is the coefficient of the i th self-equilibrium mode.

4.3 Mean Identification Error (MIE)

Consider a situation that the forces of some members are measured to estimate those of the remaining members. To reflect the effect of measurement errors on estimation errors, mean identification error (MIE) of all members is formulated in this section. The MIE will also be used as constraint, which reflects the accuracy of identification, for finding the optimal measurement members in the next section.

4.3.1 Formulation of MIE

The numbers of all members and measurement members are denoted by m and p , respectively. Let $\mathbf{s}^m \in \mathfrak{R}^p$ denote the axial force vector of the measurement members, and $\mathbf{s}^e \in \mathfrak{R}^{m-p}$ denote the vector of axial forces to be estimated. Then Eq. (4.6) can be rewritten as

$$\begin{pmatrix} \mathbf{s}^m \\ \mathbf{s}^e \end{pmatrix} = \begin{pmatrix} \mathbf{G}^m \\ \mathbf{G}^e \end{pmatrix} \alpha \quad (4.7)$$

From Eq. (4.7), we obtain

$$\mathbf{s}^m = \mathbf{G}^m \alpha \quad (4.8)$$

Since \mathbf{G} and \mathbf{G}^m are both constant matrices, the differential forms of Eq. (4.6) and Eq. (4.8) are

$$\Delta \mathbf{s} = \mathbf{G} \Delta \alpha \quad (4.9)$$

$$\Delta \mathbf{s}^m = \mathbf{G}^m \Delta \alpha \quad (4.10)$$

If \mathbf{G}^m is a full-rank matrix, the least square solution of Eq. (4.10) can be expressed in forms of the generalized inverse matrix \mathbf{G}^{m-} of it (see Appendix II) as

$$\Delta \alpha = \mathbf{G}^{a-} \Delta \mathbf{s}^m \quad (4.11)$$

Substitute α to Eq. (4.9), $\Delta \mathbf{s}$ can be calculated by the following equation

$$\Delta \mathbf{s} = \mathbf{G} \mathbf{G}^{m-} \Delta \mathbf{s}^m \quad (4.12)$$

Let $\mathbf{H} = \mathbf{G} \mathbf{G}^{m-}$, and rewrite Eq. (4.12) as

$$\Delta \mathbf{s} = (\mathbf{H}_1, \mathbf{H}_2, \dots, \mathbf{H}_p) (\Delta s_1^m, \Delta s_2^m, \dots, \Delta s_p^m)^\top \quad (4.13)$$

where $()^\top$ denotes the transpose of a vector. From Eq. (4.13), the estimation error $\Delta \mathbf{s}^i \in \mathfrak{R}^m$ of all members due to the measurement error Δs_i^m of the i th member is

$$\Delta \mathbf{s}^i = \mathbf{H}_i \Delta s_i^m \quad (4.14)$$

The MIE due to measurement errors of all p measurement members is defined as

$$E = \sqrt{\sum_{i=1}^p \Delta \mathbf{s}^{i\top} \Delta \mathbf{s}^i / h} \quad (4.15)$$

By substituting Eq. (4.14) into Eq. (4.15), we obtain

$$E = \sqrt{\sum_{i=1}^p (\Delta s_i^m)^2 \mathbf{H}_i^\top \mathbf{H}_i / h} \quad (4.16)$$

For a simpler case where $\Delta s_i^m = e$ ($= \text{const.}$), Eq. (4.16) can be rewritten as

$$E = e \sqrt{\sum_{i=1}^p \mathbf{H}_i^\top \mathbf{H}_i / h} \quad (4.17)$$

4.3.2 Characteristics of MIE

Property 1: When all members are to be measured ($p = m$), $E = e$, irrespective of the total number of members m .

Proof:

When all members are to be measured, \mathbf{G}^{a-} becomes \mathbf{G}^- ($\mathbf{G} \in \mathbb{R}^{m \times h}$). Since \mathbf{G} is a full-rank matrix and the relation $m > h$ is satisfied always, the generalized inverse matrix \mathbf{G}^- of \mathbf{G} can then be written as

$$\mathbf{G}^- = (\mathbf{G}^\top \mathbf{G})^{-1} \mathbf{G}^\top \quad (4.18)$$

so, we can obtain

$$\mathbf{H} = \mathbf{G} \mathbf{G}^- = \mathbf{G} (\mathbf{G}^\top \mathbf{G})^{-1} \mathbf{G}^\top \quad (4.19)$$

Since \mathbf{H} is a symmetrical matrix, so $\mathbf{H}^\top \mathbf{H}$ can be written as

$$\mathbf{H}^\top \mathbf{H} = \mathbf{H} \mathbf{H} = \mathbf{G} (\mathbf{G}^\top \mathbf{G})^{-1} \mathbf{G}^\top \mathbf{G} (\mathbf{G}^\top \mathbf{G})^{-1} \mathbf{G}^\top = \mathbf{H} \quad (4.20)$$

4.4 Formulation of Optimization Problem

from which we know that all the eigenvalues of $\mathbf{H}\mathbf{H}$ are equal to 1 so the trace of this matrix is h . On the other hand, $\mathbf{H}^\top\mathbf{H}$ can be written in another form as

$$\mathbf{H}^\top\mathbf{H} = \begin{pmatrix} \mathbf{H}_1^\top\mathbf{H}_1 & \mathbf{H}_1^\top\mathbf{H}_2 & \cdots & \mathbf{H}_1^\top\mathbf{H}_m \\ \mathbf{H}_2^\top\mathbf{H}_1 & \mathbf{H}_2^\top\mathbf{H}_2 & \cdots & \mathbf{H}_2^\top\mathbf{H}_m \\ \vdots & \vdots & \ddots & \vdots \\ \mathbf{H}_m^\top\mathbf{H}_1 & \mathbf{H}_m^\top\mathbf{H}_2 & \cdots & \mathbf{H}_m^\top\mathbf{H}_m \end{pmatrix} \quad (4.21)$$

It is obvious that the sum of diagonal elements of $\mathbf{H}^\top\mathbf{H}$, also called *trace* of the matrix which should be equal to h from the discussion previously, is the one used to formulate the mean identification error in Eq. (4.17).

Therefore, we have proved that when all members are to be measured ($p = m$), $E = e$, irrespective of the total number of members m .

4.4 Formulation of Optimization Problem

In the process of identification of the stress distribution of a tension structure, it is clear that the precision of measurement, the number of measurement and the locations of measurement are the key parameters. The precision of the measurement depends on the measurement device, which is not a scope and not discussed in this study.

It should be noted that it is not always true that the more the number of measurements, the more accurate identification result one can achieve. In order to find the optimal measurement positions, or optimal sensor deployment, some researches have been done for the conventional types of structures (Sanayei et al., 1992; Pothisiri and Hjelmstad, 2002; Abdullah et al., 2001; Zavoni et al., 1999).

To find the optimal measurement members with minimum number, the following optimization problem subjected to the constraint of the upper-bound \bar{E} of the MIE, is formulated as

$$\begin{aligned} & \text{minimize} && p \\ & \text{subject to} && E \leq \bar{E} \end{aligned} \quad (4.22)$$

where p denotes the number of measurement members and \bar{E} the upper-bound constraint on mean identification error. The problem turns to be a combinatorial

optimization problem that is to find an optimal set of measurement members with the minimal number of elements satisfying the constraint on upper-bound of MIE.

To solve this kind of problem, there have been many heuristic methods proposed, such as genetic algorithm, simulated annealing and tabu search, since it is very hard to get an exact solution due to the possibility of huge number of combination. Two basic methods, *Stingy* method and *Greedy* method, are considered here.

4.5 Stingy Method

Stingy method is a basic heuristic method for combinatorial optimization problem. It starts from a complete set with all elements, and drop the element contributing the least to the value of objective function one by one from the current set. While no more element can be dropped due to all the constraint conditions having to be satisfied, the last set is then considered to be the optimal solution of the problem, although there is no proof that it is the exact optimal solution.

The stingy method in this study begins from a complete set of measurement members, in which all members or specified members are set to be measurement members. The member, removal of which leads to the least of MIE, is dropped out from the current set, since it is considered to have the minimal influence on MIE so dropping of it will not make much worse on identification accuracy. The removal operation is executed consecutively until the upper-bound constraint on MIE is violated if any element of the current set is dropped.

By letting \mathcal{J} denote the set of measurement members, and p denote the size of \mathcal{J} , stingy method adopted can be summarized as

Algorithm 1 – Stingy method:

Step 0 Set $\mathcal{J} = \{1, 2, \dots, m\}$. The number of measurement members p is equal to m .

Step 1 Find $k = \underset{j \in \mathcal{J}}{\operatorname{argmin}}(E_p^j - E_p^0)$, where E_p^0 and E_p^j denote the MIEs of sets \mathcal{J} and $\mathcal{J} - \{j\}$, respectively.

Step 2 If $E_p^k > \bar{E}$, then terminate. Otherwise, $\mathcal{J} := \mathcal{J} - \{k\}$ because it has the minimum effect on MIE in set \mathcal{J} ; set $p := p - 1$ and return to Step 1.

4.6 Greedy Method

The greedy method, whose idea is exactly opposite to the stingy method introduced early, is a method that starts from the set with least elements, and adds the elements with the greatest contribution to the objective function to the current set consecutively until all the constraint conditions are satisfied.

In this study, Simulated Annealing (SA) is used to determine an independent set of measurement members with the minimal number, which should be h calculated by Eq. (4.5), at the first step, and then adds the one, inclusion of which leads to the minimum MIE, which is considered to have the greatest influence on MIE so it should be included to the current set. The inclusion operation is executed consecutively until the upper-bound constraint on MIE is satisfied. The algorithm is summarized as follows

Algorithm 2 – Greedy method:

Step 0 Determine the minimal independent set of measurement members \mathcal{J} , with h elements, by using SA. Set $p = h$.

Step 1 Find $k = \underset{j \in \mathcal{J}}{\operatorname{argmax}}(E_p^0 - E_p^j)$, where E_p^0 and E_p^j denote the MIEs of sets \mathcal{J} and $\mathcal{J} \cup \{j\}$, respectively.

Step 2 Let $\mathcal{J} := \mathcal{J} \cup \{k\}$, because member k is the most effective member to be measured to reduce MIE. Set $p := p + 1$.

Step 3 Terminate if $E_i^k \leq \bar{E}$. Otherwise, return to Step 1.

4.6.1 Simulated annealing (SA)

In the greedy method mentioned above, the minimal independent set of measurement members is determined by Simulated Annealing.

As its name implies, the Simulated Annealing (SA) exploits an analogy between the way in which a metal cools and freezes into a minimum energy crystalline structure (the annealing process) and the search for a minimum in a more general system (SA) (Kirkpatrick et al., 1983). The major advantage of SA over some other heuristic methods is its ability to avoid becoming trapped at local optima. It is among the most popular iterative methods that have been applied widely to solve not only many combinatorial problems but also the real world problems.

The disadvantage of SA is, as is well known, the long annealing time. Computation cost of SA relates to the number of the measurement members, the initial solution.

4.6.1.1 Feasible Solutions

The algorithm starts from an initial feasible solution, employs a random search. A random and small change in one or a combination of some variables can generate a neighboring solution.

As mentioned, the sufficient and necessary condition for Eq. (4.10) has a least square solution is that:

The matrix \mathbf{G}^m corresponding to the estimation members has to be full-rank: $\text{rank}(\mathbf{G}^m) = h$.

To generate a feasible neighboring solution satisfying the above condition, we use the following scheme:

Finding Feasible Neighboring Solution:

Step 0: Let $\mathbf{G}^a \in \mathfrak{R}^{h \times h}$ denote the matrix corresponding to the current independent set of measurement members, and \mathbf{G}^{b0} corresponding to the estimation ones.

Step 1: Select one row randomly from \mathbf{G}^b , denoted as \mathbf{G}_i^b .

Step 2: Solve the equation

$$\beta = \mathbf{G}_i^b (\mathbf{G}^a)^{-1} \quad (4.23)$$

of which the nonzero j th elements shows that if the j th row of \mathbf{G}^a is taken the place by \mathbf{G}_i^b , the new matrix $\bar{\mathbf{G}}^a$ is full-rank too.

Step 3 Change the randomly chosen j th row \mathbf{G}_j^a , where the j th element of β is nonzero, \mathbf{G}^a and \mathbf{G}_i^b in \mathbf{G}^b to get new ones of them.

This way, an estimation member is changed to be measurement member, vice versa, letting the new set of measurement members to be independent. If needed changes of measurement members is more than one, the above algorithm can be implemented specific times in the iteration of finding a feasible neighbor.

4.6.1.2 Transition of Solutions

Whether the current solution is substituted by the candidate one or not is decided by the following probability function:

$$P = \min\{1, e^{\Delta f_i/t_i}\} \quad (4.24)$$

where Δf_i is the cost difference between the candidate solution and the current solution in iteration i , and t_i is the control parameter known as temperature.

Random numbers uniformly distributed in the interval $(0, 1)$, used in this study, are a convenient means of implementing the random part of the algorithm. In each iteration, the above transition probability is compared with one such uniform random number. In the case of a better candidate solution, a move is always made since the probability of transition P is equal to 1, and there is still a chance even for a worse one to be accepted since P will always larger than 0 at nonzero temperature. If the transition from the current solution to the candidate solution is rejected, another solution in the neighborhood will be generated and evaluated. This scheme allow SA to escape local optima without getting stuck.

4.6.1.3 Cooling Schedule & Termination Conditions

The temperature decreases during the search according to a function known as the *cooling schedule* or annealing schedule. There are several theoretical and empirical cooling schedules suggested in the literature that could be categorized into classes such as monotonic schedules, adaptive schedules, geometric schedules and

quadratic cooling schedules (Azizi and Zolfaghari, 2004). A lower temperature contributes to a lower transition probability.

The cooling schedule adopted in this study is a monotonic one which can be defined as

$$t_i = \eta^i t_0 \quad (4.25)$$

where the annealing schedule starts at a high temperature t_0 , then cools exponentially with the ratio $\eta (= t_1/t_0)$ after neighbors of the current solution have been attempted sufficiently at each current temperature. By applying this schedule, the end of the search has less chance of escaping local optima, while in the beginning the search is more likely to move out of local optimal solutions.

There are many tricks to terminate the algorithm regarding the optimal solution has been achieved, e.g., when the current temperature is very low that there is highly impossible to make any improvement, or the desired number of acceptances is not achieved at specific times of successive temperatures that the system is considered "frozen".

So the process of SA adopted here can be summarized as follows

Algorithm of Simulated Annealing:

Step 0: Generate an initial solution randomly. Specify a value to the cooling ratio η and initial temperature t_0 . Set $i = 0$.

Step 1: Search the neighborhood of the current solution p times, and move to a new one with the solution transition criterion in Eq. (4.24). Record the solution with minimum objective value in the iterations.

Step 2: Set the recorded solution to be the current one, update $i =: i + 1$. If there is any change of solution in Step 1, then decline the temperature by Eq. (4.25); otherwise, remain the temperature unmodified.

Step 3: If the temperature is low enough, $t_i < \bar{t}$, or there is not any new solution in Step 1 at j times of successive temperatures, then terminate the algorithm; Otherwise, return Step 1 with the updated temperature t_i .

4.7 SLS & GLS

By using Algorithm 1 or Algorithm 2, we can find the minimal set of measurement members \mathcal{J} , with p elements, subjected to the upper-bound constraint on MIE.

The solution, obtained by the simple operation of removing or adding measurement members mentioned above, however, may not have enough accuracy as expected. If the computation cost is not a significant factor considered in the implementation of finding measurement positions of tension structures, *Local Search Strategy* has capability of finding iterative improvement by searching neighborhood of the current solution.

Based on the ideas of the two proposed heuristic methods, *SLS* (Stingy method with Local Search) and *GLS* (Greedy method with Local Search), adopting local search strategy at each iteration of removing or adding a measurement member in Algorithm 1 or Algorithm 2, may have much higher accuracy but more time-consuming at the same time. The local search strategy adopted in this study is described as follows.

Algorithm 3 – local search strategy:

Step 0 Let q denote the number of trials of local search at each step of Stingy or Greedy method. Set the loop counter $l = 1$.

Step 1 Choose $j \in \mathcal{J}$ and $k \notin \mathcal{J}$ randomly. Calculate E_l^0 and E_l^k , which denote the MIEs of member sets \mathcal{J} and $\mathcal{J} - \{j\} \cup \{k\}$, respectively.

Step 2 If $E_l^k \leq E_l^0$, update $\mathcal{J} := \mathcal{J} - \{j\} \cup \{k\}$.

Step 3 Let $l := l + 1$. If $l > q$, then terminate local search; otherwise, return to Step 1.

4.8 Numerical examples

To illustrate the efficiency and accuracy of the proposed approaches, both tensegrity structure and cable net model of membrane structure are used as examples.

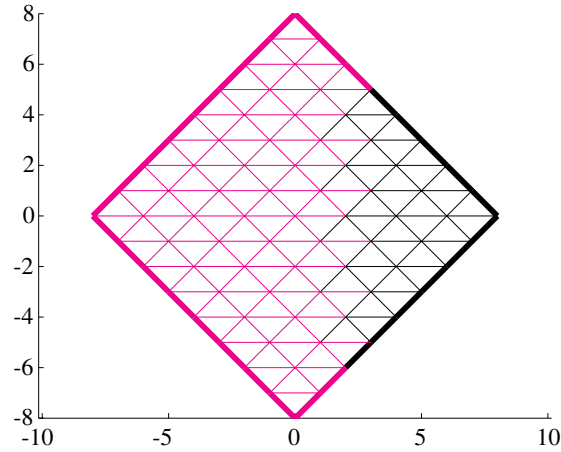


Figure 4.2: Top view of the 176-member cable net model.

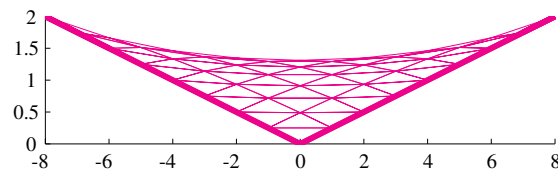


Figure 4.3: Side view of the 176-member cable net model.

4.8.1 Cable Net Model of Membrane Structure

For simplicity, the membrane structure is modelled by a virtual cable net (Maurin and Motro, 1998). This way, the problem of finding the optimal measurement positions of stress in a membrane structure is transformed into that of searching for the optimal set of the members whose axial forces are to be measured, called *measurement members*, in a cable net.

An HP-shaped membrane structure, of which the diagonal span length is 16 m and the height is 2 m, with different cable net approximations is used in this section. Fig. 4.2 and Fig. 4.3 show the top view and side view of the structure modelled by a 176-member cable net, respectively.

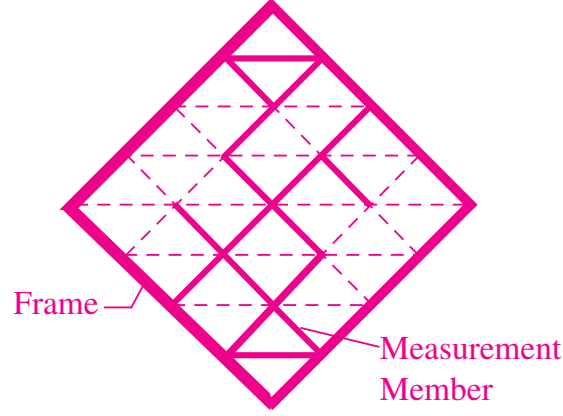


Figure 4.4: Optimal measurement members - $m = 40$, $h = 13$, $\bar{E}/e = 1.5$.

4.8.1.1 21-member Cable Net Model

To investigate the efficiency and accuracy of each method, a cable net model with only 21 cable members of the membrane structure is used.

The minimum number of members that have to be measured is $h = 9$ calculated by Eq. (4.5). The exact set of the optimal measurement members with this minimum number and its corresponding \bar{E}/e are obtained by enumeration method, $p = h (= 9)$, and is compared to the same case by the proposed methods, as listed in Table 4.8.1.1. Since the first step of Greedy Method and SLS use the SA to determine the optimal independent set of measurement, only the result of SA is listed in the table. The parameters used in the implementation of SA are set as: initial temperature $t_0 = 10$, ratio of cooling schedule $t_1/t_0 = 0.92$, neighbors of the current solution at each temperature are search $2.5h$ times, and the annealing terminates when there is no change in three consecutive updated temperature.

From the table, we can see that Simulated Annealing and SLS can find the globally optimal solution by enumeration method. And although Stingy method may not have high enough accuracy, it has great advantage in computation cost.

Note that computation cost of SA is dependent on the initial solution and the setting of parameters, also the cost of local search is dependent on the setting of parameter q .

Table 4.1: Efficiencies and accuracies by comparison with enumeration method.

	Enumeration	SA	Stingy	SLS
Computation Cost	33528	1642	162	1254
Minimum MIE	1.5793	1.5793	1.9953	1.5793
Relative Error		0.00%	26.34%	0.00%

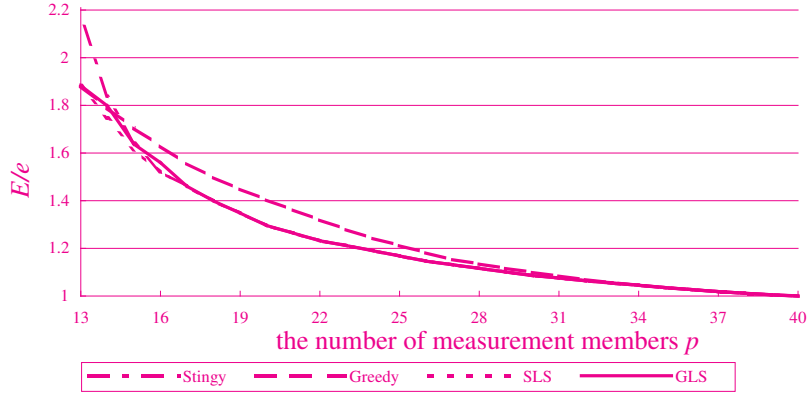


Figure 4.5: Numerical experiments of the proposed methods ($m = 40$, $h = 13$).

4.8.1.2 40-member Cable Net Model

Fig. 4.4 shows the structure modelled by a 40-member cable net. The minimal number of measurement members calculated by Eq. (4.6) is $h = 13$.

In order to compare the efficiency and accuracy of the proposed methods, MIEs of all feasible number of measurement members ($h \leq p \leq m$) are computed by each method and shown in Fig. 4.5. The vertical and horizontal axes denote the values of E/e and the number of measurement members p , respectively.

From all these numerical experiments, we can draw conclusions that

1. SLS can always attain better than or at least the same good solution as other methods.
2. When the constraint on MIE is tight, which we can also say that more measurement members are needed, SLS, Stingy and GLS have exactly the same high accuracy.

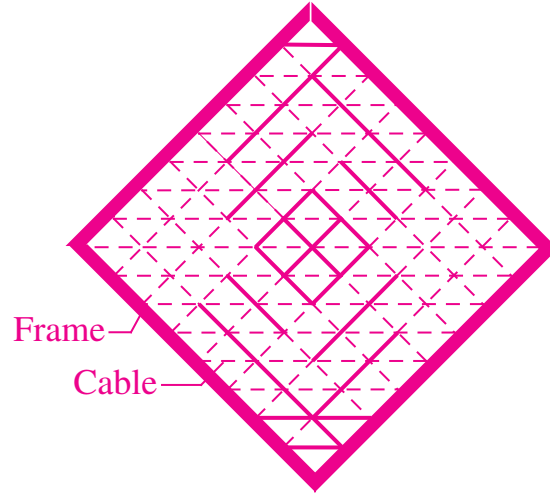


Figure 4.6: Optimal measurement members - $m = 176$, $h = 29$, $\bar{E}/e = 2.0$.

3. GLS or SLS always has higher or the same accuracy comparing to the Stingy or Greedy method, which indicates the advantage of local search strategy in view of accuracy.
4. Greedy method is not a good choice in view of not only accuracy but also efficiency.

4.8.1.3 Optimal Measurement Positions by Stingy Method

Knowing that SLS is of high accuracy and efficiency among the proposed methods, it is used to find the optimal set of measurement members for the following examples.

Fig. 4.4 shows the structure modelled by a 40-member cable net. If to upper bound constraint of MIE (E/e) is set to be 1.5, 17 optimal measurement members are found as shown in solid lines.

In another case of 176-member cable net model subjected to $\bar{E}/e \leq 2.0$, 40 optimal measurement members are obtained by SLS as shown in Fig. 4.6.

From these two examples, we can see that the measurement members locate at the neighborhood of vertical diagonal of the structure, reflecting the fact that the middle of the structure has more significant influence on the mean identification

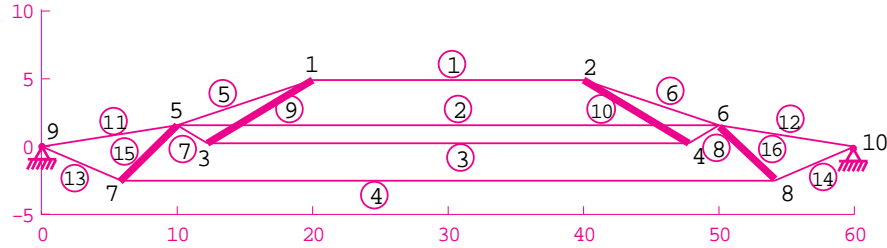


Figure 4.7: A two-dimensional tensegrity structure.

error. The meshing method adopted for the structure is also considered to be an factor of the distribution of optimal measurement positions.

4.8.2 Two-dimensional Cable Dome

A two-dimensional prestressed tensegrity structure as shown in Fig. 4.7, of which the span is 60m and height is 7.4386m obtained by the form-finding process proposed in Chapter 2, is used as another numerical example. The structure consists of 16 members - 4 struts and 12 cables, which is simplified from a three-dimensional cable dome, used as an example by [Ohsaki and Kanno \(2003\)](#), by using its symmetry properties. Note here that the horizontal cables represent two adjacent cables actually.

h of the structure is calculated to be 2, which means that force distribution of the whole structure can be determined by only two measurement members.

Example 2-1: The dotted line with triangle marks in Fig. 4.8 demonstrates the relation of the number of measurement members p to the mean identification error E/e calculated by Stingy Method.

Member 2 and 11 are found finally by the Stingy method. And the maximal and minimal MIEs of the structure for all the cases with different measurement members are calculated to be 1.8914 and 1, respectively.

Example 2-2: In many cases, measurements of compressive members are very difficult to obtain high enough accuracy, unlike the tensile members, of which axial forces can be measured with high accuracy by inserting sensors in them. So it is desired to measure only the tensile members of a tensegrity structure, which can be accomplished very easily by using the proposed methods by neglecting the

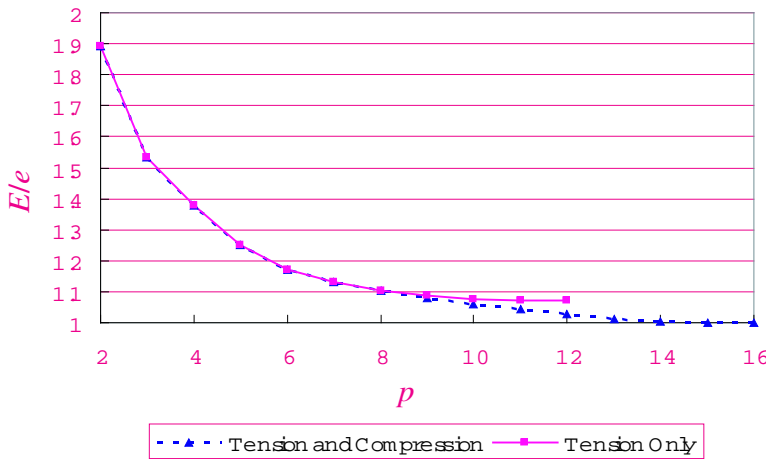


Figure 4.8: MIE of a 2D tensegrity structure by Stingy Method.

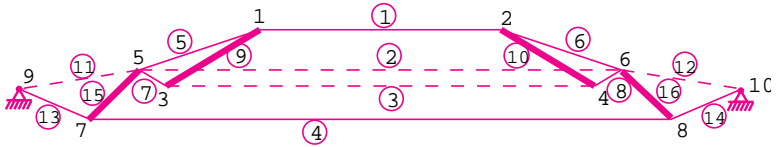


Figure 4.9: Optimal measurement members by Stingy method ($\bar{E}/e = 1.5$).

compressive members in each operation of removal or inclusion of measurement members in Algorithm 1 or Algorithm 2.

Since there are four compressive members, the Stingy method starts from the complete set of 14 tensile members, and find the relation of number of measurement members p to MIE E/e , shown as solid lines with square marks in Fig. 4.8.

It can be seen that, Example 1 and Example 2 find the same set of measurement members when the number of them are equal to or less than 8, and have a little difference since the measurements of compressive members have not been considered in Example 2.

Example 2-3: When the upper-bound constraint on the mean identification error is set to be $E/e = 1.5$ and only tensile members are to be measured, both Stingy method and Greedy method, in which the parameters are set as $t_0 = 5$ and $\eta = 0.92$, find us four measurement members, $\{ 2, 3, 11, 12 \}$, shown as dotted lines in Fig. 4.9.

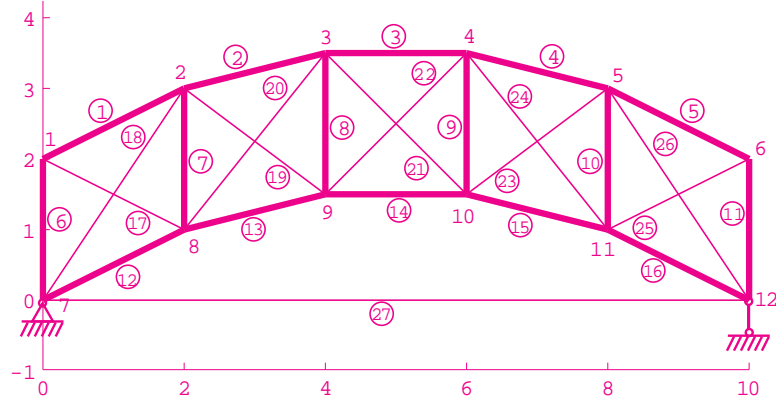


Figure 4.10: A two-dimensional prestressed pin-jointed arch.

4.8.3 Two-dimensional Self-stressing Pin-jointed Arch

As shown in Fig. 4.10, a two-dimensional pin-jointed arch consisting of 12 nodes and 27 members. The span of it is $10m$, and the height is $3.5m$. The thicker lines denote the compressive members and the thinner ones the tensile. Since node 7 is fixed while node 12 can have displacement in x -direction, and there is no self-weight nor external load, the structure belongs to the category of self-stressing tensegrity structure. The minimal number of measurement members of this structure is calculated to be $h = 6$.

Example 3-1: Subjected to the upper-bound constraint on MIE $\bar{E}/e = 1.5$, 11 measurement members - $\{3, 4, 7, 13, 14, 15, 18, 20, 22, 23, 25\}$ are found by applying the proposed Greedy method.

Example 3-2: However, by applying GLS instead of Greedy method for the same case, 10 measurement members $\{7, 9, 13, 14, 15, 18, 20, 22, 23, 25\}$, one less than Greedy method, are found to satisfy the constraint on MIE, which shows again the ability of local search strategy of finding better solution in the neighborhood of the current one but with much higher computation cost on the other hand.

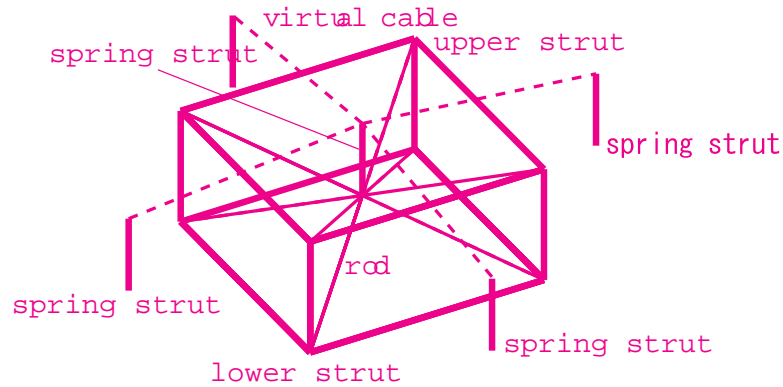


Figure 4.11: System truss unit.

4.8.4 Three-dimensional Tensegric Truss Dome

A three-dimensional tensegric truss dome, made of system truss units, is used here as an example for finding the optimal measurement members. The basic idea of the system truss unit is shown in Fig. 4.11 - it consists of a tensegric truss, four upper and four lower struts connected by 8 rods with high tension to the central node, and a spring strut, of which one end is connected to the central node and the other with spring to the membranes. The membrane materials are substituted by virtual cables, shown as dotted thinner lines in the figure. It is obvious that the spring strut cannot remain stable without pre-tension in the virtual cables.

Because of the light-weight and stability by introducing pre-tension in the membrane, the system is first adopted in the Multi-objective Dome of Kirara Sports Park built in Yamaguchi-ken, Japan, of which outer appearance and internal space are shown in Fig. 4.12.

In order to identify the prestress distribution of struts, rods and membrane materials, measurements without considering the mechanical properties of the structure may lead to significantly uneconomic, because of the high complexity and highly indetermination of the system.

Fig. 4.13 shows the three-dimensional tensegric dome used here as a numerical example, red and yellow thicker lines denote struts and spring struts, respectively, green and blue thinner lines denote rods and virtual cables, respectively. The



Figure 4.12: Multi-objective Dome of Kirara Sports Park.

membrane on the upper boundaries is fixed to the abutment around the structure but not the upper struts. Span of the structure is $20m$ in each directions in the $x - y$ plane, and the height is $4.5792m$. Each unit of the structure is about $4m \times 4m \times 2m$, and the spring rod is $1.3m$. The nodes of upper struts are located on an arch, of which radius is $20m$ and angle is 60° . There are 441 members and 142 nodes totally.

Since the least number of measurement members is calculated to be $h = 87$, and the high-tension rods can provide only 82 independent measurement members, we specify 8 lower struts and 8 virtual cables in the four corners to be measurement members for convenience and requirement of the number of independence. The complete set of measurement members consists of all 200 high-tension rods, 8 struts and 8 virtual cables.

Due to the high computation cost of this case, we use Stingy method, which is considered the fastest one in the proposed method but with relatively high accuracy, to find 103 measurement members while giving the upper-bound constraint on MIE to be $E/e = 2.9$, shown as dotted lines in Fig. 4.14.

4.9 Conclusions & Discussions

For identification of the stress distribution of tension structures, four heuristic methods with high accuracy have been proposed for finding optimal measurement

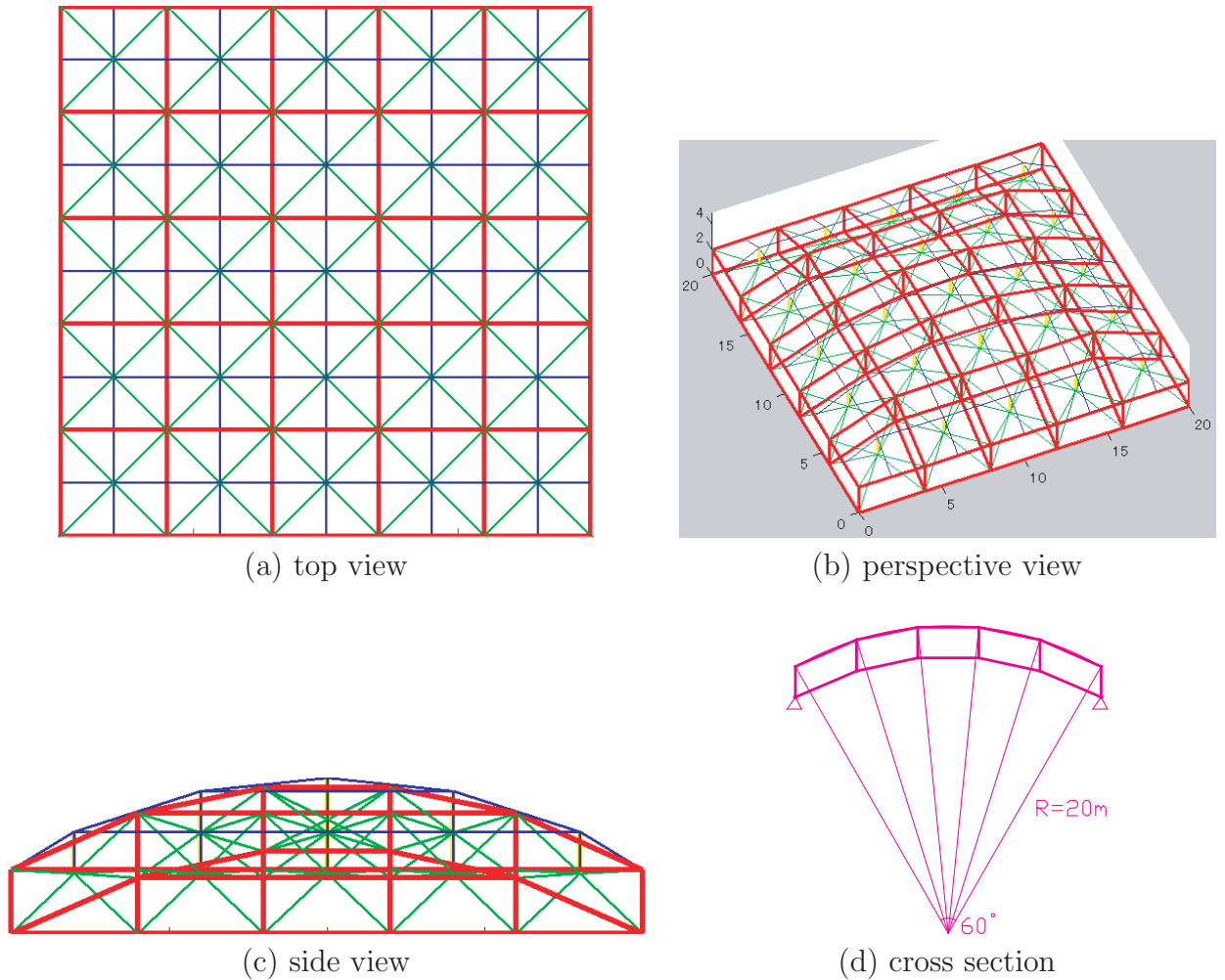


Figure 4.13: A three-dimensional tensegric dome.

positions of the stresses. To the problem of membrane structure with continuum membrane material, cable net model has been introduced to transformed it into a prestressed pin-jointed structure consisting of only tensile members. This way, the proposed methods are suitable for all kinds of tension structures.

Their accuracies and efficiencies have been shown by using several numerical experiments and comparing with the numeration method. Although we have shown the high accuracy and efficiency of the proposed methods in this study, there is no proof that the solution attained by any of these methods is globally optimal. Also as shown in the numerical examples, there is no method that is

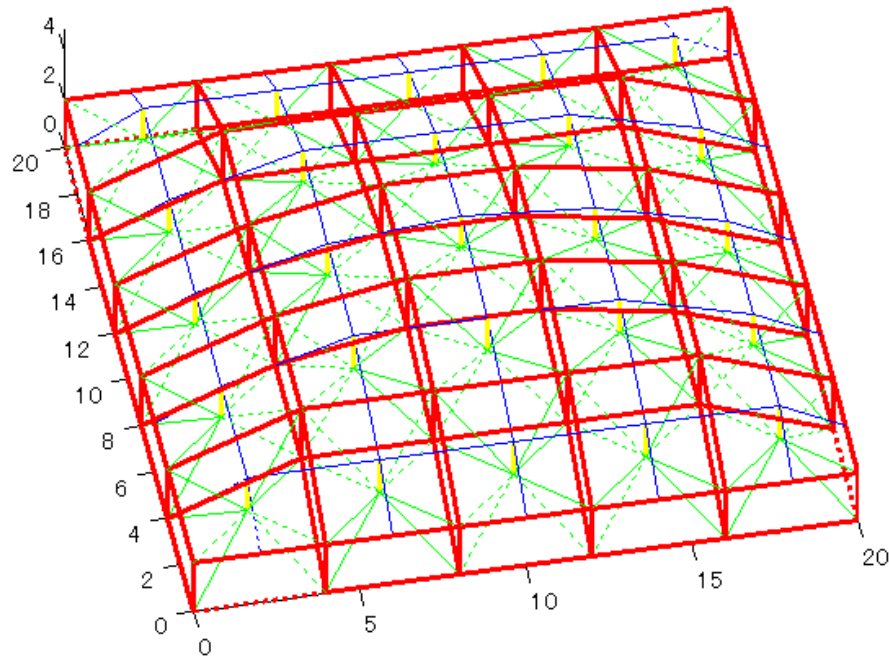


Figure 4.14: A three-dimensional tensegric dome.

most accurate and fastest for all cases. The method should be selected in view of desired accuracy and efficiency, subjected to the constraint on MIE. Generally, SLS is always not a bad choice.

Chapter 5

Optimal Measurement Positions II

A new formulation of identification considering the measurement errors both of member forces and nodal coordinates is given. A new version of simulated annealing starting from an initial solution found by Stingy method is used to find a specific number of measurement members which minimizes the identification error.

5.1 Introduction

In the previous chapter, we have formulated the mean identification error (MIE) to reflect the accuracy of identification of prestress distribution, based on the sensitivity analysis of the equilibrium equations of a tension structure. In this formulation, only the measurement errors of forces have been taken into consideration, while assuming that the configuration of the structure in terms of nodal coordinates are known a priori or measured without any error. Four heuristic methods based on the basic idea of Stingy, Greedy methods and local search strategy are then proposed to find an optimal set of measurement members with the minimal number, subjected to an upper-bound constraint on the MIE specified by users.

5.1.1 Motivation

However, the measurement errors of nodal coordinates and the forces should be taken into account at the same time to reflect the identification error exactly, although the errors of nodal coordinates may sound very small because of the high capability of the measurement devices. So the identification error should be reformulated. On the other hand, the upper-bound constraint on identification may be difficult to decide since it is dependent on the model or type of structure. To this problem, simulated annealing (SA) turns to be a very efficient tool. Therefore, by adopting some new strategies in a standard SA, a specific number of measurement members are to be found in this chapter.

5.1.2 Outline

In the follows of this chapter, the equilibrium equations of the tension structures based on the idea of force density method are used and summarized in Section 2.

Section 3 implements sensitivity analysis of the equilibrium equations considering forces and nodal coordinates as variables. And Section 4 formulates the equation of identification error (IE), by applying sensitivity analysis and probability theory, to reflect the influence of the measurement errors of nodal coordinates and axial forces on it.

An optimization problem, in which a specific number of measurement members are found to minimize the identification error IE, is formulated in Section 5. And then an Improved Simulated Annealing (ISA) starting from a better initial solution by Stingy method instead of a random one is proposed for the problem.

Accuracy and efficiency of the proposed method are illustrated by several numerical examples in Section 6 and 7, and some discussions and conclusions are then given in Section 8.

5.2 Equilibrium Analysis

In order to simply the problem, the following assumptions, similar to the ones in Chapter 4, are introduced as:

1. Members of the structure are connected by pin joints.
2. Topology of the structure, which defines the relation of members and nodes, is known.
3. Geometrical configuration of the structure is in terms of nodal coordinates.
4. Coordinates of free nodes are determined by measurement with measurement errors, while there is no error for the fixed ones.
5. No external load is applied and the self-weight of the structure is neglected.

Let m , n and n^f denote numbers of members, free nodes and fixed nodes, respectively. Since external loads and self-weight of the structure are not considered, the free nodes are in a state of self-equilibrium that the equilibrium equations of them can be written as (details can be found in Chapter 3)

$$\mathbf{D}\mathbf{s} = 0 \tag{5.1}$$

where \mathbf{s} denotes the axial force vector, and the equilibrium matrix $\mathbf{D} \in \mathfrak{R}^{3n \times m}$ is defined as $\mathbf{D} = \begin{pmatrix} \mathbf{C}^\top \mathbf{U} \\ \mathbf{C}^\top \mathbf{V} \\ \mathbf{C}^\top \mathbf{W} \end{pmatrix} \mathbf{L}^{-1}$, in which \mathbf{C} is an incidence matrix defining topology of the structure; \mathbf{U} , \mathbf{V} and \mathbf{W} are diagonal matrices of which diagonal elements represent coordinate differences in x -, y - and z - directions of each member, respectively. They can be calculated by the nodal coordinates in these directions of each node and the incidence matrix \mathbf{C} ; and \mathbf{L} is a diagonal matrix whose diagonal elements represent the length of each member.

The number of self-equilibrium modes is

$$h = m - \text{rank}(\mathbf{D}) \tag{5.2}$$

Only the underdetermined case, when $h > 0$, is considered here since the tension structure falls into this category always.

5.3 Sensitivity Analysis of Equilibrium Matrix

From the definition of \mathbf{D} , the partial derivative of it respect to nodal coordinate x is

$$\frac{\partial \mathbf{D}}{\partial x} = \begin{pmatrix} \mathbf{C}^\top \frac{\partial \mathbf{U}}{\partial x} \mathbf{L}^{-1} + \mathbf{C}^\top \mathbf{U} \frac{\partial \mathbf{L}^{-1}}{\partial x} \\ \mathbf{C}^\top \frac{\partial \mathbf{V}}{\partial x} \mathbf{L}^{-1} + \mathbf{C}^\top \mathbf{V} \frac{\partial \mathbf{L}^{-1}}{\partial x} \\ \mathbf{C}^\top \frac{\partial \mathbf{W}}{\partial x} \mathbf{L}^{-1} + \mathbf{C}^\top \mathbf{W} \frac{\partial \mathbf{L}^{-1}}{\partial x} \end{pmatrix} \quad (5.3)$$

since the matrix \mathbf{C} , which defines the topology of free nodes, is a constant matrix. And x can denote the coordinate of free node i in x -, y - or z - direction, which is x_i , y_i or z_i respectively.

Here, the unknown parameters in Eq. (5.3) are $\frac{\partial \mathbf{U}}{\partial x}$, $\frac{\partial \mathbf{V}}{\partial x}$, $\frac{\partial \mathbf{W}}{\partial x}$, and $\frac{\partial \mathbf{L}^{-1}}{\partial x}$, which are formulated in the following.

5.3.1 Sensitivity Analysis of Length Matrix

Since length matrix \mathbf{L} is a diagonal matrix, whose diagonal elements are the lengths of the members, so \mathbf{L} to the power 2 in terms of nodal coordinate differences \mathbf{U} , \mathbf{V} and \mathbf{W} is

$$\mathbf{L}^2 = \mathbf{U}^2 + \mathbf{V}^2 + \mathbf{W}^2 \quad (5.4)$$

The partial derivative of Eq. (5.4) with respect to nodal coordinate x is

$$\frac{\partial \mathbf{L}}{\partial x} = \mathbf{L}^{-1} \left(\mathbf{U} \frac{\partial \mathbf{U}}{\partial x} + \mathbf{V} \frac{\partial \mathbf{V}}{\partial x} + \mathbf{W} \frac{\partial \mathbf{W}}{\partial x} \right) \quad (5.5)$$

Since the partial derivative of \mathbf{L}^{-1} with respect to x is

$$\frac{\partial \mathbf{L}^{-1}}{\partial x} = -\mathbf{L}^{-2} \frac{\partial \mathbf{L}}{\partial x} \quad (5.6)$$

substitute Eq. (5.5) into Eq. (5.6), the partial derivative of \mathbf{L}^{-1} with respect to x can be written as

$$\frac{\partial \mathbf{L}^{-1}}{\partial x} = -\mathbf{L}^{-3} \left(\mathbf{U} \frac{\partial \mathbf{U}}{\partial x} + \mathbf{V} \frac{\partial \mathbf{V}}{\partial x} + \mathbf{W} \frac{\partial \mathbf{W}}{\partial x} \right) \quad (5.7)$$

5.3.2 Sensitivity Analysis of Coordinate Difference Matrices

Let x_i denote the coordinate of free node i in x - direction, then the partial derivative of \mathbf{u} with respect to x_i is

$$\frac{\partial \mathbf{u}}{\partial x_i} = \frac{\partial(\mathbf{C}\mathbf{x})}{\partial x_i} + \frac{\partial(\mathbf{C}^f \mathbf{x}^f)}{\partial x_i} \quad (5.8)$$

Since the topology in terms of \mathbf{C} and \mathbf{C}^f is assumed to be known, and there is no measurement error in coordinates of fixed nodes, so Eq. (5.8) can be written as

$$\frac{\partial \mathbf{u}}{\partial x_i} = \mathbf{C}_i \quad (5.9)$$

where \mathbf{C}_i denote the i th column of \mathbf{C} . The influence of construction errors of fixed nodes (supports) can be formulated in a similar way to Eq. (5.9) by assuming the topology matrix \mathbf{C}^f not to be constant, although it is not an objective of this paper.

Because $\mathbf{U} = \text{diag}(\mathbf{u})$, so

$$\frac{\partial \mathbf{U}}{\partial x_i} = \text{diag}(\mathbf{C}_i) \quad (5.10)$$

Knowing that \mathbf{U} and \mathbf{W} are not functions of x_i , so their partial derivatives with respect to x_i are

$$\begin{aligned} \frac{\partial \mathbf{V}}{\partial x_i} &= \mathbf{0} \\ \frac{\partial \mathbf{W}}{\partial x_i} &= \mathbf{0} \end{aligned} \quad (5.11)$$

In the cases of $x = y_j$ or $x = z_k$, the partial derivatives of \mathbf{U} , \mathbf{V} and \mathbf{W} with respect to them can be calculated similarly to Eq. (5.10) and Eq. (5.11) as

$$\left\{ \begin{array}{l} \frac{\partial \mathbf{U}}{\partial y_j} = \mathbf{0} \\ \frac{\partial \mathbf{V}}{\partial y_j} = \text{diag}(\mathbf{C}_j) \\ \frac{\partial \mathbf{W}}{\partial y_j} = \mathbf{0} \end{array} \right. \text{ and } \left\{ \begin{array}{l} \frac{\partial \mathbf{U}}{\partial z_k} = \mathbf{0} \\ \frac{\partial \mathbf{V}}{\partial z_k} = \mathbf{0} \\ \frac{\partial \mathbf{W}}{\partial z_k} = \text{diag}(\mathbf{C}_k) \end{array} \right. \quad (5.12)$$

respectively.

Substituting $\frac{\partial \mathbf{U}}{\partial x}$, $\frac{\partial \mathbf{V}}{\partial x}$ and $\frac{\partial \mathbf{W}}{\partial x}$ calculated by the formulation above into Eq. (5.7) and Eq. (5.3), $\frac{\partial \mathbf{D}}{\partial x}$ can then be calculated.

5.4 Formulation of Identification Error (IE)

In Chapter 4, we have attained a formulation of mean identification error by using the equilibrium equations extensively, in which the measurement errors of axial forces have been considered, based on the assumption that the geometrical configuration of the structure is known without any measurement errors. However, the geometrical configuration of a structure, in terms of nodal coordinates, has to be determined by measurement, so that the measurement errors of coordinates should be considered at the same time.

5.4.1 Formulation of Force Errors

Let p denote the number of measurement members, $\mathbf{s}^m \in \mathfrak{R}^p$ denote the axial force vector of the measurement members, and $\mathbf{s}^e \in \mathfrak{R}^{m-p}$ denote the one of estimation members. Eq. (5.1) can then be rewritten in another form as

$$\mathbf{D}^m \mathbf{s}^m + \mathbf{D}^e \mathbf{s}^e = \mathbf{0} \quad (5.13)$$

where the columns of matrices \mathbf{D}^m and \mathbf{D}^e are the column components in \mathbf{D} corresponding to the elements of axial force vectors \mathbf{v}^m and \mathbf{v}^e .

The least squares solution of Eq. (5.13) is (see Appendix B)

$$\mathbf{s}^e = -(\mathbf{D}^e)^- \mathbf{D}^m \mathbf{s}^m \quad (5.14)$$

where $()^-$ denotes the Moore-Penrose matrix inverse.

The total differential equation of Eq. (5.14) is

$$\sum_{i=1}^{3n} \frac{\partial \mathbf{D}^m}{\partial x_i} \Delta x_i \mathbf{s}^m + \mathbf{D}^m \Delta \mathbf{s}^m + \sum_{i=1}^{3n} \frac{\partial \mathbf{D}^e}{\partial x_i} \Delta x_i \mathbf{s}^e + \mathbf{D}^e \Delta \mathbf{s}^e = \mathbf{0} \quad (5.15)$$

where Δx_i and $\Delta \mathbf{s}^m$ can be considered as the measurement errors of nodal coordinates and axial forces of measurement members, respectively. On the other hand, $\Delta \mathbf{s}^e$ denotes the estimation errors of axial forces of the estimation members. The details of calculation of $\frac{\partial \mathbf{D}^m}{\partial x_i}$ and $\frac{\partial \mathbf{D}^e}{\partial x_i}$ in Eq. (5.15) can be found in Appendix C.

From Eq. (5.14) and Eq. (5.15), the estimation error vector $\Delta \mathbf{s}^e$ can be written as

$$\Delta \mathbf{s}^e = -(\mathbf{D}^e)^- \left(\sum_{i=1}^{3n} \left[\frac{\partial \mathbf{D}^m}{\partial x_i} - \frac{\partial \mathbf{D}^e}{\partial x_i} (\mathbf{D}^e)^- \mathbf{D}^m \right] \mathbf{s}^m \Delta x_i + \mathbf{D}^m \Delta \mathbf{s}^m \right) \quad (5.16)$$

5.4 Formulation of Identification Error (IE)

Eq. (5.16) can be written in a simpler form, by applying $\mathbf{H} \in \mathfrak{R}^{(m-p) \times 3n} = (\mathbf{H}_1, \dots, \mathbf{H}_i, \dots, \mathbf{H}_{3n})$ and $\mathbf{G} \in \mathfrak{R}^{(m-p) \times p} = -(\mathbf{D}^e)^{-1} \mathbf{D}^m$, where $\mathbf{H}_i = -(\mathbf{D}^e)^{-1} [\frac{\partial \mathbf{D}^m}{\partial x_i} - \frac{\partial \mathbf{D}^e}{\partial x_i} (\mathbf{D}^e)^{-1} \mathbf{D}^m] \mathbf{s}^m$, as

$$\Delta \mathbf{s}^e = (\mathbf{H}, \mathbf{G}) \begin{pmatrix} \Delta \mathbf{x} \\ \Delta \mathbf{s}^m \end{pmatrix} \quad (5.17)$$

Since the measurement and estimation errors of axial forces can be written as $\Delta \mathbf{s}^\top = (\Delta \mathbf{s}^{m\top}, \Delta \mathbf{s}^{e\top})$, called *force error vector* here, Eq. (5.17) can then be rewritten in terms of force error vector as follows

$$\Delta \mathbf{s} = \begin{pmatrix} \mathbf{O} & \mathbf{I}_p \\ \mathbf{H} & \mathbf{G} \end{pmatrix} \begin{pmatrix} \Delta \mathbf{x} \\ \Delta \mathbf{s}^m \end{pmatrix} \quad (5.18)$$

where \mathbf{I}_p denotes an identity matrix with $p \times p$ elements. This way, the force error vector $\Delta \mathbf{s}$ is formulated as a function of measurement errors of nodal coordinates $\Delta \mathbf{x}$ and axial forces $\Delta \mathbf{s}^m$.

5.4.2 Mean and Variance-covariance

By assuming that

All the elements of measurement error vectors of nodal coordinates $\Delta \mathbf{x}$ and axial forces $\Delta \mathbf{s}^m$ satisfy independent normal distribution $(0, e_c^2)$ and $(0, e_f^2)$, respectively.

Therefore, $\Delta \mathbf{x}$ and $\Delta \mathbf{s}^m$ satisfy normal distributions of $(\mathbf{0}, e_c^2 \mathbf{I}_{3n})$ and $(\mathbf{0}, e_f^2 \mathbf{I}_p)$, respectively. From Eq. (5.18), we know that the mean error vector of all the axial forces $\Delta \mathbf{s}$, both measured and estimated, is

$$\mathbf{E}[\Delta \mathbf{s}] = \mathbf{0} \quad (5.19)$$

since $\mathbf{E}[\Delta \mathbf{x}] = \mathbf{0}$ and $\mathbf{E}[\Delta \mathbf{s}^m] = \mathbf{0}$. And its variance-covariance matrix \mathbf{A} is

$$\mathbf{A} = \begin{pmatrix} e_f^2 \mathbf{I}_p & e_f^2 \mathbf{G}^\top \\ e_f^2 \mathbf{G} & e_c^2 \mathbf{H} \mathbf{H}^\top + e_f^2 \mathbf{G} \mathbf{G}^\top \end{pmatrix} \quad (5.20)$$

5.4.3 Definition of Identification Error (IE)

Since axial forces and nodal coordinates have different dimensions, it is more convenient to transform them into dimensionless factors, by introducing $\Delta \mathbf{x}/e_c$ and $\Delta \mathbf{s}^m/e_f$, to reflect the force errors due to the relative measurement errors of axial forces and nodal coordinates, so Eq. (5.18) is rewritten as follows

$$\Delta \mathbf{s} = \begin{pmatrix} \mathbf{O} & e_f \mathbf{I}_p \\ e_c \mathbf{H} & e_f \mathbf{G} \end{pmatrix} \begin{pmatrix} \Delta \mathbf{x}/e_c \\ \Delta \mathbf{s}^m/e_f \end{pmatrix} \quad (5.21)$$

or in another form as follows for simplicity

$$\Delta \mathbf{s} = \mathbf{B} \Delta \mathbf{r} \quad (5.22)$$

where

$$\mathbf{B} = \begin{pmatrix} \mathbf{O} & e_f \mathbf{I}_p \\ e_c \mathbf{H} & e_f \mathbf{G} \end{pmatrix} \quad (5.23)$$

and

$$\Delta \mathbf{r} = \begin{pmatrix} \Delta \mathbf{x}/e_c \\ \Delta \mathbf{s}^m/e_f \end{pmatrix} \quad (5.24)$$

From Eq. (5.22), it is clear that different combination of measurement errors, corresponding to the change of $\Delta \mathbf{r}$, with a specific set of measurement members, corresponding to a constant \mathbf{B} , may lead to very different force errors. The worst situation of the force errors with a specific set of measurement members is defined as the maximum Euclidean vector norm of $\Delta \mathbf{s}$:

$$\text{Max} \quad \|\Delta \mathbf{s}\| \quad (5.25)$$

This worst situation of force errors is adopted as the definition of *Identification Error (IE)*, E , in this chapter.

To find out the maximum vector norm of force error vector directly, the 2-norm of matrix \mathbf{B} , $\|\mathbf{B}\|_2$, can be used:

$$E = \|\Delta \mathbf{s}\| = \|\mathbf{B}\|_2 = \max_{\|\Delta \mathbf{r}\|_2=1} \|\mathbf{B} \Delta \mathbf{r}\|_2 \quad (5.26)$$

where it is to find a vector $\Delta \mathbf{r}$, of which vector norm is equal to 1, leading $\|\Delta \mathbf{s}\|$ to be maximal.

5.5 Formulation and Solution of Optimal Positions

It can be proved that the 2-norm of matrix \mathbf{B} is equal to the square root of its largest eigenvalue (Borse, 1997), λ_{max} , which may simplify the calculation greatly

$$E = \sqrt{\lambda_{max}} \quad (5.27)$$

When all the members are to be measured ($p = m$) and the measurement errors of nodal coordinates are assumed to be zero ($e_c = 0$), the maximum norm of force error vector is e_f , since at this situation

$$\mathbf{B} = e_f \mathbf{I}_m \quad (5.28)$$

5.5 Formulation and Solution of Optimal Positions

In the earlier chapter, we have proposed four methods, based on the idea of Stingy method, Greedy method and local search strategy, for finding the optimal set of measurement members subjected to the upper-bound of Mean Identification Error (MIE). The accuracy and efficiency of them have been shown and discussed at the end of it. But to different structures or even the same structure with different models, the constraint on identification error is not easy to specify, although it has been shown that when all the members are to be measured it turns to be e_f , the variance of measurement error of axial forces.

In many cases in practice, the measurement may be desired to be specific number taking the cost and availability of measurement devices into consideration. So, this chapter formulates an optimization problem to represent this requirement and solution of it based on standard simulated annealing is then proposed.

5.5.1 Formulation

From the definition of identification error (IE) in Eq. (5.27), it is clear that different sets of measurement members, corresponding to the changes of matrix \mathbf{B} , may have different identification errors, even if the number of measurement members were identical.

5.5 Formulation and Solution of Optimal Positions

With the specific number of measurement members, it is always strongly desired to find the set of it to minimize the identification error, so the optimization problem can be formulated as follows

$$\begin{aligned} & \text{minimize } E \\ & \text{subject to } p = \bar{p} \end{aligned} \tag{5.29}$$

where \bar{p} denotes the specific number of measurement members. Note here that there is actually another innate constraint condition that the matrix \mathbf{D}^e have to be full-rank to make its least square solution meaningful (see Appendix B).

5.5.2 Solution

It has been shown and discussed in the earlier chapter that Simulated Annealing may have very high accuracy and the ability of finding near optimal solution without entrapping in the local optimum. The accuracy and efficiency of it are affected by the following factors:

1. initial solution,
2. initial temperature,
3. local search in the neighborhood,
4. cooling schedule,
5. and termination conditions.

Among these, the initial solution and cooling schedule may play critical roles: a better solution which is closer to the strictly optimal one may lead to less effort and faster convergence; and the faster the cooling schedule may certainly cause faster termination but may not achieve a accurate enough solution due to the deficiency of searching for better solution in the neighborhood of the current one. So, the Standard Simulated Annealing (SSA) begins from a random initial solution with monotonically decrease of temperature at a constant ratio, may need slower cooling schedule to find the near optimal solution.

5.6 Numerical Example 1: 21-member Cable Net Model

In practical implementation of standard Simulated Annealing (SSA), it is really important, but difficult on the other hand, to specify appropriate parameters especially the cooling ration η : too high may cost more significant computation time, but too low will cool the system down faster and may make it terminate on a local minima.

5.5.2.1 Improved Simulated Annealing (ISA)

From the numerical examples shown in the earlier chapter, which will be given again for a 21-member cable net model of a membrane structure in the next numerical example section using the new definition of identification error, we have got to know that the proposed Stingy method has relatively high accuracy while just little computation cost.

These characteristics promise it to be a good tool, which can provide us a good initial solution rather than a random one, to reduce computation cost and, the most important, to improve accuracy.

As has been mentioned in the previous chapter, Stingy method starts from a complete set of members, and keep removing the members, which has the minimal influence on identification error, consecutively until the upper bound constraint on identification error has been satisfied. In order to make use of the idea of Stingy method to find us a better initial solution for the beginning of Simulated Annealing, with specific number of measurement members, the Stingy method can be implemented by dropping the members from a complete set one by one until there remains the specific number \bar{p} .

5.6 Numerical Example 1: 21-member Cable Net Model

In order to investigate the influence of measurement errors of nodal coordinates and axial forces on the estimation errors of axial forces, and the efficiency and accuracy of the proposed methods for finding the optimal measurement positions, this section gives out some numerical examples.

Although tension membrane structure is made of continuum membrane material, it can be discretized and substituted by a cable net model, e.g. described

5.6 Numerical Example 1: 21-member Cable Net Model

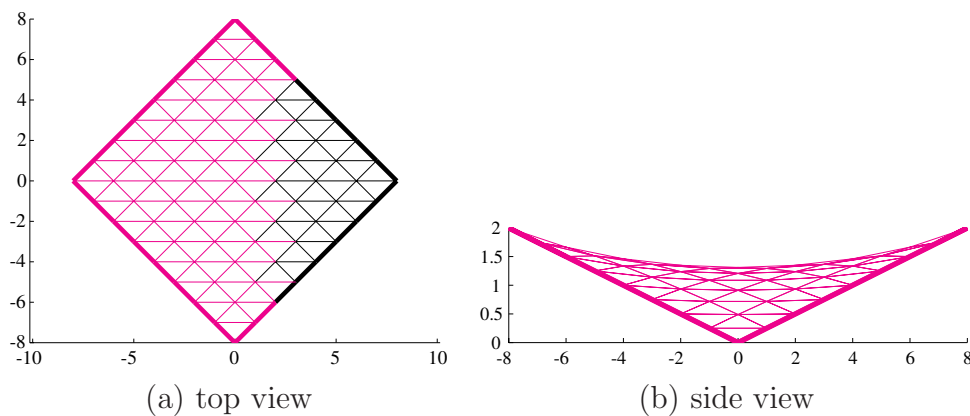


Figure 5.1: A membrane structure modeled by a cable net with 176 members.

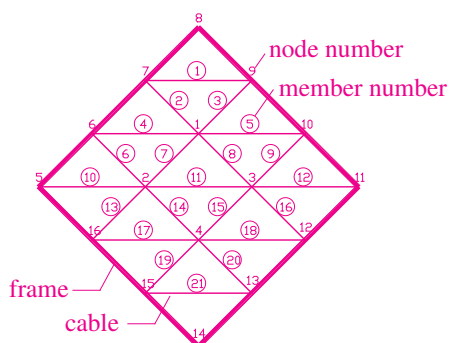


Figure 5.2: A membrane structure modeled by a cable net with 21 members.

by [Maurin and Motro \(1998\)](#). This way, membrane structure can also be treated as a special kind of prestressed pin-jointed structure.

An HP-shaped membrane structure, of which the diagonal span length is 16 m and the height is 2 m, is used as numerical example. Fig. 5.1 shows the top view and side view of the structure substituted by an 176-member cable net model.

5.6.1 Enumeration method

To investigate the exact influence of number of measurement members on the identification error, enumeration method is applied first. And a simpler cable net model with only 21 cable members as shown in Fig. 5.2, in which at least 9 independent measurement members are needed, is used instead because the

5.6 Numerical Example 1: 21-member Cable Net Model

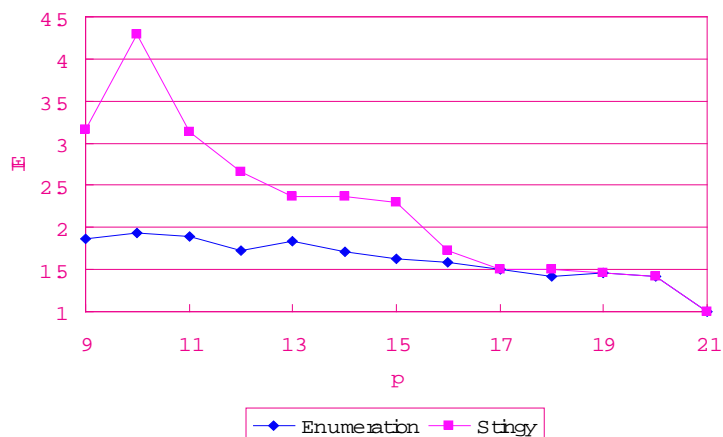


Figure 5.3: 21-member cable net.

computation cost is very high for combinatorial problem; e.g. in order to find an optimal set of measurement with 9 measurement members for this relatively simple model, totally $({}^9C_{21} =)293930$ iterations are necessary. The cost may increase exponentially with the increasing number of cable net members. Stingy method proposed in the last chapter is used to show the relation in the same case for comparison.

In the case of neglecting measurement errors of nodal coordinates ($e_c = 0$) and setting $e_f = 1$, the relationships between p and IE calculated by enumeration method and Stingy method are shown in Fig. 5.3.

It can be seen from this figure that

1. the relation of the number of measurement members (p) to the identification error (IE) by enumeration method has a basic tendency that more measurement members may lead to higher accuracy of identification, although it is not absolutely true for all cases. So the proposed methods in Chapter 4 based on adding or removing elements consecutively can also be applied here.
2. The Stingy method is of very high accuracy while p is large since it begins from a complete set of measurement members. It can reflect the trend of the relationship between p and IE properly although not highly accurately.

5.6.2 Efficiency and Accuracy of Improved SA (ISA)

To investigate the efficiency and accuracy of the Improved Simulated Annealing (ISA) comparing to the standard one (SAS), the 21-member cable net model of the tensile membrane structure described previously is used.

The parameters of SSA and ISA used here to find optimal \bar{p} measurement members are set as follows:

- neighborhood of the current solution in each iteration step is searched 50 times;
- initial temperature is set to be $t_0 = 5$;
- cooling ratio is $\eta = 0.99$ or $\eta = 0.95$;
- terminate while $t_i < 10^{-6}$ or no update of solution at 5 consecutive temperature.

The identification errors calculated by SSA and ISA and their computation costs are listed in Table 5.1, Table 5.2 and Table ??, Table ?? for the cases of CASE 1 and CASE 2, where $\eta = 0.99$ and $\eta = 0.95$, respectively.

Table 5.1: SSA with random initial solution

No. of Trials	1	2	3	4	5	6	Mean
Identification Error	1.9219	1.7302	1.7302	1.8252	1.8252	1.9219	1.8258
Computation Cost	24378	19941	16626	18768	16422	27795	20655

Table 5.2: ISA with initial solution by Stingy

No. of Trials	1	2	3	4	5	6	Mean
Identification Error	1.7302	1.7302	1.8252	1.7302	1.8252	1.7302	1.7619
Computation Cost	18666	18513	17085	17901	15198	18411	17629

The mean values of these results by SSA and ISA are summarized and compared to the enumeration method and Stingy method as in Table 5.3 to investigate their efficiencies and accuracies.

From these results, we can see that

5.7 Other Numerical Examples

Table 5.3: Comparison of EM, RSA, Stingy and ISA for $\bar{p} = 12$.

	Enumeration	Stingy	SSA	ISA
Identification Error	1.7302	2.6607	1.8258	1.7619
Relative Error ^a	0%	53.78%	5.53%	1.83%
Computation Cost	293930	165	20655	17629
Relative Cost ^b	100%	0.056%	7.03%	6.0%

^aProportion of the difference of identification error by each method and the enumeration method to the optimal minimum.

^bProportion of the computation cost of each method to the enumeration method.

1. Greater the cooling ratio η , more accurate the result one can achieve, however, with heavier computation burden, because the slower cooling schedule may provide sufficient search for better solutions.
2. ISA can find the strict optimal solution with higher frequency and a little less computation cost than SSA.

Therefore, it is likely possible for us to draw the conclusion that a better solution gained from Stingy method, rather than a random one, is more reliable to achieve more accurate solution with a similar efficiency.

5.7 Other Numerical Examples

5.7.1 Example 2: Two-dimensional Self-stressing Arch

To illustrate the suitability of ISA to any other kind of tension structure, a two-dimensional self-stressing pin-jointed arch, which is described in the previous chapter and shown in Fig. 4.10, is used again to find specific number of measurement members. The minimal number of measurement members of it is $h = 6$.

Example 2-1: Set the specific number of measurement members to be $\bar{p} = 13$ and the parameters as $t_0 = 10$, $\eta = 0.95$, without considering any measurement error of nodal coordinates. The ISA finds the optimal set of measurement members as $\{2, 4, 13, 15, 17, 18, 20, 21, 22, 23, 25, 26, 27\}$, which are shown as dotted lines in Fig. 5.4.

It is clear that locations of the measurement members are symmetric since the structure is symmetric too.

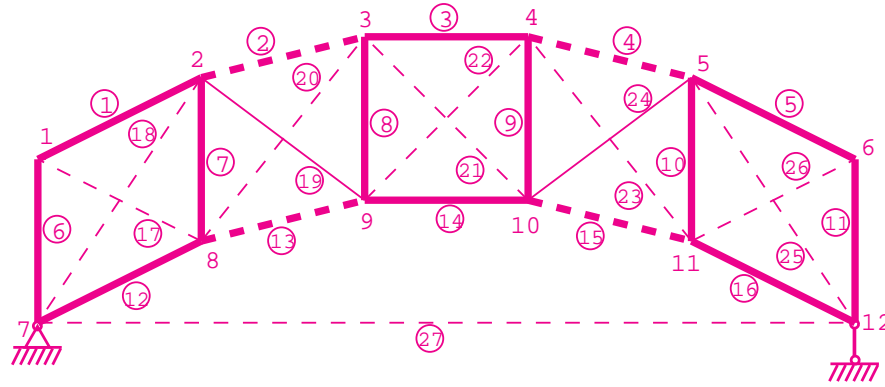


Figure 5.4: Ex. 2-1 of optimal measurement members ($\bar{p} = 13$).

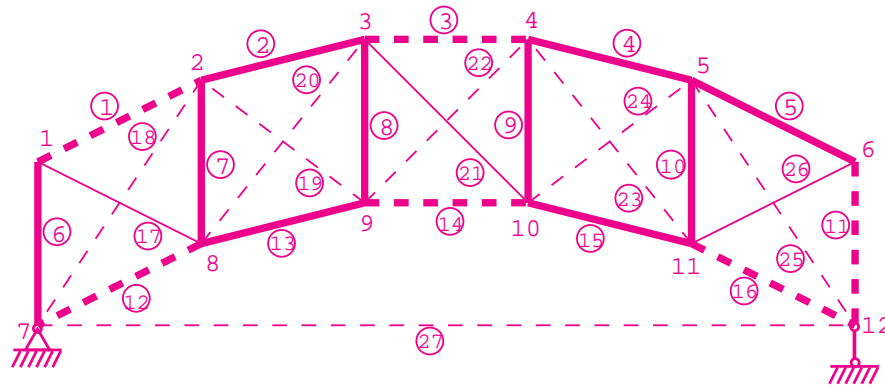


Figure 5.5: Ex. 2-2 of optimal measurement members ($\bar{p} = 13$).

Example 2-2: Since measurement devices used nowadays may have very high accuracy for the measurement of nodal coordinates, of which measurement error is said to be within 1mm, so we set the variance of measurement error of each nodal coordinate e^c for this example to be $1\text{mm}(10^{-3}\text{m})$. The maximum of absolute value of the axial forces is $-2.5697 \times 10^3\text{kN}$ (minus means it is a compressive member), in this example we use 1% of this maximal force as the variance of the measurement, so $e^f = 25.697(\text{kN})$.

By implementation of ISA, it finds the optimal set of 13 measurement members as $\{1, 3, 11, 12, 14, 16, 18, 19, 20, 22, 23, 24, 25\}$, which is shown in Fig. 5.5.

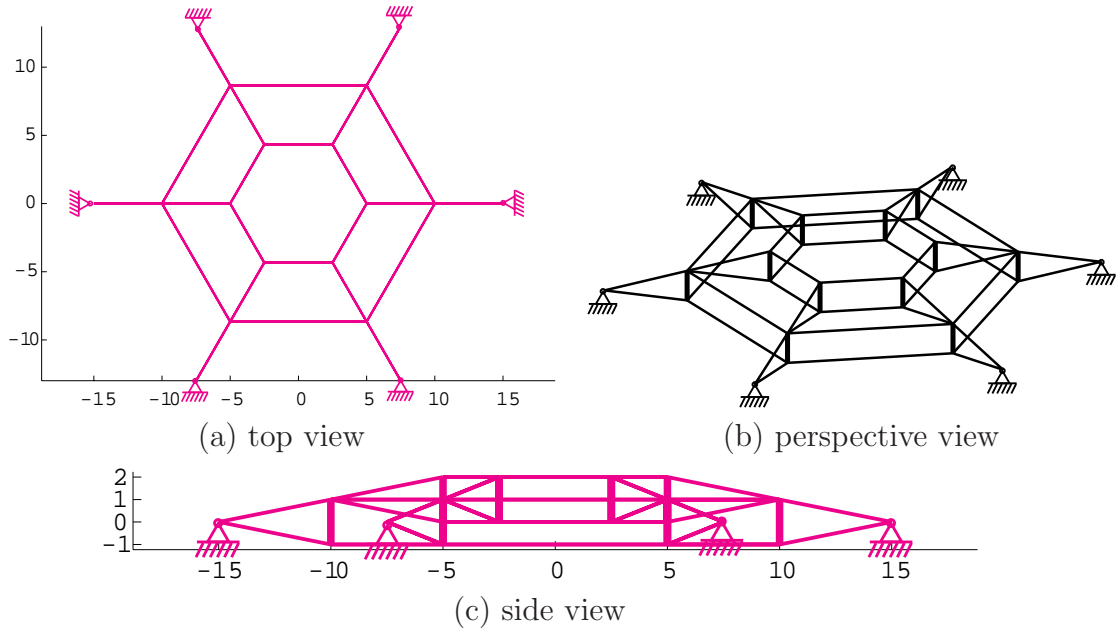


Figure 5.6: A three-dimensional cable dome.

5.7.2 Example 3: A Three-dimensional Cable Dome

Fig. 5.6 shows a three-dimensional cable dome, consisting of 12 struts and 48 cables. Nodes of the structure are located on three circles with different radius — $5m$, $10m$ and $15m$, and four different elevations — $-1m$, $0m$, $1m$ and $2m$.

The variance of each measurement error of nodal coordinate e_c is set to be $1mm$, and the one of force is $e_f = 0.5(kN)$, which is about 1.7% of the largest prestress of the structure. The object of this example is to find 12 measurement members in tension to minimize the identification error (IE).

Example 3-1: First, we use Stingy method, which starts from a complete set of tensile members and drops measurement members from the current set one by one, to find the 12 measurement members, as the dotted lines shown in Fig. 5.7(a), where the IE is 1.1988.

Example 3-2: The 12 measurement tensile members found in the Ex. 3-1 are used as initial solution for ISA, the find the near-optimal solution as the dotted lines shown in Fig. ??, where the IE is calculated to be 1.0418.

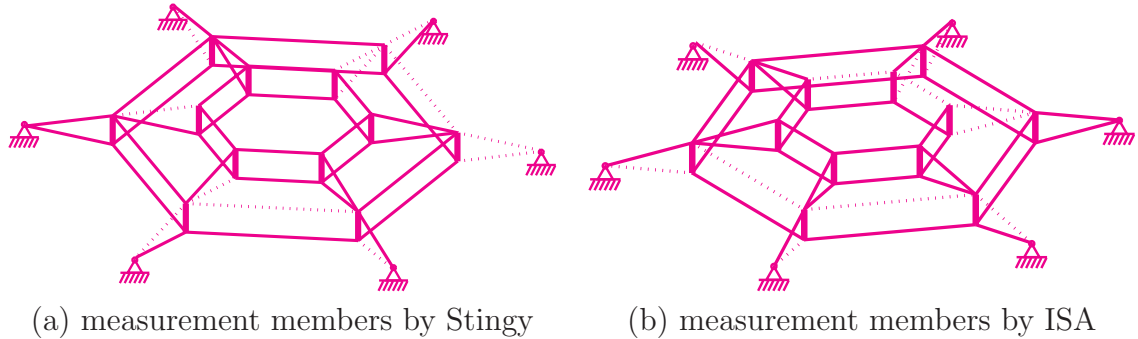


Figure 5.7: 12 optimal measurement members of a three-dimensional cable dome.

5.8 Conclusion

This chapter formulate the identification error (IE) for evaluation of the accuracy of the prestress distribution of tension structures, taking measurement errors both of forces and nodal coordinates into consideration. An optimization problem is formulated to reflect the requirement of minimizing the identification error with a specific number of measurement. And an improved simulated annealing (ISA), of which initial solution is found by the Stingy method rather than a random one, is proposed for the problem. A number of numerical examples have been given to illustrate the efficiency and accuracy of the proposed (ISA) and the influence of measurement errors of nodal coordinates on the optimal measurement members.

The improved simulated annealing is proved to have the ability of finding the near-optimal solution more stably and faster. According to the requirement, the case of only the tensile members being measured can also use the proposed method simply.

Chapter 6

Conclusions

In this study, we have proposed two form-finding methods for design of tensegrity structures, one is a direct approach and other is an adaptive force density method, and heuristic methods for finding the optimal measurement positions of tension structures based on two different formulations to evaluate the identification error of prestresses distribution.

6.1 Form-finding Problem of Tensegrity Structures

The less control on mechanical and geometrical properties of a tensegrity structure in the current methods has motivated us to propose an efficient direct approach for the form-finding problem of it. And the complexity of design process of a tensegrity structure leads to another powerful method based on the idea of force density method.

6.1.1 Direct Approach

In the direct approach for the design of tensegrity structures, the geometrical and mechanical properties of a structure which is desired by architects and structural engineers can be formulated as linear equations in terms of nodal coordinate

6.1 Form-finding Problem of Tensegrity Structures

vector and member force vector, respectively, in addition to the equilibrium equations. The geometrical properties can be direction of specific members, locations of supports and symmetry properties of some groups of members etc. In order to transform a prestressed tensegrity structure into a self-stressed or self-stressing one since only the nodes in the state of self-equilibrium can be considered in the formulation of equilibrium of the structure, a concept of virtual auxiliary member, which connects the supports, is introduced.

By specifying an independent set of member forces and then nodal coordinates consecutively according to the proposed algorithms, the approach can calculate the others directly and exactly, that the designers can have direct and exact control on the configuration and mechanics of the structure. Since only linear equations need to be solved in the proposed method, it is highly efficient. And some numerical examples have been given to illustrate the ability of searching new configuration by adjusting the values of the parameters.

However, to a relatively complicated structure where there are too much member forces need to be specified, which maybe exceed the expectation of designers, it comes to be an additional burden rather than benefit. And the final configuration of the structure may collide into a plan, line or even one point by the poorly specified values of the parameters, to which the designers are expected to have more advanced knowledge about the structure.

In these cases, more geometrical constraints, s on the structure can be introduced to reduce the number of member forces that can be specified, or introduce some optimization problems, in which the designers can specify only the parameters they want to control and hand to release the designers from this problem.

6.1.2 Adaptive Force Density Method

For the purpose of finding feasible configuration of the structures with relatively complicated topology and high rank deficiency of the equilibrium matrix, a new numerical method - Adaptive Force Density Method, which is extended from the idea of force density method originated for the design problem of tensile structures and considered a powerful tool for searching new configuration with

only linear equations, is proposed to deal with the complications arising in the design problem of tensegrity structure.

Singular value decomposition of the equilibrium matrix, which is formulated in terms of force densities and topology of the structure, is used to find a feasible set of force densities starting from a given initial one to make the equilibrium matrix satisfy the required rank deficiency. After that, we utilize the algorithm proposed in Chapter 2 to specify an independent set of nodal coordinates to achieve a unique configuration of the structure.

Some simple and complicated examples have been given to show its efficiency in computation cost and high ability of finding new configuration with the only requirements on a given topology of the structure and an initial set of force densities, irrespective of the complexity of the structure. A very good and fast convergence of the proposed method has also been shown.

The main drawback of the method is that it has no exact control over the mechanical and geometrical properties of the structure, unlike the direct approach in Chapter 2. This is considered as the main disadvantage of the force density method as well, since the parameters are force-to-length ratios.

6.2 Optimal Measurement Positions

In the problems of maintenance and health monitoring of a tension structure, the prestress distribution is necessary for the adjustment of it to achieve a desired shape. The optimal positions for measurement or deployment of sensors can reduce the costs on construction and measurement devices significantly or improve the accuracy of identification error with the same number of measurement devices, which have been discussed in Chapter 4 and 5, respectively.

6.2.1 Consider Measurement Errors of Forces only

In Chapter 4, the equilibrium equations of a tension structure is given and the minimal number of measurement members needed to identify the prestress distribution is discussed.

6.2 Optimal Measurement Positions

By separating the members into measurement members and identification members and sensitivity analysis of the equilibrium equations of the structure, a formulation of mean identification error (MIE) is then given out for evaluating the accuracy of identification.

An optimization problem, which is to minimize the number of measurement members subjected to an upper-bound constraint on the MIE is formulated, to represent the requirement of reducing the cost of measurement devices while the accuracy of identification being within an acceptable level.

Four heuristic methods based on the ideas of Stingy, Greedy methods and local search strategy are presented for finding the optimal measurement members. Since simulated annealing is a powerful method for the combinatorial optimization problem, it is adopted at the first step of Greedy method and GLS to find an optimal independent set of measurement members. Accuracies and efficiencies of the proposed methods are illustrated by several numerical examples - different cable net models of a membrane structure, a two-dimensional cable dome and a two-dimensional self-stressing tensegrity structure.

In the cases of tensegrity structure, only the tensile members are expected to be measured because of the easiness of measurement of these members. We have also shown the proposed methods are suitable to this special requirement easily in the operation of removing or adding measurement members.

6.2.2 Consider Errors of Forces and Configuration

However, the measurement problem in practice should not neglect the measurement errors configuration in terms of nodal coordinates, although they may sound very small, besides the ones of member forces. So Chapter 5 formulates a new identification error based on the sensitivity analysis of equilibrium equations of the structure, to reflect the influence of measurement errors of forces and configuration at the same time. This way, the measurement errors of nodal coordinates and/or member forces can be considered separately according to requirement. It should be noted that forces of the measurement members are needed in this formulation, which can be obtained after the design process.

Rather than finding the minimal number of measurement members in Chapter 4, we formulate an optimization problem, which is to find a set of measurement members with specific number to minimize the identification error. Simulated annealing used as the first step in Greedy method and GLS has been proved to be efficient and be of high accuracy at the same time. So we use an improved version of it, which starts from an initial solution found by the Stingy method, to find the optimal measurement members. By using a example of the 21-member cable net model of a membrane structure, the improved simulated annealing (ISA) is shown to work better than the standard one starting from a random initial solution.

Therefore, we use ISA to find optimal measurement members with the specific number in the case of considering only measurement errors of forces and case of both of configuration and forces.

6.3 Future Study

In order to reduce the number of member forces that can be specified in the proposed direct approach for the design of tensegrity structures, introduction of optimization problem is considered a promised way.

How to have more control over the geometrical and mechanical properties by the adaptive force density method is a future goal for the next version of this method. The problem turns out to how to linearly formulate the equations of geometrical properties, such as symmetry and lengths of the members, in terms of nodal coordinates.

Since the accuracy of simulated annealing is highly sensitive to the adopted cooling schedule, how to reduce this sensitivity by adopting some adaptive cooling schedules is now under consideration.

Appendix A

Reduced Row-Echelon Form

Any (possibly not square) finite matrix \mathbf{A} can be reduced by a finite sequence of linear elementary row operation $\mathbf{E}_1, \mathbf{E}_2, \dots, \mathbf{E}_l$, each one invertible, to a *Reduced Row-Echelon Form* (RREF) $\mathbf{U} := \mathbf{E}_m \cdots \mathbf{E}_2 \mathbf{E}_1 \mathbf{A}$ characterized by the following three properties:

- a. The first nonzero element in any nonzero row is 1.
- b. The leading 1 of each nonzero row 1 appears in a column of which all the other elements are 0.
- c. Each such leading 1 comes in a column after every preceding row's leading zeros.

Matrix \mathbf{A} determines its RREF \mathbf{U} uniquely, even though \mathbf{A} does not determine uniquely the sequences of Elementary Row-Operations that reduce \mathbf{A} to \mathbf{U} .

For example, the RREF of matrix

$$\mathbf{A} = \begin{pmatrix} 16 & 2 & 3 & 13 \\ 5 & 11 & 10 & 8 \\ 9 & 7 & 6 & 12 \\ 4 & 14 & 15 & 1 \end{pmatrix} \tag{A.1}$$

is

$$\mathbf{U} = \left(\begin{array}{ccc|c} 1 & 0 & 0 & 1 \\ 0 & 1 & 0 & 3 \\ 0 & 0 & 1 & -3 \\ \hline 0 & 0 & 0 & 0 \end{array} \right) \quad (\text{A.2})$$

We can easily see that the rank of \mathbf{U} is 3. Since the rank of \mathbf{A} is unchanged by pre multiplication by invertible matrices, $\text{rank}(\mathbf{A}) = \text{rank}(\mathbf{U})$. From the fact that we have applied only row operations on \mathbf{A} to get \mathbf{U} , we can know from \mathbf{U} that the first three columns of \mathbf{A} are independent.

Appendix B

Least Square Solution

The error of Eq. (5.13) can be written as

$$\epsilon = \mathbf{D}^m \mathbf{s}^m + \mathbf{D}^e \mathbf{s}^e \quad (\text{B.1})$$

where $\mathbf{D}^m \in \mathfrak{R}^{3n \times p}$ and $\mathbf{D}^e \in \mathfrak{R}^{3n \times (m-p)}$ are the equilibrium matrices corresponding to the axial forces to be measured and estimated. The square of this error is

$$\phi = \epsilon^\top \epsilon = (\mathbf{D}^m \mathbf{s}^m + \mathbf{D}^e \mathbf{s}^e)^\top (\mathbf{D}^m \mathbf{s}^m + \mathbf{D}^e \mathbf{s}^e) \quad (\text{B.2})$$

To be minimized, the following stationary condition of the square of errors ϕ have to be satisfied

$$\frac{\partial \phi}{\partial \mathbf{s}^e} = \mathbf{0} \quad (\text{B.3})$$

which can be written as

$$(\mathbf{D}^e)^\top \mathbf{D}^m \mathbf{s}^m + (\mathbf{D}^e)^\top \mathbf{D}^e \mathbf{s}^e = \mathbf{0} \quad (\text{B.4})$$

Since $2n > m$ and $3n > m$ are the usual cases for a typical 2D and 3D prestressed structures respectively, so if the inverse of $(\mathbf{D}^e)^\top \mathbf{D}^e$ exists, or in another term, $\text{rank}(\mathbf{D}^e) = m - p$, Eq. (B.4) can be solved as

$$\mathbf{s}^e = -((\mathbf{D}^e)^\top \mathbf{D}^e)^{-1} (\mathbf{D}^e)^\top \mathbf{D}^m \mathbf{s}^m \quad (\text{B.5})$$

Note here that $((\mathbf{D}^e)^\top \mathbf{D}^e)^{-1}(\mathbf{D}^e)^\top$ satisfies the definitions of Moore-Penrose matrix inverse, which are

$$\begin{aligned}
(AA^-)^\top &= AA^- \\
(A^-A)^\top &= A^-A \\
AA^-A &= A \\
A^-AA^- &= A^-
\end{aligned} \tag{B.6}$$

where $()^-$ denotes the Moore-Penrose matrix inverse, so $((\mathbf{D}^e)^\top \mathbf{D}^e)^{-1}(\mathbf{D}^e)^\top$ can be written in terms of Moore-Penrose matrix inverse \mathbf{D}^- for simplification that Eq. (B.5) can be rewritten as

$$\mathbf{s}^e = -\mathbf{D}^- \mathbf{D}^{m,m} \tag{B.7}$$

Bibliography

- Ishii, K., 1999. Membrane designs and structures in the world. Shinkenchiku-sha Co., Ltd., Tokyo. [1](#)
- Wakefield, D. S., 1999. Engineering analysis of tension structures: theory and practice. *Engineering Structures*. 21, 680–690.
- Fuller, R. B., 1975. *Synergetics, Explorations in the Geometry of Thinking*. Collier Macmillan, London. [1.1.2](#)
- Motro, R., 1996. Structural morphology of tensegrity systems. *Int. J. Space Structures*. 11(1&2), 233–240. [1.1.2](#)
- Haber, R. B., Abel, J. F., 1982. Initial equilibrium solution methods for cable reinforced membranes part I — formulations. *Comp. Meth. Appl. Mech. and Engng*. 30, 263–284. [2](#), [4.2](#)
- Caspar, D.L.D., and Klug, A., 1962. Physical principles in the construction of regular viruses. *Proceedings of Cold Spring harbor Symposium on Quantitative Biology*. 27, 1-24. [1.1.2](#)
- Ingber, D.E., 1993. Cellular tensegrity: defining new rules of biological design that govern the cytoskeleton. *Journal of Cell Science*. 104, 613–627. [1.1.2](#)
- Marks, R. and Fuller, R.B., 1960. *The dymaxion world of Buckminster Fuller*. Reinhold Publications, New York.
- Snelson, K.D., Feb. 16, 1965. Continuous tension, discontinuous compression structures. United States Patent 3,169,611.

- Fest, E., Shea, K., Domer, B. and Smith, I.F.C., 2003. Adjustable tensegrity structures. *Journal of Structural Engineering*. 129(4), 515–526. [1.1.2](#)
- Lay, D.C., 1996. *Linear algebra and its applications*, 2nd ed. Reading, MA Addison-Wesley. [3.4.2](#)
- Connelly, r. and Terrell, M., 1995. Globally rigid symmetric tensegrities. *Structural Topology*. 21, 59-78. [2.1.1](#)
- Hanaor, A., 1988. Prestressed pin-jointed structures — flexibility analysis and prestress design. *Comp. & Struct.* 28(6), 757–769. [2.1.1](#)
- Pellegrino, S., 1990. Analysis of prestressed mechanisms. *Int. J. Solids and Struct.* 26(23), 1329–1350. [2.1.1](#)
- Pellegrino, S., Calladine, C.R., 1986. Matrix analysis of statically and kinematically indetermined frameworks. *Int. J. Solids and Struct.* 22(4), 409–428. [2.1.1](#)
- Sultan, C., Corless, M., Skelton, R.E., 2001. The prestressability problem of tensegrity structures: some analytical solutions. *Int. J. Solids and Struct.* 38, 5223–5252. [2.1.1](#), [3.5.1](#)
- Jager, B.D., Skelton, R.E., 2004. Symbolic stiffness optimization of planar tensegrity structures. *J. of Intelligent Material Sys. and Struct.* 15, 181–193 [2.1.1](#)
- Motro, R., Najari, S., Jouanna, P., 1986. Static and dynamic analysis of tensegrity systems. *Proc. Int. Symp. on Shell and Spatial Structures: Computational Aspects*, Springer, NY. 270-279. [2.1.1](#)
- Barnes, M. R., 1999. Form finding and analysis of tension structures by dynamic relaxation. *Int. J. Space Struct.* 14(2), 89–104. [2.1.1](#)
- Motro, R., 1984. Forms and forces in tensegrity systems, in: H.Nooshin, ed.. *Proc. 3rd Int. Conf. on Space Struct.*, Elsevier, Amsterdam. 180–185. [2.1.1](#)
- Schek, H. J., 1974. The force density method for form finding and computation of general networks. *Comp. Meth. Appl. Mech. Engng.* 3, 115–134. [2.1.1](#), [3.2](#), [3.3](#), [3.3.1](#), [4.2](#)

- Vassart, N. and Motro, R., 1999. Multiparametered formfinding method: application to tensegrity systems. *Int. J. Space Struct.* 14(2), 147–154. [2.1.1](#), [3.1](#), [3.3.1](#), [3.3.2](#)
- Tibert, G., Pellegrino, S., 2003. Review of form-finding methods for tensegrity structures. *Int. J. Space Struct.* 18(4), 209–223. [2.1.1](#), [3.6](#)
- Ohsaki, M., Kanno, Y., 2003. Form-finding of cable domes with specified stresses by using nonlinear programming. *Proc. IASS-APCS 2003, Taipei, Taiwan, 2003.* [2.1.2](#), [2.5.1](#), [4.1.3](#), [4.8.2](#)
- Harary, F., 1969. *Graph Theory*. Addison-Wesley, Reading, MA. [2.1.2](#), [2.2](#), [3.3.1](#)
- Kaveh, A., 1992. *Structural Mechanics: Graph and Matrix Methods*. Wiley, NY. [2.1.2](#)
- Williamson, D., Skelton, R. E., 2003. Equilibrium conditions of a tensegrity structure. *Int. J. Solids Struct.* 40, 6347–6367. [2.1.2](#)
- Borse, G. J., 1997. *Numerical Method with MATLAB*. International Thomson Publishing Inc. [2.4.1](#), [3.4.1](#), [3.5](#), [5.4.3](#)
- Maurin, B., Motro, R., 1998. The surface stress density method as a form-finding tool for tensile membranes. *Engineering Structures.* 20(8), 712–719. [3.2](#), [4.2](#), [4.8.1](#), [5.6](#)
- Sultan, C., Corless, M., Skelton R.,E., 2002. Symmetrical reconfiguration of tensegrity structures. *International Journal of Solids and Structures.* 39, 2215–2234.
- Sanayei, M., et al, 1992. Selection of noisy measurement locations for error reduction in static parameter identification. *AIAA J.* 30(9), 2299–2309. [4.4](#)
- Pothisiri, T., Hjelmstad, K.D., 2002. Strategy for finding a near-optimal measurement set for parameter estimation from modal response. *J. of Sound and Vibration.* 257(1), 89–106. [4.4](#)

- Abdullah, M.M., Richardson, A., Hanif, J., 2001. Placement of sensors/actuators on civil structures using genetic algorithms. *Earthquake Engng Struct. Dyn.* 30, 1167–1184. [4.4](#)
- Zavoni, E.H., Iturrizaga, R.M., Esteva, L., 1999. Optimal instrumentation of structures on flexible base for system identification. *Earthquake Engng Struct. Dyn.* 28, 1471–1482. [4.4](#)
- Lundy, M., and Mees, A., 1986. Convergence of an annealing algorithm. *Math Prog.* 34, 111–124.
- Kirkpatrick, S., Gelatt, C.D., Jr., Vecchi, M.P., 1983. Optimization by simulated annealing. *Science.* 220(4598), 671–680. [4.6.1](#)
- Azizi, N., Zolfaghari, S., 2004. Adaptive temperature control for simulated annealing: a comparative study. *Computers & Operations Research.* 31, 2439–2451. [4.6.1.3](#)